REVIEW

Thin and transient meltwater layers and false bottoms in the Arctic sea ice pack—Recent insights on these historically overlooked features

Madison M. Smith[1],*, Hélène Angot[2,3], Emelia J. Chamberlain[4], Elise S. Droste[5,6], Salar Karam[7], Morven Muilwijk[8], Alison L. Webb[9,10], Stephen D. Archer[11], Ivo Beck[2], Byron W. Blomquist[12,13], Jeff Bowman[4], Matthew Boyer[14], Deborah Bozzato[15], Melissa Chierici[16], Jessie Creamean[17], Alessandra D'Angelo[18], Bruno Delille[19], Ilker Fer[20], Allison A. Fong[6], Agneta Fransson[8], Niels Fuchs[21], Jessie Gardner[22], Mats A. Granskog[8], Clara J. M. Hoppe[6], Mario Hoppema[6], Mario Hoppmann[6], Thomas Mock[5], Sofia Muller[19,23], Oliver Müller[24], Marcel Nicolaus[6], Daiki Nomura[25], Tuukka Petäjä[14], Evgenii Salganik[8,26], Julia Schmale[2], Katrin Schmidt[27], Kirstin M. Schulz[28], Matthew D. Shupe[12,13], Jacqueline Stefels[15], Linda Thielke[29], Sandra Tippenhauer[6], Adam Ulfsbo[30], Maria van Leeuwe[15], Melinda Webster[31], Masaki Yoshimura[25], and Liyang Zhan[32]

The rapid melt of snow and sea ice during the Arctic summer provides a significant source of low-salinity meltwater to the surface ocean on the local scale. The accumulation of this meltwater on, under, and around sea ice floes can result in relatively thin meltwater layers in the upper ocean. Due to the small-scale nature of these upper-ocean features, typically on the order of 1 m thick or less, they are rarely detected by standard methods, but are nevertheless pervasive and critically important in Arctic summer. Observations during the Multidisciplinary drifting Observatory for the Study of Arctic Climate (MOSAiC) expedition in summer 2020 focused on the evolution of such layers and made significant advancements in understanding their role in the coupled Arctic system. Here we provide a review of thin meltwater layers in the Arctic, with emphasis on the

[1] Woods Hole Oceanographic Institution, Woods Hole, MA, USA

[2] Extreme Environments Research Laboratory, Ecole Polytechnique Federale de Lausanne Valais Wallis, Sion, Switzerland

[3] University of Grenoble Alpes, CNRS, INRAE, IRD, Grenoble INP, IGE, Grenoble, France

[4] Scripps Institution of Oceanography, University of California San Diego, La Jolla, CA, USA

[5] University of East Anglia, Norwich Research Park, Norwich, UK

[6] Alfred-Wegener-Institut, Helmholtz-Zentrum für Polar- und Meeresforschung, Bremerhaven, Germany

[7] Department of Earth Sciences, University of Gothenburg, Gothenburg, Sweden

[8] Norwegian Polar Institute, Fram Centre, Tromsø, Norway

[9] University of Warwick, Coventry, UK

[10] University of York, York, UK

[11] Bigelow Laboratory for Ocean Sciences, East Boothbay, ME, USA

[12] Cooperative Institute for Research in Environmental Sciences, University of Colorado, Boulder, CO, USA

[13] NOAA Physical Sciences Laboratory, Boulder, CO, USA

[14] Institute for Atmospheric and Earth System Research (INAR), University of Helsinki, Helsinki, Finland

[15] Groningen Institute for Evolutionary Life Sciences, University of Groningen, Groningen, the Netherlands

[16] Institute of Marine Research, Tromsø, Norway

[17] Colorado State University, Fort Collins, CO, USA

[18] Graduate School of Oceanography, University of Rhode Island, Narragansett, RI, USA

[19] Unité d'Océanographie Chimique, Université de Liège, Liège, Belgium

[20] Geophysical Institute, University of Bergen, Bergen, Norway

[21] Center for Earth System Sustainability, Institute of Oceanography, Universität Hamburg, Hamburg, Germany

[22] UiT—The Arctic University of Norway, Tromsø, Norway

[23] PROPICE, Laboratoire de Glaciologie, Université Libre de Bruxelles, Brussels, Belgium

[24] Department of Biological Sciences, University of Bergen, Bergen, Norway

[25] Hokkaido University, Hakodate, Hokkaido, Japan

[26] Norwegian University of Science and Technology, Trondheim, Norway

[27] School of Geography, Earth and Environmental Sciences, University of Plymouth, Plymouth, UK

[28] Oden Institute for Computational Engineering and Sciences, The University of Texas at Austin, Austin, TX, USA

[29] Institute of Environmental Physics, University of Bremen, Germany

[30] Department of Marine Sciences, University of Gothenburg, Gothenburg, Sweden

[31] Polar Science Center, University of Washington, Seattle, WA, USA

[32] Third Institute of Oceanograhy, Ministry of Natural Resources, Xiamen, People's Republic of China

* Corresponding author:
Email: madisonmsmith@whoi.edu

new findings from MOSAiC. Both prior and recent observational datasets indicate an intermittent yet long-lasting (weeks to months) meltwater layer in the upper ocean on the order of 0.1 m to 1.0 m in thickness, with a large spatial range. The presence of meltwater layers impacts the physical system by reducing bottom ice melt and allowing new ice formation via false bottom growth. Collectively, the meltwater layer and false bottoms reduce atmosphere-ocean exchanges of momentum, energy, and material. The impacts on the coupled Arctic system are far-reaching, including acting as a barrier for nutrient and gas exchange and impacting ecosystem diversity and productivity.

Keywords: Arctic sea ice, MOSAiC expedition, Meltwater, Atmosphere-ice-ocean interactions, Air-sea gas exchange, Arctic ecosystem

1. Introduction

Sea ice is an expansive cover on much of the Arctic Ocean, but in the vertical dimension it is only a relatively thin veneer separating the often-deep ocean below from the atmosphere above. Despite this discrepancy between horizontal and vertical scales, sea ice has far-reaching impacts on the Arctic system. This paper explores similarly thin yet impactful features that often evade our measurements—thin layers of meltwater that pool under, around, and on sea ice during the melt season. Compared to their sea ice precursor, meltwater layers under sea ice and in leads are challenging to identify visually and have thus been often overlooked in observations and analyses of Arctic processes.

Unlike other oceans, the Arctic Ocean is predominantly stratified by salinity rather than temperature (Carmack, 2007). Fresher waters can remain relatively undiluted near the surface with more saline water masses below when dynamic processes (wind, waves, and currents) are generally low. On the basin scale, large freshwater fluxes are provided by Arctic rivers as well as inflows from Pacific and even Atlantic Oceans (Carmack, 2000). Locally, however, summer sea ice and snow melt provide a significant freshwater flux. This flux can result in notably thin layers of meltwater right at the interface between the ocean and the overlying sea ice and atmosphere.

Since the first recorded observation of a meltwater layer by Fridtjof Nansen in 1894 (Nansen, 1902; 1906), such features have been the subject of sporadic observation across the Arctic pack ice. Their presence is often overlooked due to the disconnect in scales with those that are typically measured in the ocean, often beginning meters below the surface. When observed, the critical importance of these layers in the Arctic climate system has been acknowledged (e.g., Vihma et al., 2014). Such meltwater stratification in the upper ocean has the potential to impact many physical, biological and biogeochemical processes occurring near the air-ice-ocean interface, including species diversity, distribution, and productivity. Further, meltwater layers can act as a barrier to air-sea gas exchange and inhibit ice-water nutrient exchange.

The sparsity of observations of this layer and differences in terminology used by different disciplines has prevented a comprehensive view of the role of sea ice and snow meltwater layers in the Arctic system. This overview aims to provide a comprehensive summary of prior observations and works describing the presence and implications of these layers. Our review will include the results from a new set of inter-disciplinary observations and studies from the Multidisciplinary drifting Observatory for the Study of Arctic Climate (MOSAiC) that were, in part, designed to understand these features and their implications.

We start by defining the terminology that will be used for the meltwater layers discussed in Section 2, followed by a summary of observational methods in Section 3. A short overview of the MOSAiC expedition follows in Section 4, which provides many new insights on meltwater layers reviewed herein. We then describe the key features of the physical evolution and previous observations of thin meltwater layers in Section 5, and proceed through sections reviewing the implications of thin meltwater layers for different components of the Arctic system. These include sea ice, ocean, organism diversity, community structure, biogeochemical gradients, and air-sea exchanges across meltwater layer interfaces in Sections 6–9, respectively. We conclude with perspectives on the expected impacts of climate change in Section 10 and highlight key challenges and propose future directions for this area of research in Section 11.

2. Terminology

This manuscript focuses on the evolution and implications of thin meltwater layers that form in the Arctic Ocean during the melt season (**Table 1**). We define thin meltwater layers as layers with a thickness on the order of 0.1 m to 1.0 m and a relatively low salinity of <20 g kg^{-1} compared to seawater. These layers have also been referred to in the literature and by the community as "freshwater lenses" and "freshwater layers," but we note here that they are not strictly freshwater. Meltwater is used to distinguish the freshwater as locally derived from in situ melt, rather than from other sources such as terrestrial/riverine input or land ice melt inflows. Based on the vertical scale of focus here, these thin meltwater layers are also distinct from larger-scale meltwater-freshened mixed layers such as in Crews et al. (2022). The possibility of meltwater layers on the 0.1–1.0 m scale in the Southern Ocean is not discussed, but, to our knowledge, they have not been documented in Antarctic sea ice.

Snow and ice meltwater can be conceptualized as spreading across the heterogeneous sea ice cover in a thin

Table 1. Definitions of meltwater layer locations and associated features

| Feature	Definition
Melt ponds	The pooling of snow and sea ice meltwater on the surface of the sea ice. Ponds can be connected to the ocean below or separated from the ocean below by impermeable sea ice or a "false bottom." Also referred to as melt puddles (JCOMM Expert Team on Sea Ice, 2014).
Under-ice meltwater layers	Thin meltwater layers that occur below the sea ice. These layers are analogous to melt ponds in that they are constrained topographically and contain meltwater; also referred to as under-ice melt ponds.
Lead meltwater layers	Thin meltwater layers in leads or cracks between floes.
False bottoms	Ice growth separated vertically from the main ice floe by a liquid-filled void. False bottoms typically form during the melt season below the base of under-ice meltwater layers in contact with cold, ambient seawater or at the base of a drainage hole where a melt pond connects to the ocean surface layer below.
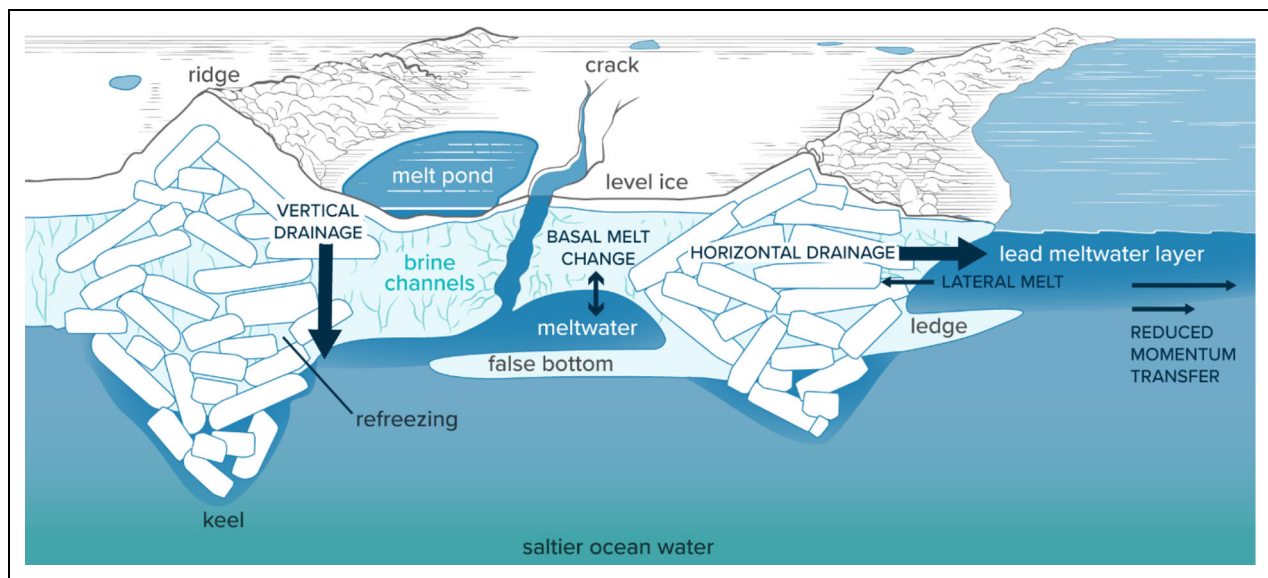
Figure 1. Schematic of thin meltwater layer locations in sea ice-covered regions. Thin meltwater layers can occur in melt ponds, under the ice, and in leads. Meltwater additionally refreezes within voids of ridge keels, and into false bottoms at the base of under-ice meltwater layers. Schematic also shows the key drivers in the physical evolution of layers, with ecological and biogeochemical implications summarized in a later figure. Not to scale. Figure by Madison Smith and Natalie Renier © Woods Hole Oceanographic Institution.

layer, thus including three primary locations: melt ponds, under-ice meltwater layers also known as under-ice melt ponds, and lead meltwater layers between floes (**Figure 1**). Melt ponds are included in the definition here as an important sink in the meltwater budget where stratification can occur, but the focus in this review is on the unique and less well-described presence of meltwater layers between and underneath sea ice floes. It is not uncommon for meltwater in leads and under ice to refreeze at the interface with the colder and saltier ocean water below. This refreezing is most commonly observed below the ice, where the refrozen layer is referred to as a false bottom (**Table 1**). Other possible sinks of meltwater include refreezing in voids within ridge keels or at the base of lead meltwater layers (**Figure 1**). False bottoms have not been included previously in the World Meteorological Organization (WMO) Sea Ice Nomenclature (JCOMM Expert Team on Sea Ice, 2014), but have been proposed for inclusion in future versions due to the

increasing capability to observe this common subsurface feature.

In this review, we focus on meltwater layers formed from snow and ice meltwater, with a view towards the relevance for pack ice in the Central Arctic. Snow and ice meltwater layers also commonly occur in and under landfast ice (e.g., Perovich and Maykut, 1990; Ehn et al., 2011; Hop et al., 2011; Mundy et al., 2011; Elliot et al., 2015; Kirillov et al., 2018), as described throughout the review, with some differences in the formation and evolution due to increased snowmelt, reduced sea ice drift, and tidal effects. Landfast ice can also have distinct "freshwater" layers from terrestrial runoff or from glacial melt, which are not included here.

3. Sampling and observational techniques
Limited methods are available for sampling and observing meltwater layers under and surrounding sea ice. Traditional profiling instruments for conductivity, temperature,

and depth (CTDs), whether free-falling or deployed by winch, are unable to fully resolve thin meltwater layers due to the minimum required averaging interval of tens of centimeters. These features typically cannot be observed from ships due to the mixing of the upper water column by the ship's wake. Additionally, temperature and conductivity sensors on CTD rosette samplers are usually mounted at the bottom, such that the shallowest measurable depth is around 1 m. These measurement limitations have further implications for the ability to identify associated changes in ecological and biogeochemical parameters on the relevant scale, where low salinity layers are easily mixed and disturbed.

The majority of observations of under-ice and lead meltwater layers have come from on-ice point measurements of water properties. The lowering of a probe to collect in situ point measurements of temperature and salinity has been employed in leads (Nansen, 1902; 1906; Perovich and Maykut, 1990; Richter-Menge et al., 2001; Pegau, 2002; Nomura et al., 2023) and under ice (e.g., Smith et al., 2022b). Observations of under-ice meltwater were typically made by collecting water either using a pump (Eicken, 1994) or by SCUBA divers (Ehn et al., 2011); the water was subsequently measured for salinity using a conductivity probe or salinometer. Values for salinity reported on the practical salinity scale are dimensionless, whereas absolute salinity is reported in g kg^{-1}. The latter better reflects the effect of global spatial gradients in the composition of the dissolved material on conductivity measurements (Wright et al., 2011; McDougall et al., 2012). For the purpose of examining the large salinity gradients associated with meltwater layers in this study, the small differences between using practical and absolute salinity are negligible. Although they can be used interchangeably effectively, we report values in absolute salinity whenever possible, in accordance with the official description of seawater, TEOS-10 (McDougall and Barker, 2011). Profiling measurements from a hole in drifting sea ice using buoyant, ascending profilers, such as the vertical microstructure profiler (VMP; Fer et al., 2022b), can resolve the meltwater layer with minimal disturbance to the water structure. Recent developments in equipping remotely operated vehicles (ROV) with CTD sensors allow fine scale and high vertical resolution profiles directly under sea ice (Katlein et al., 2017).

Under-ice meltwater layers have been indicated using measurements of temperature, such as from active profiling or buoys with thermistor chains (Langleben, 1966; Provost et al., 2019; Lei et al., 2022). However, the lack of conductivity/salinity observations creates challenges in differentiating meltwater from ice (Lei et al., 2022), as estimates from temperature alone are ambiguous. Sea ice drilling, such as for measuring thickness and coring, can be a reliable, yet destructive, method to determine the presence of false bottoms. In addition to false bottoms serving as a concrete indicator of relatively fresh meltwater, the desalinization of the bottom of the ice core can indicate prior under-ice meltwater layers (Eicken, 1994). Similarly, the ease of drilling can serve as a qualitative

indicator of prior meltwater layers as fresher ice is harder to drill through than more saline ice. In addition to the salinity of the ice, false bottoms can be distinguished from ridged ice by the structure of the ice (Eicken, 1994), d^{18}O signatures (e.g., Smith et al., 2022b), and the typical false bottom thickness (tens of cm at most; e.g., Smith et al., 2022b). The presence of under-ice meltwater layers and associated false bottoms have also been assessed qualitatively using imagery (Assmy et al., 2013; Perovich, personal communication, 29/07/2022) and from under-ice sonar data (Wang et al., 2013; Salganik et al., 2023). At present, thin meltwater features and false bottoms cannot be observed by airborne or satellite remote sensing, as these features cannot be detected through sea ice and meltwater layers in leads typically occur on a smaller spatial scale than can be resolved.

Relative to under-ice and lead meltwater layers, methods to measure melt ponds are relatively straightforward, and the observational record of melt ponds extends as far back as the 1950s (e.g., Nazintsev, 1964). Given the extensive work on melt ponds, a complete description of melt pond properties and processes is beyond the scope of this review. Instead, we refer readers to the cited references for more information on melt pond observations (Fetterer and Untersteiner, 1998; Eicken et al., 2002; Eicken et al., 2004; Petrich et al., 2012; Polashenski et al., 2012; Landy et al., 2014; Polashenski et al., 2017; Wright et al., 2020; Webster et al., 2022), highlighting here the key linkages that melt ponds have with other meltwater layers.

Melt ponds undergo different stages of evolution as melt progresses: (1) initial formation and growth, during which the surface of ponds can be above sea level; (2) vertical drainage due to permeable ice or macroscopic flaws, including cracks or enlarged brine channels, draining ponds to sea level; (3) continued deepening of ponds, at which point thaw holes form and pond floors melt through; and (4) either complete melt-out or refreezing. Prior to stage 2, the size (or areal extent) and depth of a melt pond are adequate for estimating the meltwater content within a given pond. Melt pond depth can be measured through a variety of methods, including manual measurements with a marked ski pole or ruler (e.g., Perovich et al., 2003; Polashenski et al., 2015) or by using an automated depth probe (Webster et al., 2022), all of which tend to have a maximum uncertainty of 1 cm. Recently, pond depths have been derived from airborne photogrammetry (Divine et al., 2016) and remotely sensed data (e.g., Farrell et al., 2020; König and Oppelt, 2020), though assessments are ongoing to quantify retrieval uncertainties and biases. Melt pond size and areal coverage can be quantified using high-resolution imagery from kites (e.g., Petrich et al., 2012), drones (e.g., Calmer et al., 2023), aircraft (e.g., Miao et al., 2015; Wright et al., 2020), and satellites (e.g., Fetterer and Untersteiner, 1998; Rösel and Kaleschke, 2012) using supervised and unsupervised classification methods. Methods to estimate melt pond coverage and depth are continuing to evolve rapidly with advancing technology.
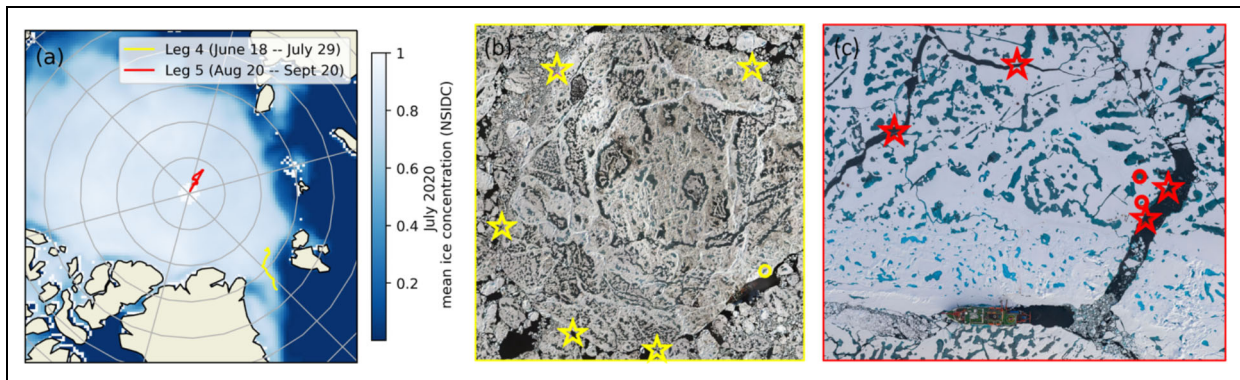
Figure 2. Maps of MOSAiC meltwater layer sampling areas. (a) Drift tracks of MOSAiC Legs 4 (June 18–July 29; yellow) and 5 (August 20–September 20; red). Blue to white shading shows the average July 2020 ice concentration (from the National Snow and Ice Data Center, NSIDC). Aerial imagery of floes (Neckel et al., 2022) indicate primary lead sampling sites with stars and melt pond sampling sites with circles for (b) Leg 4 and (c) Leg 5.

4. Overview of observations on the MOSAiC expedition

Thin meltwater layers were observed during the course of the MOSAiC expedition, which was a year-long drift expedition in the Central Arctic from October 2019 to October 2020. An overview of the drift and highlights of physical evolution can be found in Nicolaus et al. (2022), Shupe et al. (2022) and Rabe et al. (2022). The expedition was divided into 5 legs; observations of relevance for the questions addressed here derive primarily from summer, spanning June–July (Leg 4) and August–September (Leg 5). Drift tracks were spatially discontinuous due to drift of the original floe and its break-up upon reaching the ice edge in late July (**Figure 2**). Nevertheless, the expedition collected an unparalleled density of observations of the Arctic air-ice-ocean system, measuring key parameters for nearly the entire year.

The science approach utilized disciplinary teams making coordinated observations to facilitate interdisciplinary analysis and understanding. The importance of fine-scale stratification during the summer melt season had been identified during planning as a key undersampled feature. Thus, interdisciplinary sampling was undertaken to capture the implications of meltwater features. In particular, coordinated sampling of leads with semi-continuous and discrete observations made by teams studying sea ice (Nicolaus et al., 2022), ocean (Rabe et al., 2022), atmosphere (Shupe et al., 2022), ecology, and biogeochemistry were undertaken during both Legs 4 and 5 (**Figure 2**). These dedicated observations provide the most complete picture of meltwater layer processes that exist, while numerous other sensors provide opportunistic and supplementary insight into the evolution and implications of meltwater layers.

The summer conditions during the MOSAiC expedition can be considered anomalous in terms of air temperature and typical in terms of wind speeds (Rinke et al., 2021). The July and August conditions at the moving position of MOSAiC were among the warmest in the climatology (1979–2020), with temperature being above the 75th percentile of climatological records 52% and 60% of the time in July and August, respectively. These

anomalous temperatures are likely related to the fact that the expedition was closer to the ice edge than it would have been at the same location earlier in the climatological period due to the low summer ice extent (Rinke et al., 2021). In contrast, wind speeds at 10-m height in July were nearly perfectly aligned with historical distributions, with 26% both above and below the interquartile range of the climatology. August and September wind speeds were slightly anomalously low with 32% and 30% below the 25th percentile, respectively (Rinke et al., 2021).

5. Physical evolution of thin meltwater layers

The first recorded observation of thin meltwater layers in leads or cracks was made by Nansen during the drift of Fram in 1894 (Nansen, 1902; 1906; **Figure 3**). He described a "nearly fresh layer of water [between floes], with a temperature about or even above 0°C." The layer was approximately 2 m thick on July 11, with a salinity of 1–2 and noticeable clumps of algae floating near the bottom boundary of the layer (Nansen, 1902; 1906; **Figure 4**). Subsequent observations of these difficult-to-observe meltwater layers below sea ice, in cracks and leads, suggest that these features likely occur in the pack ice across most of the Arctic Ocean during the melt season.

While false bottoms were likely first described by Untersteiner and Badgley (1958), Hanson (1965) provides the first detailed quantification of associated under-ice meltwater layers or "under-ice melt ponds." Under-ice meltwater layers, inferred by the presence of false bottoms below, were observed with ablation stakes at sites near both a natural and artificial drainage hole in the Chukchi Sea in 1958 (Hanson, 1965). The superposition of two meltwater layers and false bottoms infers two subsequent drainage events prior to observation, after which the layers and false bottoms gradually thinned through August and into September, when observations ceased. In 1965 in the Canadian Arctic (Ellesmere Island), the temperature evolution of a likely low-salinity under-ice meltwater layer was measured more directly during the melt season, with water temperature increasing from −1.4°C to −0.4°C (Langleben, 1966). While submarine
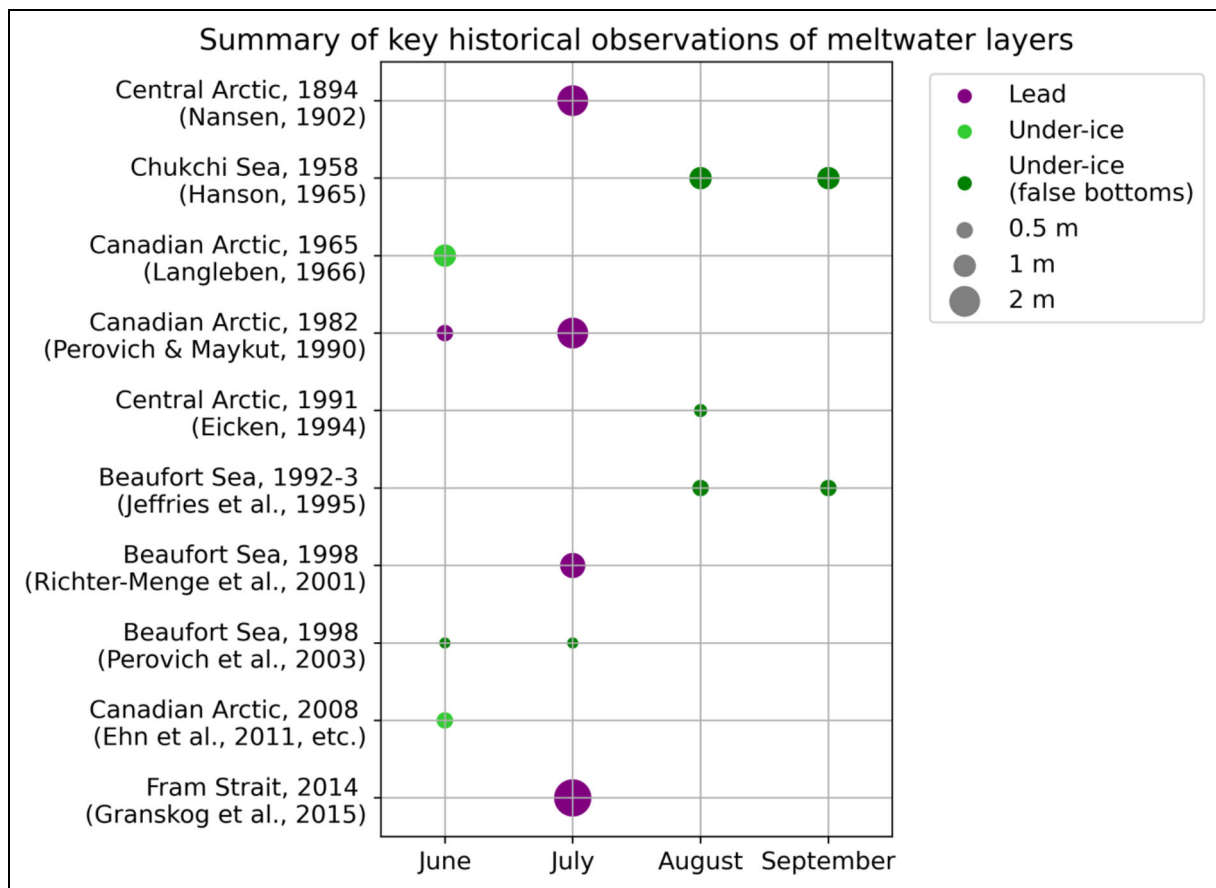
Figure 3. Summary of key historical observations of meltwater layers. Timing, by month, of key historical records of meltwater layers in leads (purple) and under ice (green, with dark green indicating inferred from false bottoms) in the Arctic. Size of circles corresponds to the approximate maximum thickness of the observed layer in meters.

sonar measurements indicated that under-ice meltwater layers may be common under the Arctic ice pack (Wadhams and Martin, 1990), Perovich and Maykut (1990) documented the development of a warm, relatively fresh layer in a stable lead with an initial width of 3 m during summer of 1982 in the Canadian Arctic (Mould Bay). By July 6, there was an approximately 2 m thick, well-mixed, relatively fresh (practical salinity of approximately 3) surface layer that warmed over mid-July to a maximum temperature above 0°C. Horizontal variations in the lead temperature structure were small. During the Surface Heat Budget in the Arctic Ocean (SHEBA) study in the Beaufort Sea in 1998, a stable lead developed a strongly stratified, relatively fresh meltwater layer (practical salinity <4) down to a maximum depth of 1.4 m around July 25 (Richter-Menge et al., 2001), with the highest fraction of this meltwater coming from surface snow and ice melt (Perovich et al., 2021). A helicopter survey (July 22) of 8 additional leads around the SHEBA camp showed that thin (<1.5 m) low-salinity (practical salinity <10) lead meltwater layers were present in all of them (Richter-Menge et al., 2001). Meltwater layers in cracks and ice holes were indicated by observations in the Eastern Central Arctic in 2012 by visual imagery of density gradients and the presence of floating algal aggregates at the meltwater-saltwater interface (Assmy et al., 2013; **Figure 4**). In contrast to these observations, leads in the Arctic pack under

stormier conditions have been observed to remain well-mixed throughout the summer melt season (e.g., McPhee et al., 1987).

A more detailed investigation of under-ice meltwater layers was completed in the Central Arctic in 1991 (Eicken, 1994), with meltwater layers characterized by a practical salinity of 1.5 reaching a thickness of 0.3 m. Using false bottoms as an indication of the lower-bound of coverage of under-ice meltwater layers, others found that they occurred under approximately 10% of level-ice core locations in the Beaufort Sea in 1992 and 1993 (Jeffries et al., 1995), and at least 15% of locations that were observed in the Beaufort Sea during SHEBA in 1998 (Perovich et al., 2003). Observations under landfast sea ice in the Amundsen Gulf, in the Canadian Arctic, indicated evolution of a 0.5-m thick meltwater layer over June 2008 (Ehn et al., 2011; Hop et al., 2011; Mundy et al., 2011). Measurements showed practical salinities <10 on two of the three observation dates, with the meltwater layer generally becoming thicker and more saline over the June sampling period (Mundy et al., 2011). Sea ice meltwater-affected layers in the upper few meters of the ocean were inferred from ship-based optical measurements in late summer 2014 in the Fram Strait, where the meltwater signal was typically associated with a decrease in absorption but an increase in scattering (Granskog et al., 2015).
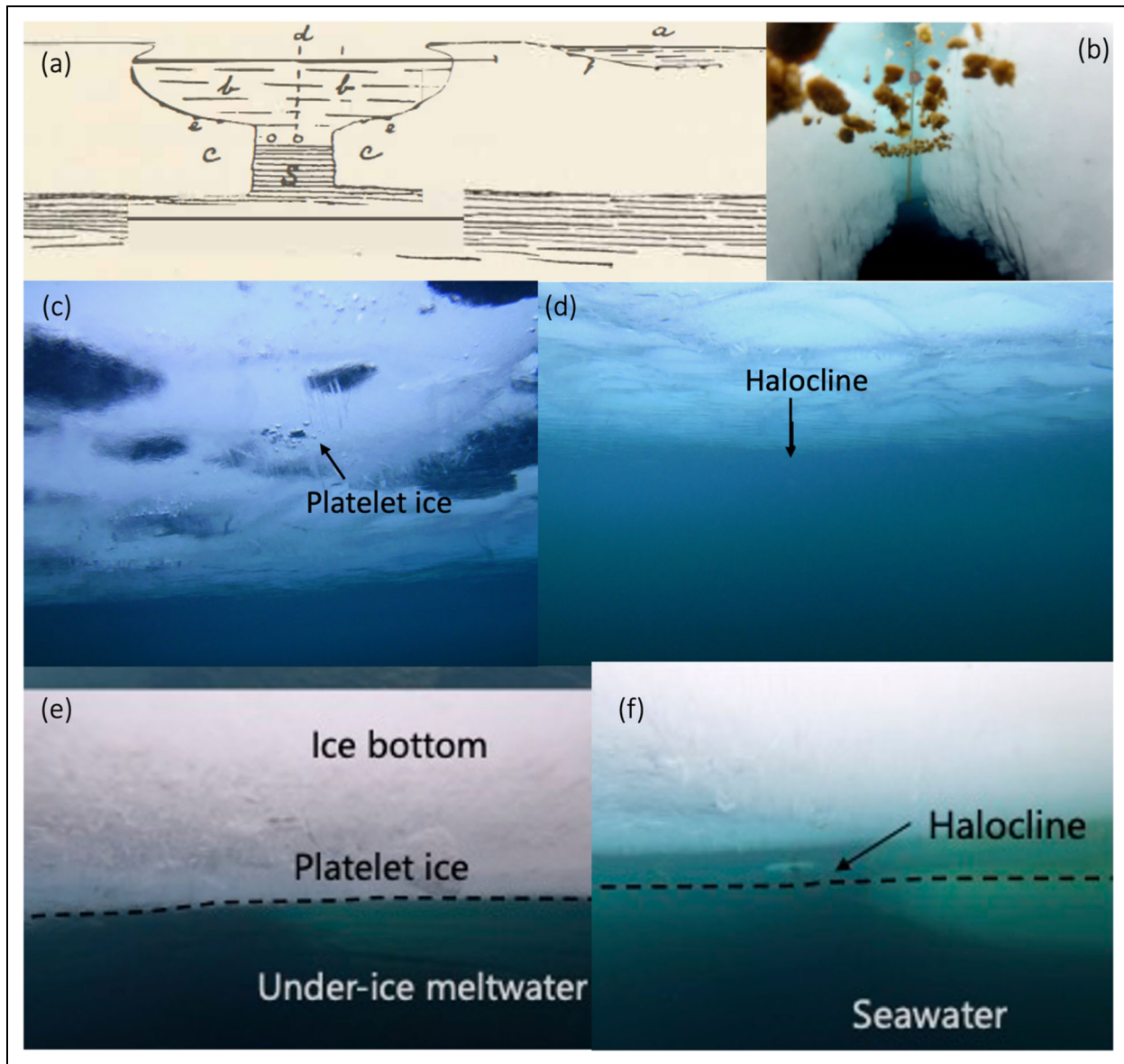
Figure 4. Visualizations of meltwater layers in cracks (a, b) and under ice (c–f). Meltwater layer interfaces in cracks can sometimes be delineated by the accumulation of algal aggregates at the density gradient between meltwater and underlying seawater, as (a) sketched by Nansen (1906) and (b) captured by GoPro (Assmy et al., 2013), both in the Central Arctic. Under-ice meltwater layers formed beneath landfast ice in the Canadian Arctic in spring 2008 (CFL-IPY project) had (c) thickness of 30–40 cm at initial observation, and (d) developed to 40–50 cm by June. (e, f) Imagery of a 10 cm thick under-ice meltwater layer from the MOSAiC expedition similarly showing the halocline and interface with platelet ice (dashed lines) growing within the meltwater layer (Smith et al., 2022b). Photos (c, d) courtesy of Haakon Hop.

The physical evolution of these thin meltwater layers underneath ice and in leads is determined by the balance of the stratification of freshwater, reduced momentum transfer, and mixing (e.g., Smith et al., 2022b). In particular, the stratification is determined by inputs of relatively fresh meltwater. While sea ice melt onset can begin as early as April, meltwater input from snow and sea ice in most of the Arctic begins in earnest in June (e.g., Perovich et al., 2021). Meltwater flux from melting snow and ice often continues through August and sometimes September, until freeze-up begins. A relatively small fraction of meltwater remains on the ice in melt ponds, while the majority drains into the ocean laterally or vertically, where it may accumulate in meltwater layers (Perovich et al., 2021). The majority of pond drainage occurs through horizontal transport on the ice to macroscopic flaws formed from enlarged brine channels (Polashenski et al., 2012). In situ precipitation in the summer is not well quantified, but likely plays a small role in the freshwater budget relative to the melting of sea ice and accumulated snow. Mixing of meltwater with the ocean mixed layer below is largely driven by wind and ice motion, which can result in intermittent or rapid changes in stratification and presence of meltwater layers (e.g., Richter-Menge et al., 2001;

Smith et al., 2022b; Nomura et al., 2023). Shear within the ocean from wind-driven ice drift may be more important than air-sea surface stress or waves for narrow leads under typically light summer winds. This turbulence can propagate upwards to erode the density gradient at the base of the meltwater layer. Under-ice and lead meltwater layers are thus hypothesized to be more common and more persistent in landfast ice regions, due to the generally negligible ice drift and thus lower mixing rates, which is supported by relatively abundant observations of meltwater layers in these locations (e.g., Perovich and Maykut, 1990; Ehn et al., 2011; Hop et al., 2011; Mundy et al., 2011; Elliot et al., 2015; Kirillov et al., 2018).

Various modeling efforts have contributed to our understanding of the general drivers of meltwater evolution in the Arctic upper ocean. A one-dimensional model applied to the upper ocean of the Nansen Basin (Rudels, 2016) suggested that the under-ice meltwater layer is self-sustaining by driving ice melt. The mixed-layer models typically simulate a thicker surface layer than the meltwater layers reported here (e.g., Rudels, 2016), but the implications and principles of evolution will largely be the same. Maintenance of meltwater layers is a balance between buoyancy, the addition of fresher meltwater and entrainment of water below by wind or shear-driven mixing. Buoyancy input from above is both positive, from melting of snow and sea ice, and negative, as a result of cooling and sea ice brine rejection during both ice formation and melt. Floe-scale simulations using the MIT General Circulation Model (MITGCM; Horvat et al., 2016) incorporate the horizontal mixing resulting from ocean eddies, and also simulate the evolution of a relatively fresh lens beneath sea ice during the melt season. In contrast to the definition of meltwater as salinity <20 g kg^{-1} used herein, the melt layers in the MITGCM study had relatively small differences from the ocean below with salinity of approximately 33 g kg^{-1}, but nonetheless had stable enough stratification to persist across large spatial scales.

During the MOSAiC expedition, continuous observations of thin meltwater layers from melt onset to freeze-up were limited by logistical constraints (Nicolaus et al., 2022), but the evolution was captured by a combination of continuous and focused observation periods during July (Leg 4) and September (Leg 5; **Figure 5**). Following the short-lived melt onset and pond formation in late May (CJ Cox et al., personal communication, 16/02/2023; Webster et al., 2022) the formation of melt ponds began in earnest in mid-June. Meltwater layers in leads and under ice likely began forming days to weeks after the first visual indications of meltwater layers in leads observed on July 1. Under-ice meltwater was indicated by the presence of a false bottom at an oceanographic observation site in late June (Schulz et al., 2022) and at the long-term first-year ice (FYI) coring site on July 6 (Salganik et al., 2023). The anomalously warm conditions during July and August possibly contributed to larger meltwater fluxes than might be expected in earlier years in the climatological record (Rinke et al., 2021).

We summarize the evolution of the meltwater layer, during Legs 4 and 5 of the MOSAiC expedition, in the three primary sinks as observed by a variety of platforms: leads (in purple), melt ponds (in blue), and under-ice layers (in green; **Figure 5**). The average meltwater layer thickness is defined here as the depth relative to the relevant air-water or ice-water interface at which the maximum change in density occurs; the salinity is characterized using the average of all available measurements above this depth, which should have salinity <20 g/kg. This definition of meltwater layer thickness is distinct from the equivalent freshwater thickness, as used in other publications (i.e., Smith et al., 2022b), due to the requirement of a reference ocean salinity in the latter which may evolve spatially and temporally. Estimates of under-ice meltwater layer thickness come primarily from in situ profiling using a Yellow Springs Instruments (YSI) conductivity and temperature probe (Smith et al., 2022a), ice mass balance (IMB) buoys and ice coring (Salganik et al., 2023), and a microstructure probe (MSS; Schulz et al., 2022) where spatial variability in locations leads to some of the temporal variability. In addition, false bottoms were mapped spatially using multibeam sonar from ROV surveys, with the results suggesting under-ice spatial coverage of about 20% in mid-July (Salganik et al., 2023). Lead meltwater layer estimates come primarily from in situ profiling with YSI (Smith et al., 2022a), a Castaway CTD (Smith et al., 2022a), Fishing-Rod CTD (Karam et al., 2023), and a VMP "upriser" (Fer et al., 2022b). Melt pond depths are averages from repeated mass balance transect measurements which had slightly lower pond coverage than the broader area and did not include the deepest ponds in the vicinity (Webster et al., 2022). Melt pond salinities on select dates were obtained from a combination of isotope samples (Lange et al., 2022) and profiles using a Rinke CTD. Due to variability in measurement type, location, and interval, results are not often directly comparable. Instruments were calibrated individually, as described in the appendix (Text S1), but no intercalibration was completed. We expect the lack of intercalibration to have little impact on the results presented here given the definition of meltwater layer thickness used. Combining these diverse datasets gives us insight into key features of the temporal evolution.

Following the initial formation and observation of meltwater layers in leads and under ice at the beginning of July, the thickness initially increased before gradually declining (**Figure 5**). Salinities of meltwater layers were generally lowest in the middle of the melt season when meltwater inputs were highest, gradually increasing over time as a result of mixing and entrainment of ocean water from below and release of brine from the ice above (Salganik et al., 2023). Example profiles of lead meltwater layers on three dates in July (**Figure 6a** and **b**) demonstrate the general trend towards a thinner meltwater layer, with gradual decrease in the strength of stratification at the halocline. Melt ponds represented a relatively small but consistent meltwater reservoir throughout much of July. The thickness of lead meltwater layers correlated negatively with lead width as a result of conservation of volume (Nomura et al., 2023). The disappearance of meltwater layers in September was synchronous across
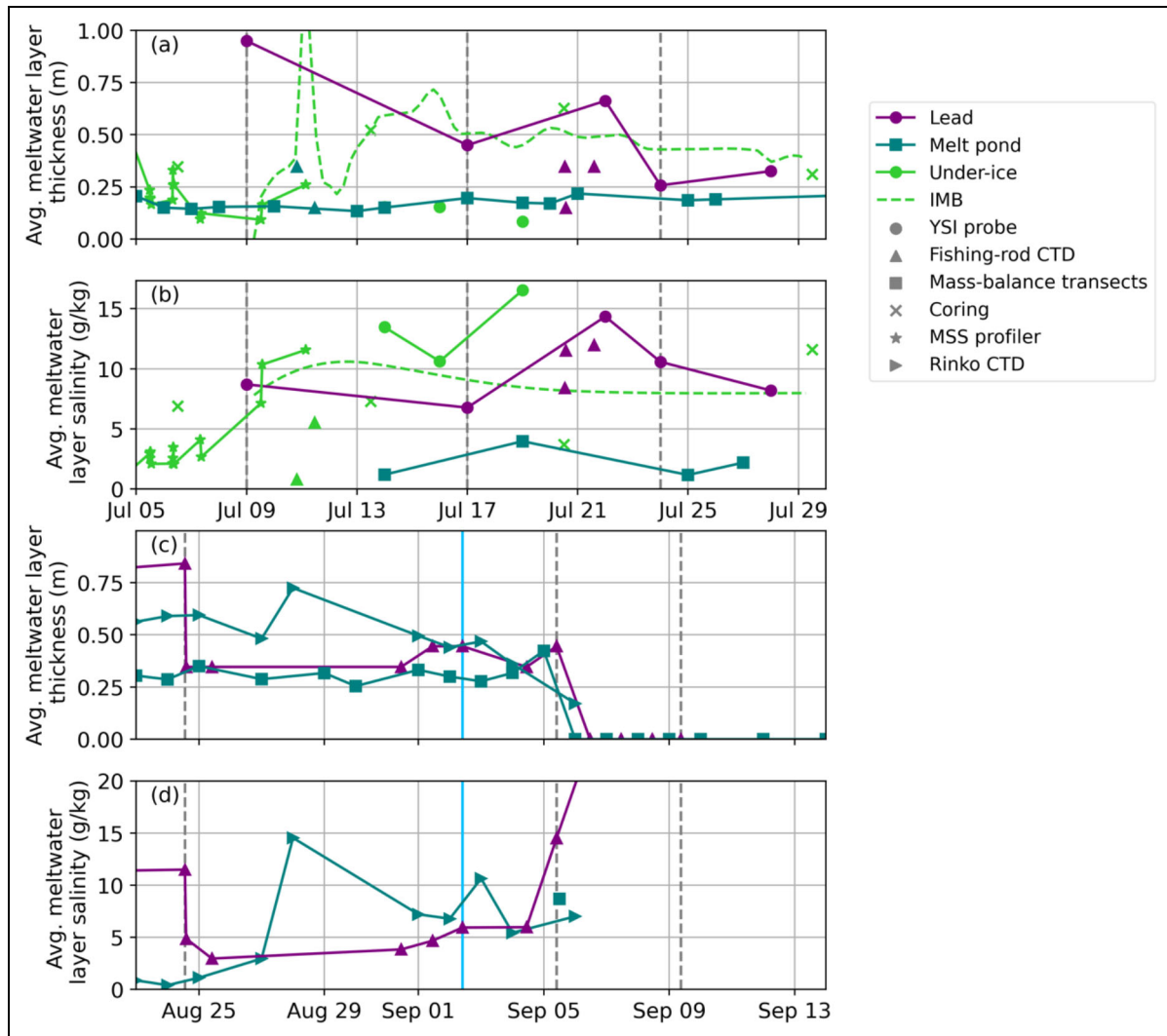
Figure 5. Temporal evolution of physical properties of meltwater layers from the MOSAiC expedition. Summary of the evolution of physical properties of meltwater layers during (a, b) melt season, July 2020, and (c, d) freeze-up, August–September 2020, including average estimated thickness (a, c) and absolute salinity (b, d) of meltwater layers in leads (purple), melt ponds (blue), and under ice (green). Meltwater layer thickness is defined here as the depth of maximum change in density. Symbols indicate different measurement platforms; circles, YSI probe (Smith et al., 2022a); triangles, fishing-rod CTD; squares, mass-balance transects (Webster et al., 2022; Itkin et al., 2023); x's, coring observations (Smith et al., 2022a; Salganik et al., 2023); stars, MSS profiler, where an approximate ice thickness of 2 m was assumed (Schulz et al., 2022); and right-facing triangles, Rinko CTD (Nomura et al., 2023). Dashed lines (a, b) are estimates from ice-mass balance (IMB) buoys using mass balance calculations (Salganik et al., 2023). Vertical grey dashed lines (c, d) correspond to dates of profiles in **Figure 6**. Vertical blue lines (c, d) indicate the first date of surface freezing on leads and ponds.

locations of leads and melt ponds (**Figure 5**). The differences in temporal and spatial factors between the time periods make comparisons difficult, as July observations occurred on a mix of multi-year ice (MYI) and first-year ice (FYI) near Fram Strait while August to September observations occurred on FYI near the North Pole. However, the observed dissolution of the meltwater layers under ice and in leads during both July and September correspond to the timing of anomalously high winds above the climatological 75th percentile (Rinke et al., 2021; Smith et al., 2022b). Example profiles from leads on three dates during August–September (**Figure 6c** and **d**) show the dissolution of stratification between September 5 and September 9 following a storm.

In future work, additional MOSAiC datasets will be compiled to estimate a complete budget of freshwater sources and sinks from melt into freeze-up. Quantifying the relative contribution of direct precipitation, snow melt, and sea ice melt to freshwater reservoirs and their fate on the ice, in meltwater layers, or in the ocean below will improve predictions of how these features vary spatially and are likely to evolve in the future.

6. Implications for the sea ice
The presence of a relatively fresh meltwater layer directly below the sea ice impacts how the sea ice evolves over the course of the melt season and how it interacts with the ocean below. Notably, the meltwater layer impacts the sea
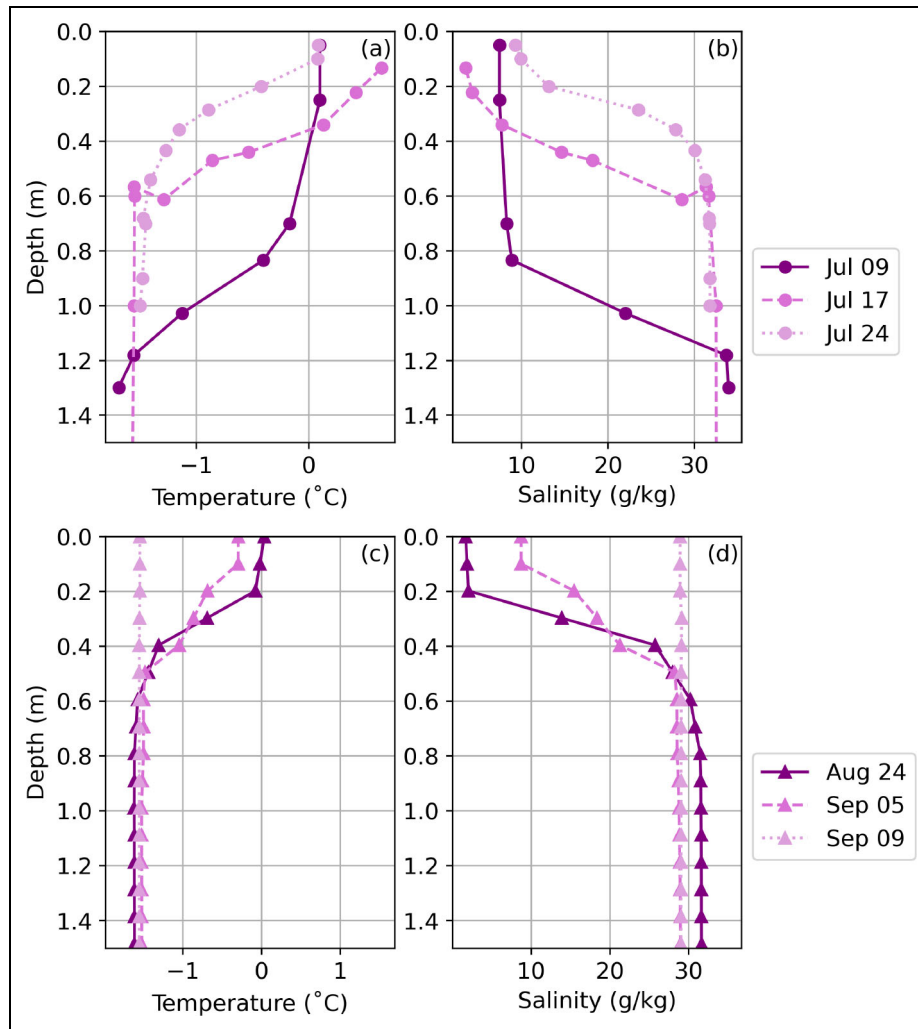
Figure 6. Example temperature and salinity profiles in leads with meltwater layers from the MOSAiC expedition. (a, b) Example melt season profiles from July 9, 17, and 24 of (a) temperature and (b) absolute salinity, measured by YSI probe. Dates correspond to vertical grey dashed lines in **Figure 5a** and **b**. (c, d) Example freeze-up season profiles from August 24, September 5, and September 9 of (c) temperature and (d) absolute salinity, measured using fishing-rod CTD. Dates correspond to vertical grey dashed lines in **Figure 5c** and **d**.

ice volume with implications for larger scale ice mass balance. The presence of the meltwater layer can slow bottom ablation (Smith, 2019), and even contribute to growth of additional ice as false bottoms through diffusion at the stratified interface. False bottom formation occurs due to the difference in freezing temperature of the fresher water above and saltier water below. Double diffusion processes at the boundary move heat from the fresher water to the saltwater, which causes supercooling and growth of platelet ice (Martin and Kauffman, 1974; Hoppmann et al., 2020). False bottom growth proceeds both laterally across the interface and also upwards—through the meltwater layer—with the continued diffusion of heat to the colder ocean below.

The contribution of the meltwater layer to false bottom formation is perhaps the best documented impact of meltwater layers in prior literature. Thickness estimates for false bottoms typically range from 0.02 m when initially growing to 0.2 m when fully developed (Untersteiner and Badgley, 1958; Hanson, 1965; Eicken, 1994). In various

sectors of the Arctic, they have been observed from 10% to 20% (Eicken, 1994; Perovich et al., 2003) of observation locations. False bottoms were observed to have about 20% spatial coverage from both under-ice multibeam surveys and dedicated drilling on the MOSAiC expedition (Smith et al., 2022b; Salganik et al., 2023), with average thickness of 0.08 m (Smith et al., 2022b). The temporal evolution of false bottom thickness observed from multiple sites is summarized in **Figure 7**, with photos from selected days showing the physical structure and appearance from below. False bottom thickness increased over the first half of July, to a maximum thickness of just over 0.1 m on average, then subsequently thinned and largely disappeared as mixing increased and warmer, saltier water reached the false bottom (Smith et al., 2022b; Salganik et al., 2023).

Process models have provided insights on the expected evolution and impact of false bottoms (Notz et al., 2003; Alexandrov and Nizovtseva, 2008; Smith, 2019). Notz et al. (2003) presented an analytical model describing the
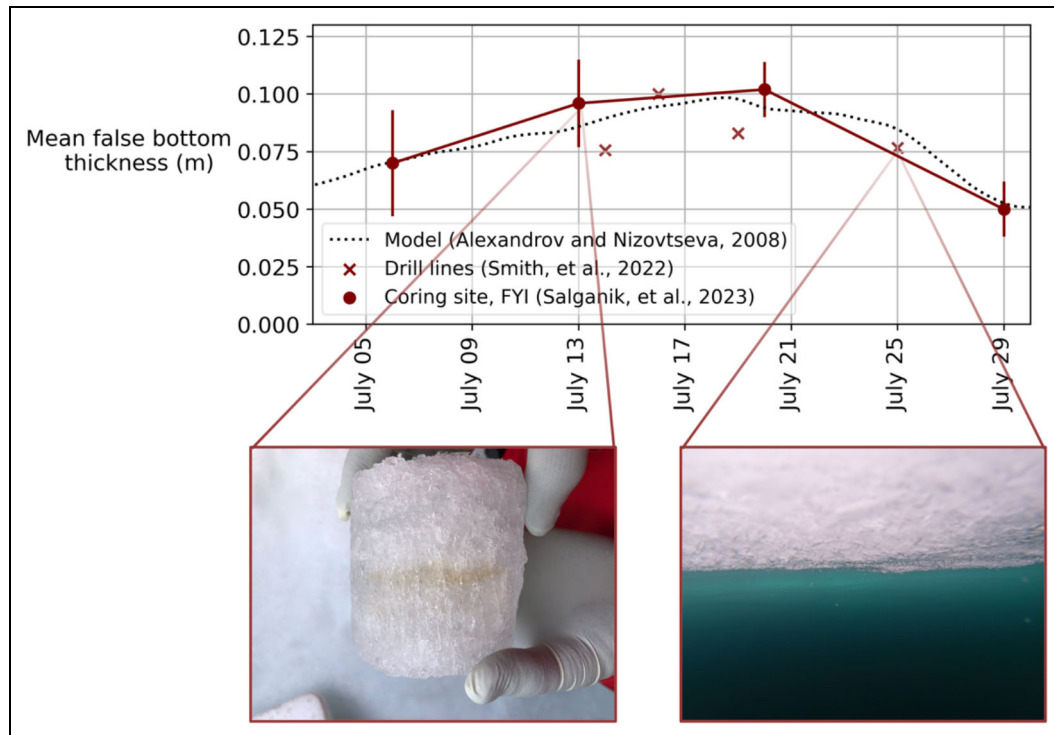
Figure 7. Temporal evolution of false bottom thickness during MOSAiC. Summary of temporal evolution of false bottom thickness, combining data from Smith et al. (2022a) and Salganik et al. (2023). Observations are compared with model results from Alexandrov and Nizovtseva (2008) using a drag coefficient of 6×10^{-4} and forced with snow and ice mass balance (IMB) observations (Salganik et al., 2023). Bottom left: Photo of false bottom collected at the MOSAiC first-year ice (FYI) coring site on July 13, 2020, with an approximate thickness of 0.09 m. The band of darker ice midway through the ice is likely indicative of a layer of ice algae (Photo credit: Allison Fong). Right: Photo still from GoPro video of false bottom observed from below near the FYI coring site IMB buoy on July 25, 2020. Videos available in Smith et al. (2022a).

formation by diffusion of heat and salt, which was able to capture features of observed evolution in the Arctic. False bottom processes were similarly modeled in one-dimension by Alexandrov and Nizovtseva (2008; **Figure 7**). Modeling by Smith (2019) incorporated the sea ice slab above and horizontal aspects of growth. This latter model suggested significant local impacts on sea ice mass balance, where ice with false bottoms would be 1%–8% thicker than ice without. Application of the Notz et al. (2003) false bottom model to MOSAiC observations captured aspects of growth but not all of the subsequent melt (Smith et al., 2022b; Salganik et al., 2023), while the model from Alexandrov and Nizovtseva (2008) compares well with MOSAiC coring site observations in **Figure 7**. Although this work and other evidence (e.g., Eicken, 1994) suggest the impact of widespread false bottoms on regional sea ice mass balance, parameterizations have not yet been developed for the basin scale. In the absence of a sufficient parameterization for large-scale application, Tsamados et al. (2015) used a simple adjustment to the heat transfer coefficient based on surface melt pond concentration to account for the formation of false bottoms. However, there is a lack of data quantifying the relationship of false bottoms with surface melt ponds and their contribution to the overall mass balance. Refinement of our understanding of the controls on meltwater layer

evolution is needed to improve modeling of false bottoms such that modeling can be applied in the future on the large scale.

Over the same time period as false bottom formation on the MOSAiC expedition, the conductive heat transfer associated with false bottom presence was observed to oppose the ocean heat flux and subsequently slow sea ice bottom melt (Salganik et al., 2023). In neighboring areas that started with the same average ice thickness, ice with false bottoms was 7%–8% thicker than ice without false bottoms, in line with the range from prior model estimates (Smith, 2019). Conversely, the stratified meltwater layer has also been proposed to accumulate heat (Langleben, 1966; Granskog et al., 2015), which alternatively could lead to an increase in bottom ablation. Such heat accumulation may be partially due directly to solar heating through the ice, but is more likely a result of drainage of warmed surface meltwater (Kirillov et al., 2018). Whether this meltwater layer ultimately increases or decreases bottom ablation of the overlying ice is a function of whether the driving factor in basal melt is local solar warming, which can lead to increased melt, or heat in the mixed layer, which can become isolated from the ice bottom. While observations during MOSAiC suggest that the latter dominates, at least in the presence of false bottoms, dominant process may vary under different

conditions, such as below thin ice. Meltwater infiltration additionally has an important and concentrated impact on the mass balance of ridges, where re-freezing of the relatively fresh meltwater can result in rapid ridge keel consolidation in the melting season (Marchenko, 2022; Lange at al., 2023). Such consolidation effectively increases the sea ice volume and slows subsequent ridge keel melt.

The infiltration of this relatively fresh layer can lead to physical changes in the sea ice above through desalinization. During the melt season, sea ice with underlying meltwater layers often exhibits reduced salinity near the bottom. Eicken (1994) observed differences in bottom salinity of level ice with and without an underlying meltwater layer of practical salinity 0.4–0.7 vs. 3.1, respectively, indicating desalination by meltwater flushing. Polashenski et al. (2015) observed low $\delta^{18}O$ and salinities at the top and bottom of ice cores in the Beaufort Sea, indicative of the infiltration and re-freezing of meltwater. During MOSAiC, FYI in the presence of an under-ice meltwater layer decreased in bulk salinity from 4.4 to 5.3 in winter and spring to 1.1 by the end of July (Salganik et al., 2023), which is half of that commonly observed for Arctic FYI with similar thickness during the melt season (Wang et al., 2020). Salganik et al. (2023) suggested that in the presence of a false bottom, the salinity of the (trapped) meltwater layer can increase due to brine flushing from the ice above.

The presence of meltwater layers in leads during the summer typically results in enhanced lateral melting of sea ice, as was observed during the SHEBA expedition (Richter-Menge et al., 2001; Perovich et al., 2003) and an experiment in Mould Bay (Perovich and Maykut, 1990). This melting can enhance the formation of undercut ice or ice shelves at the floe edge, as commonly observed and shown in Perovich et al. (2003). The strong stratification of thin meltwater layers can allow solar heat to build up in these layers depending on the levels of turbidity and absorption. For example, Perovich and Maykut (1990) noted that increased turbidity in lead meltwater layers, presumably associated with an algal bloom, led to "nearly complete absorption" of solar energy by around 10-m subsurface. During their study, similar structure was not observed in more mobile ice at a nearby site, indicating the importance of quiescence in formation of meltwater layers and subsequent accumulation of heat. When wind or ice drift causes mixing through the meltwater layer, its heat can then be released rapidly, resulting in large increases in both lateral and bottom melt. In Mould Bay, heat buildup in the layer itself was minimal as there was sufficient mixing from wind to lead directly to lateral melting, with a total of 1.5 m lateral melt over the course of the experiment surrounding the initially 3-m-wide lead (Perovich and Maykut, 1990). Due to the role that lateral melting plays in forming open water and decreasing local albedo, the basin-wide sea ice pack is very sensitive to the temperature difference in leads driving this melt (e.g., Smith et al., 2022c). The lateral melt rate abutting leads with thin meltwater layers and evolving heat content will be targeted in future MOSAiC studies to understand the role of atmospheric and oceanic factors on the resulting melt.

Following the summer season, the persistence of fresher meltwater in melt ponds and in the upper ocean into fall and winter can impact sea ice freeze-up and subsequent evolution. During fall at MOSAiC, meltwater freshening of the upper ocean resulted in increased freezing temperature, which terminated basal melting and preconditioned freeze-up (Kawaguchi et al., 2022). Meltwater layers in leads similarly may result in earlier freezing at these locations because fresher water freezes at a higher temperature than more saline water (Nomura et al., 2023), and relatively fresh ice layers in leads and under-ice may impede gas exchange (Section 9). Refrozen leads and melt ponds from the preceding summer are visible in winter as warm surface temperature anomalies (Thielke et al., 2022), which may suggest an extended impact on the annual cycle depending on the growth history.

7. Implications for the ocean

The large salinity difference between the meltwater layers and the underlying ocean water results in stratification approximately two orders of magnitude stronger than in the halocline underlying the mixed layer (**Figure 8**; Richter-Menge et al., 2001; Golovin and Ivanov, 2015; Perovich et al., 2021). However, spatial variability in ice conditions, melt rates, and turbulent mixing can set up substantial lateral gradients on scales on the order of 1 km (Timmermans and Winsor, 2013). The meltwater does not necessarily remain stationary, and so distinguishing between a newly formed meltwater layer and an already relatively fresh surface mixed layer is sometimes challenging. For example, observations from the Pacific sector of the Arctic have shown that the evolution of meltwater layers might be impacted by advection and horizontal stirring (Peralta-Ferriz and Woodgate, 2015). In the Atlantic sector of the Amundsen and Makarov Basins, observations have shown meltwater layers embedded within relatively low salinity (approximately 32.6) upper ocean layers (Rudels, 2016). Both the size of ice floes and the presence of ocean eddies likely play a role in the lateral redistribution of meltwater (Horvat et al., 2016). We can also expect that meltwater layers will reduce mixed layer instabilities by reducing mixed layer depth H and increasing stratification N, as they occur on their Rossby deformation radius, NH/f, where f is the Coriolis parameter.

Situated directly at the interface between atmosphere, sea ice, and the underlying ocean, the presence of these meltwater layers influences the vertical transfer of momentum, heat, and salt (Vihma et al., 2014). A meltwater layer stabilizes the ocean boundary layer under ice (the upper few meters) and increases the potential energy, thereby requiring more energy from turbulence to move freshwater downward against the buoyancy force. The maximum turbulent mixing scale is reduced, with impacts on the ice-ocean drag (McPhee et al., 1987; Kudryavtsev and Soloviev, 1990). The frictional coupling between the ice and ocean, hence drag, is reduced, making the mixed layer more "slippery." Furthermore, the turning angle of
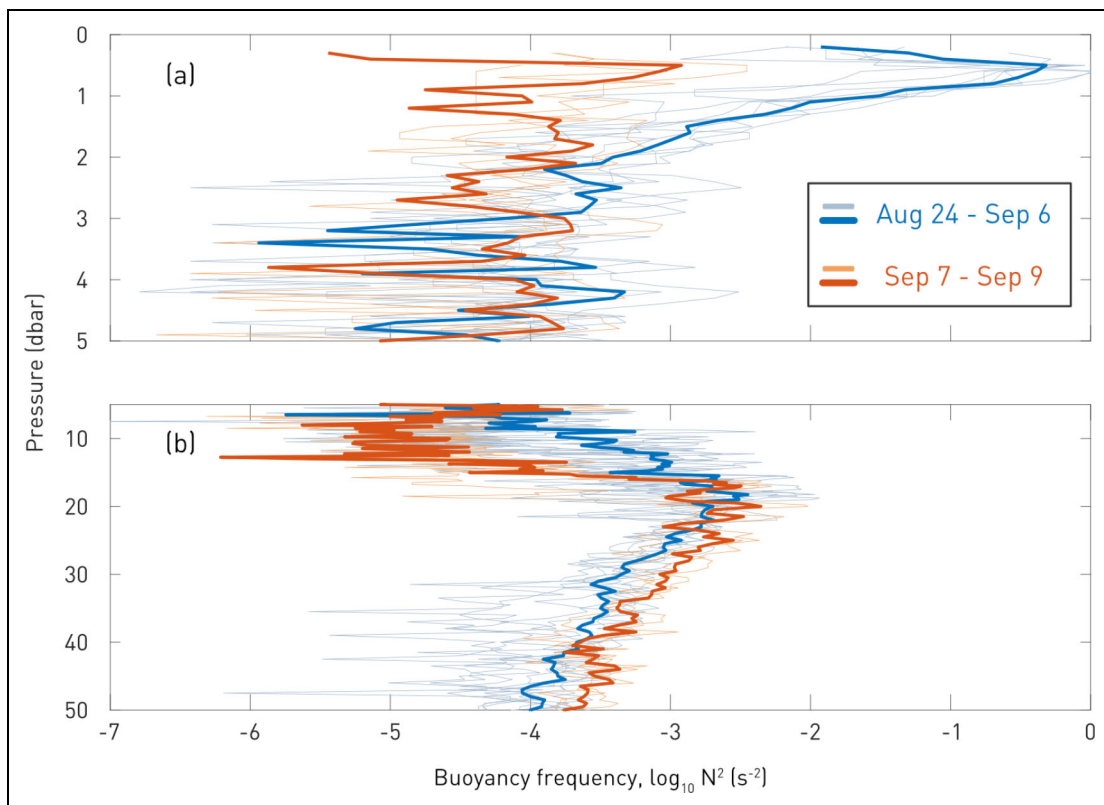
Figure 8. Buoyancy frequency N^2 of the near-surface ocean before and after a storm. Profiles from before the storm observed during MOSAiC expedition Leg 5 (August 24 to September 6; blue) show a meltwater layer in the upper meter, which is absent following mixing from storm (September 7–9; red). The stratification of the meltwater layer in (a) is approximately 2 orders of magnitude stronger than the mixed layer halocline in (b). Thick lines show the mean profile over the given time period, and thin lines show individual profiles. The profiles were collected using a hand-held fishing-rod CTD from the ice.

the Ekman layer is increased. During the N-ICE2015 campaign north of Svalbard, meltwater in the upper ocean was observed to reduce the upper ocean turbulent mixing (Randelhoff et al., 2017). While the meltwater layers they observed were an order-of-magnitude greater in thickness and salinity than those of primary interest here, the physical process likely extends to the smaller scale and higher stratification scenarios.

Similar to sea ice (Martin et al., 2014), the meltwater layer can act as a lid on the ocean, reducing the transfer of momentum from the atmosphere. Specifically, the turbulent ocean boundary layer acts as a sink for wind energy, such that the fraction of energy redistributed to the deeper layers in the water column is reduced. As a result, meltwater layers may alter the near-inertial energy propagating downwards in the Arctic Ocean (Morison et al., 1985). They can also interact with sea ice to generate ice-ocean drag in these layers mediated by internal waves (McPhee and Kantha, 1989). During the MOSAiC expedition, an upward-rising VMP was used to understand near-surface turbulence and the effect of melting on the turbulent boundary layer (Fer et al., 2022a; Fer et al., 2022b). The disruption of the under-ice meltwater layer in mid-to-late July (Section 5) has implications for the upper-ocean structure and turbulent transport. The effect of this evolution on the momentum transfer between the surface

and the mixed layer is still an open question worthy of future observations and studies.

Several profiles from the ascending VMP during MOSAiC showed indications of a thin meltwater layer (thin lines in **Figure 9**). Contrasting average dissipation profiles in the presence and absence of a meltwater layer suggest that the turbulence is suppressed by 1–2 orders of magnitude in the upper meters of the water column. This suppression is not limited to the meltwater layer (<1 m), but extends downward at least 3 m. **Figure 9** only illustrates the effect of a meltwater layer on a relatively nonturbulent environment—high turbulence, for example during strong wind events, may in turn mix and erode the meltwater layer, as observed during MOSAiC (e.g., **Figure 5**; Nomura et al., 2023).

Meltwater retention near or at the surface also affects the salt and heat balance of the mixed layer below (Kadko, 2000). The presence of these layers means that a considerable reservoir of relatively fresh and warm water is not being mixed down (e.g., **Figure 6**). Additionally, during MOSAiC, the presence of false bottoms was found to capture brine release from sea ice, as under-ice meltwater was twice as salty as the pre-melt sea ice (Salganik et al., 2023). The complete melt of false bottoms can also lead to meltwater layers rapidly mixing with the underlying ocean, resulting in a strong freshening of the upper ocean (Smith,
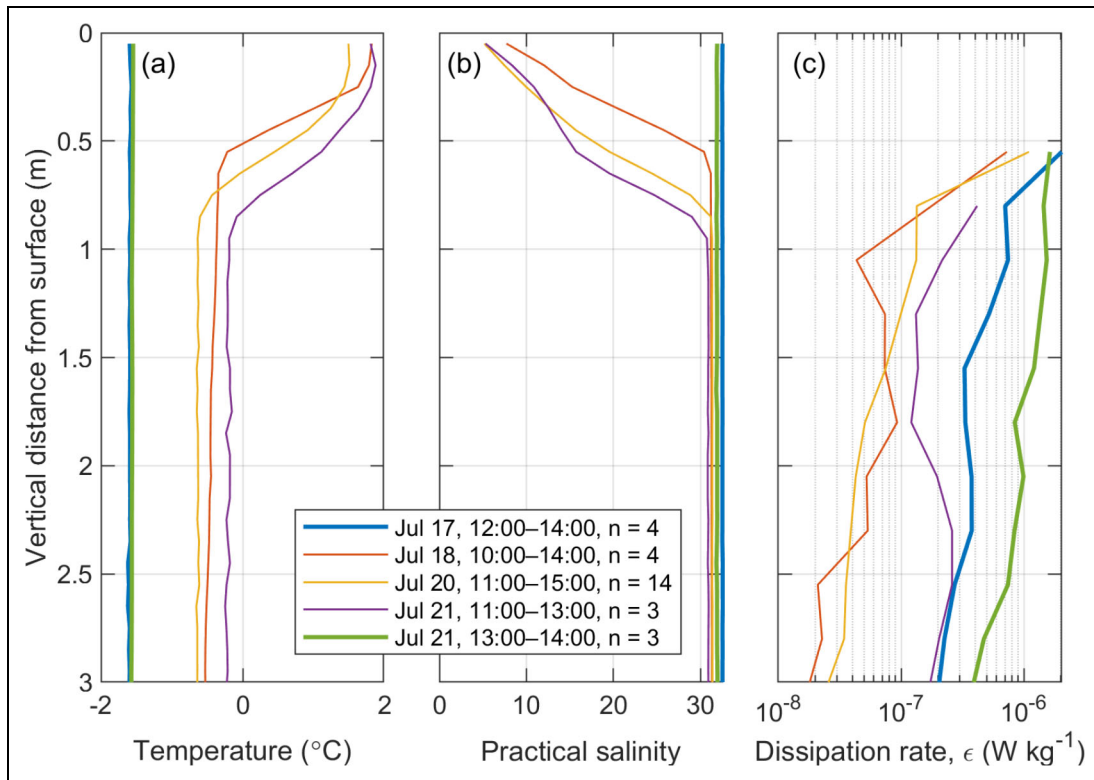
Figure 9. Profiles from the vertical microstructure profiler (VMP) in the presence and absence of a meltwater layer. All profiles were collected in the upper 3 m of leads: (a) temperature, (b) approximate practical salinity, and (c) the dissipation rate, ε. For the profiles collected on July 17 and in the afternoon of July 21 (thick lines) the profiler surfaced under pack ice or close to the ice edge where no meltwater layer was detected. Legend indicates the day, approximate start and end hour of the profiling, and the number of profiles averaged. Methods are described in Text S2; a more detailed analysis is not given due to large uncertainties in the profiles which had not targeted the meltwater layer specifically.

2019). Meltwater layers typically result in a faster temperature increase at the surface as freshening at the surface reduces downward distribution of heat into underlying mixed layers (Rudels, 2012; 2016). In this manner, the presence of meltwater layers impacts the partitioning of solar heat between ice melt and warming of the water column, resulting in more heat being retained in the ocean below (e.g., Hudson et al., 2013; Granskog et al., 2015). Idealized simulations performed by Skyllingstad et al. (2005) and observations from Randelhoff et al. (2014) show that the presence of a meltwater layer impedes downward mixing of solar heat and upward mixing of colder or warmer water. At the same time, increased turbidity in meltwater layers, such as from algal blooms, increases the absorption and solar heating of the upper few meters (Perovich and Maykut, 1990; Taskjelle et al., 2017). Indeed, observations have shown notable heat accumulated in meltwater layers in leads (Perovich and Maykut, 1990; Richter-Menge et al., 2001) and cracks (Nansen, 1902). Similarly, Langleben (1966) documented an increase in the temperature of under-ice meltwater layers associated with solar input by approximately 1°C over the melt season, which can dramatically impact the icescape (Section 6). Solar heating results in a small increase in the stability of the stratification.

However, the thermal contribution to stratification is small compared to the haline contribution, especially at low temperatures (Sigman et al., 2004).

Meltwater layers can have a notable impact on upper ocean optics (Belanger et al., 2013; Granskog et al., 2015). Ehn et al. (2011) show a peak in absorption spectra and increased scattering in turbid under-ice meltwater layers, while Pegau (2002), Belanger et al. (2013), and Granskog et al. (2015) observed that sea ice meltwater itself can act as a source of scattering particles to the under-ice and lead meltwater layers. In such cases, increased scattering at the very surface can reduce radiation in the ocean below (Belanger et al., 2013) while increasing light exposure of any organisms trapped in the meltwater layer (Section 8). The presence of such layers could cause localized impacts on satellite retrievals of chlorophyll and other relevant variables through the influence on upper ocean optics and light attenuation (Belanger et al., 2013). However, the net effect of thin meltwater layers in the ocean below depends highly on their effects on both absorption and scattering and how these properties differ from the underlying seawater (Granskog et al., 2015). High-biomass layers, including algal aggregates, are often seen within the meltwater layer or accumulated at the meltwater-seawater interface (Section 8), but the net effect on the light field is not yet known.
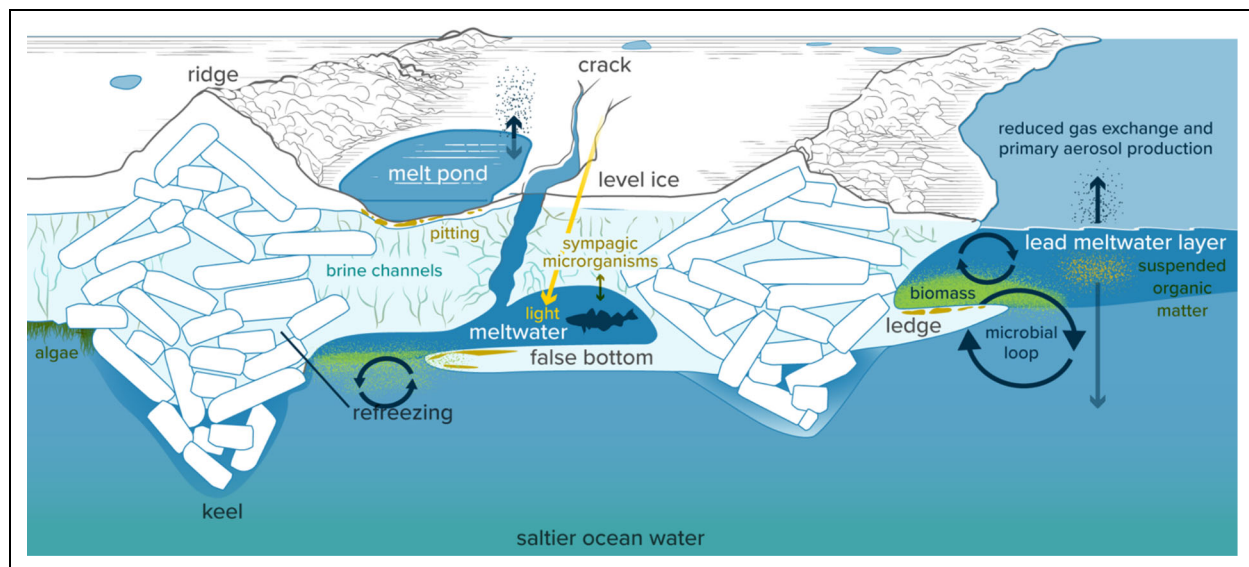
Figure 10. Schematic of key ecological, biogeochemical, and atmospheric processes associated with thin meltwater layers. Circular arrows represent microbial loops. These processes are discussed in Sections 8–10 in relation to meltwater in melt ponds, leads, and under the sea ice. Figure by Madison Smith and Natalie Renier © Woods Hole Oceanographic Institution.

8. Organism diversity and community structure within and below the meltwater layer

Melt ponds and meltwater layers in leads and underneath sea ice create ephemeral ecological habitats with microbial communities that are distinct from sea ice and bulk seawater (e.g., **Figure 10**). Distinct niches are expected to develop as the melting season progresses, causing shifts in community composition with cascading impacts on ecosystem functionality, productivity, and food quality for higher trophic levels. Past work on microbial communities of brackish and freshwater habitats in the Arctic Ocean has provided insights into how habitat transitions shape the diversity and activity of these communities (Brinkmeyer et al., 2004; Assmy et al., 2013; Fernández-Méndez et al., 2016; Xu et al., 2020; Hancke et al., 2022). However, detailed data on the evolution of these habitats, along with information on the seasonal cycle of sea ice and seawater properties, are required to understand how they recruit their microbiomes and how dispersal contributes to the development of these ephemeral ecosystems.

Melting sea ice and snow significantly shape the microbial assemblages in meltwater habitats, in part through stress responses and physiological acclimation to their shifting environmental conditions (Mundy et al., 2011; Hatam et al., 2016; Rapp et al., 2021; **Figure 11**). Microbes inhabiting sea ice are well adapted to the hypersaline conditions in sea ice brine pockets (Junge et al., 2004; Mock et al., 2017; Rapp et al., 2021). The transition into a hyposaline environment upon melt, or meltwater flushing of basal sea ice (Salganik et al., 2023; Section 6), causes osmotic, ionic, and oxidative stress, resulting in cell loss and impairing various cellular functions, such as photosynthetic activity, membrane integrity, and growth rates (Kirst, 1989; Arrigo and Sullivan, 1992; Ralph et al., 2007; Antoni et al., 2020; Chamberlain et al., 2022). In bacterial communities, fluctuations in salinity appear to be more stressful than temperature extremes, with survival depending largely on solutes for osmoprotection (Ewert and Deming, 2014). Additional stressors in thin meltwater layers, such as high irradiances and low macronutrient concentrations, can augment stress for some organisms. For example, hyposalinity and nutrient limitation increase susceptibility of microalgae to high light stress, enhancing the potential for photodamage and oxidative stress (Ralph et al., 2005; Petrou et al., 2011) and decreasing capacity for biomass production (Behrenfeld et al., 2008).

Certain species can acclimatize to the rapidly changing environmental conditions during ice melt on a timescale of days to weeks (Grant and Horner, 1976; Juhl and Krembs, 2010), by changing fatty acid composition, concentrations of osmoregulatory compounds, or light-harvesting characteristics of the photosynthetic apparatus (Kirst, 1989; Hernando et al., 2018; Bowman et al., 2021). Autotrophic flagellates generally seem to be better able to acclimate to meltwater habitats than diatoms, often dominating algal communities in persistent low-salinity meltwater layers and potentially initiating under-ice meltwater blooms (Gradinger, 1996; Mundy et al., 2011). However, a spectrum also exists within the diatom group, where some species, e.g., *Fragilariopsis, Chaetoceros, Attheya*, are more resilient to low salinity than others, e.g., *Nitzschia* and *Cylindrotheca* (Allen, 1971; Zhang et al., 1999; Ryan et al., 2004; Hernando et al., 2015; Antoni et al., 2020).

At the interface between meltwater and seawater, another unique algae community, originally termed "halocline flora," can establish (Apollonio, 1980; 1985; Apollonio and Matrai, 2011; McLaren, 2011). The halocline community typically occurs within the upper 2 m of the water column, and can persist for up to 8 weeks at consistently high biomass levels of 1–2 mg chlorophyll *a* (Chl *a*) m^{-3} (Bursa, 1963). Halocline communities have been
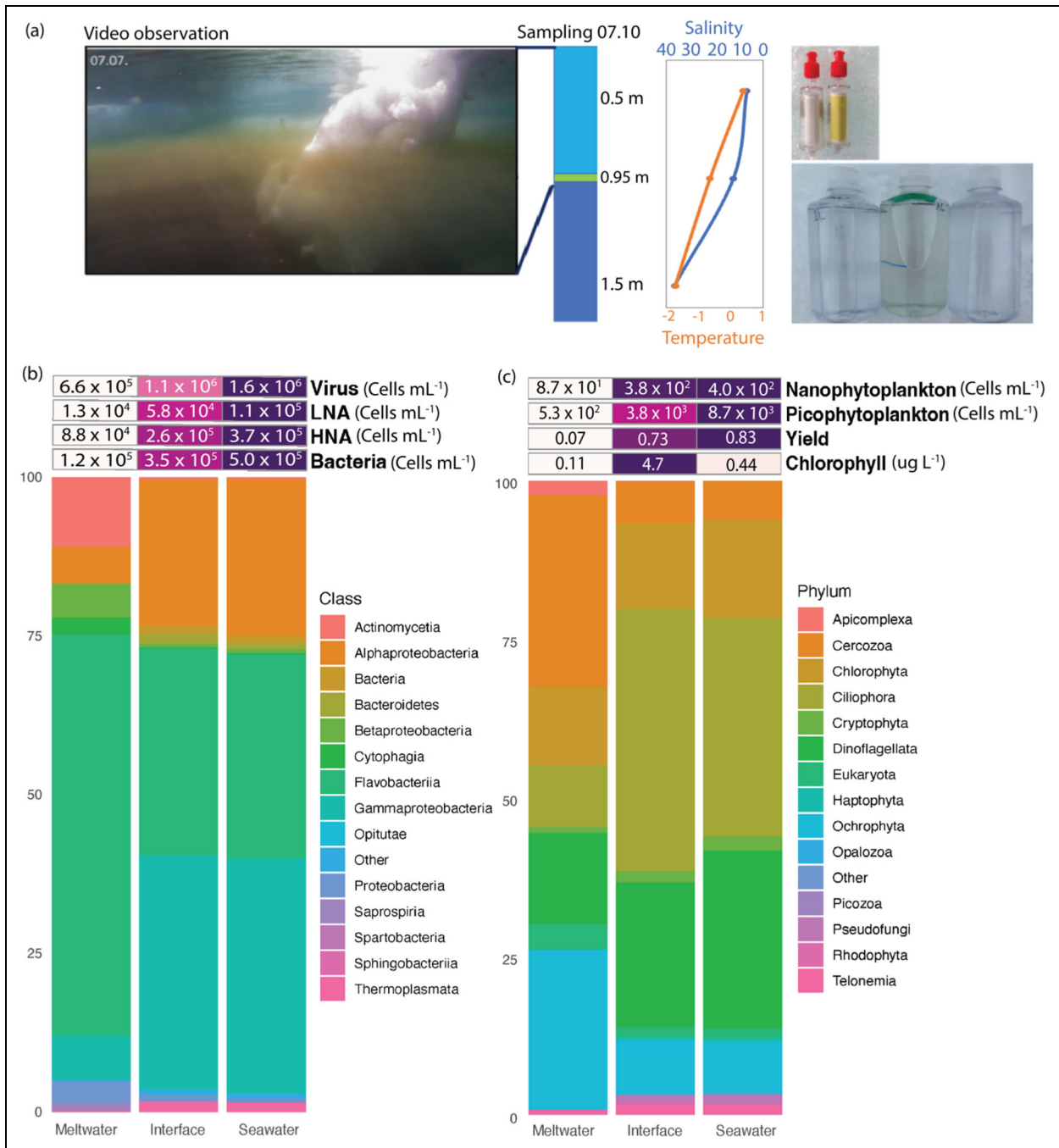
Figure 11. Example microbial community structure and ecophysiology from a stratified lead meltwater layer. Images and data are from a lead meltwater layer sampled in July during the MOSAiC expedition. (a) Image on the left shows a relatively thin (approximately 1–2 cm), high-biomass layer located at the interface between meltwater and seawater observed on July 7 (Muilwijk et al., 2022). Temperature (°C) and salinity values for these targeted layers were measured using a YSI probe prior to water sampling on July 10 (Section 5; Smith et al., 2022a). Targeted sampling of this layer took place on July 10 and 11, with the images on the right showcasing differences in water pigmentation from each layer (filtered biomass from left to right: meltwater, interface; bottles from left to right: meltwater, interface, underlying seawater). (b) The total abundances of prokaryotic cells ("bacteria," by flow cytometry), high nucleic acid (HNA)-containing bacteria, low nucleic acid (LNA)-containing bacteria, and viral particles in the meltwater layer, interface, and underlying seawater, with the relative abundances of bacterial and archaeal community members color-coded by class. (c) The total cell abundances of picophytoplankton and nanophytoplankton, chlorophyll concentration, and effective quantum yield in the meltwater layer, interface, and underlying seawater, with the relative abundances of eukaryotic community members color-coded by phylum. Data information and methods used are available in supplemental material (Text S3).

observed to be dominated by phototrophic flagellates of the Chlorophyceae and Chrysophyceae classes (Bursa, 1963). Distinctive bacterial communities have also been observed between the surface and subsurface of meltwater-rich environments (Zeng et al., 2013). These high-biomass layers likely resemble under-ice blooms, impacting the optical (Section 7) and thermal (Section 6) properties of the ice above and ocean surface layer below by increasing absorption and light scattering within visible wavebands (Ehn et al., 2011) with a positive feedback on primary productivity by ice-associated and under-ice algae (Pavlov et al., 2017). Further, increased scattering in meltwater-associated biomass layers (Section 7) leads to high scalar irradiance, and thus spatially and temporally variable conditions of high light stress. This variability is reflective of variation in light transmission, photosynthetically available radiation and UV exposure, and therefore indirectly depends on variability in snow cover, sea ice thickness, absorbers and scatterers, and stratification strength in the under-ice environment (Uusikivi et al., 2010; Alou-Font et al., 2013; Elliot et al., 2015; Matthes et al., 2020).

Regardless, organisms trapped in shallow near-surface meltwater layers (whether in leads or below ice) are relatively more exposed to high light conditions than those in a deeper mixed layer. Increased exposure to UV radiation necessitates the production of photoprotectants, such as mycosporine-like amino acids and carotenoid pigments, as observed for algae in sea ice (Uusikivi et al., 2010; Alou-Font et al., 2013), thin lead ice (Kauko et al., 2017), melt ponds (Mundy et al., 2011; Ha et al., 2014), and under-ice meltwater (Mundy et al., 2011; Elliot et al., 2015). Although photoprotectants help algae survive near the surface within sea ice and meltwater, their production can compromise biomass growth even more than high light stress alone (Kauko et al., 2017). High light-low nutrient environments, such as the meltwater habitat, where the need for energy dissipation via carbon fixation is high but biomass buildup is limited by nutrients, may be characterized by organic matter with high C:N ratios and high levels of dissolved organic matter (Lewis et al., 2019). The latter, which includes cellular exudates, enhances aggregate formation and microbial activities (Thornton, 2014). Changes in both stoichiometry and microbial loop dynamics affect food quality for higher trophic levels as well as biogeochemical cycling.

During July–September of the MOSAiC Expedition (both drift tracks in **Figure 2**), the distribution of algae was visibly stratified across salinity gradients in the upper 2 m of the surface ocean, often with community assemblages in the under-ice or lead meltwater layer that were distinct from the underlying seawater. In early July, a halocline high-biomass layer was observed accumulating at the interface between the meltwater layer and underlying seawater, when the meltwater layer thickness was still increasing (**Figure 5**). This visibly dense biomass layer was estimated to be approximately 1–2 cm thick, based on video images and sampling attempts (**Figure 11a**), with a protist community composed primarily of previously described halocline biota: pico-eukaryotes such as

pelagophytes and dinoflagellates. For example, on July 11, this biomass-dense interface was high in Chl a, with an autotrophic community structure more similar (qualitatively) to that in the underlying seawater than in the overlying meltwater layer (**Figure 11c**). Both heterotrophic and autotrophic microorganisms were more abundant below the halocline, with lowest abundances measured in the meltwater layer, indicating that biomass in the meltwater layer was also low. Additionally, particles with high Chl a content (4.7 µg L^{-1}) along the interface were likely larger than 10–15 µm, which is roughly the size limit for flow cytometry. The bacterial cells present in the meltwater layer had higher proportions of Gammaproteobacteria and Flavobacteria than the underlying seawater. These taxa are commonly enriched in sea ice and may have originated from that environment (Bowman, 2015). The melt layer also had a large proportion of Actinomycetia, or Actinobacteria, common to Arctic permafrost environments (Boetius et al., 2015), which may have originated from snow or sediment entrained in the MOSAiC ice floe (Krumpen et al., 2020). The eukaryotic community present in the meltwater layer was also enriched in taxa common in sea ice and thus similarly indicative of an originally ice-based community, supporting previous findings in related environments (Mundy et al., 2011).

Studies using high-throughput sequencing of phylogenetic marker and functional genes show that microbial communities of relatively fresh layers are largely distinct from sea ice and adjacent seawater only if the exchange is limited (Xu et al., 2020). For instance, melt ponds that are enclosed appear to be dominated by β-proteobacteria (Brinkmeyer et al., 2004) and more mixotrophic and heterotrophic microbial eukaryotes (Xu et al., 2020). However, as soon as meltwater habitats in leads and under-ice meltwater ponds are in closer exchange with nutrient-richer seawater, different microbial communities seem to thrive (Hancke et al., 2022). These communities often appear to be dominated by photosynthetic microbes, including the keystone diatom *Melosira arctica* (Hancke et al., 2022), which was observed in high biomass for ice-associated communities from July to September during MOSAiC.

Melosira arctica is a sympagic diatom that forms up to meter-long filaments. Cryoprotective and adhesive properties provided by extracellular mucus consisting of polymeric substances allow them to attach to the under-ice surface (Krembs et al., 2002; Abdullahi et al., 2006; Aslam et al., 2012). As the meltwater layer developed underneath the ice during July of MOSAiC, *Melosira arctica* strands were observed to detach from the under-ice surface (**Figure 12a**), followed by disintegration of the long filaments into smaller aggregates, many of which were bleached in appearance (**Figure 12b**). Previous studies have shown that sub-ice algal aggregates can account for up to 94% of local primary production (Fernández-Méndez et al., 2014) and associate the release of *Melosira arctica* from the sea ice with sea ice melt and subsequent sedimentation (Tremblay et al., 1989; Riebesell et al., 1991; Bauerfeind et al., 1997; Michel et al., 1997; Boetius et al., 2013), making *Melosira arctica* an important factor in the High Arctic
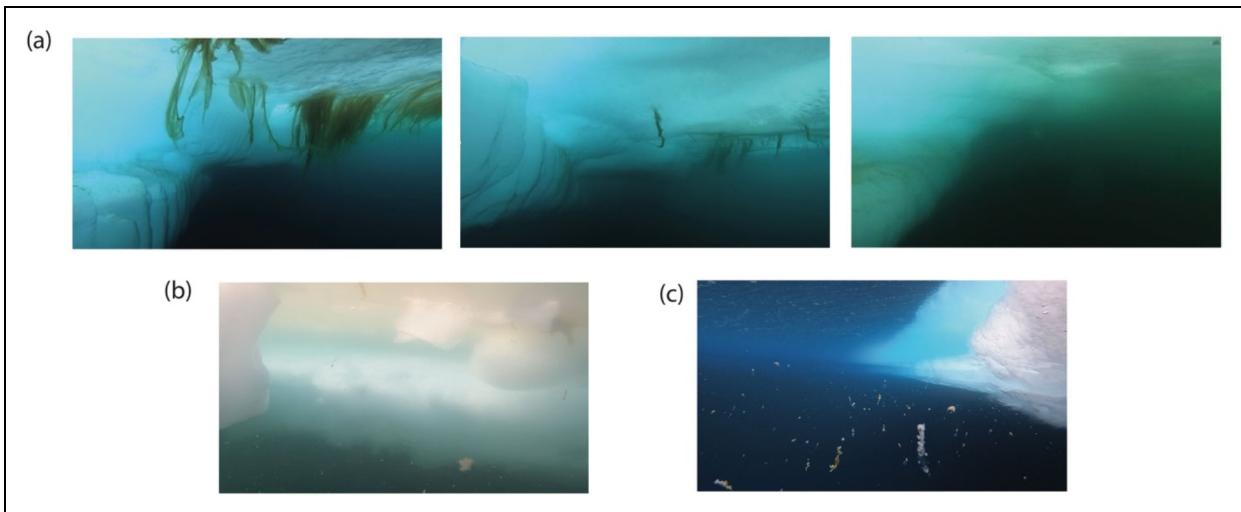
Figure 12. *Melosira arctica* progression and meltwater layer evolution. (a) Three images taken at the same spot, facing the same direction underneath a bore hole through first year sea ice. From left to right: June 28, 2020; July 5, 2020; July 19, 2020. The second image also shows platelet ice. (b) Image from beneath a lead surface with meltwater layer from July 22, 2020, taken from video footage. (c) Image from beneath a lead surface during the northern positioning of the Leg 5 drift track, with visible suspended algal aggregates taken from video footage. Original videos from which stills (b) and (c) were taken are available in the supplemental material (Videos S1–S3).
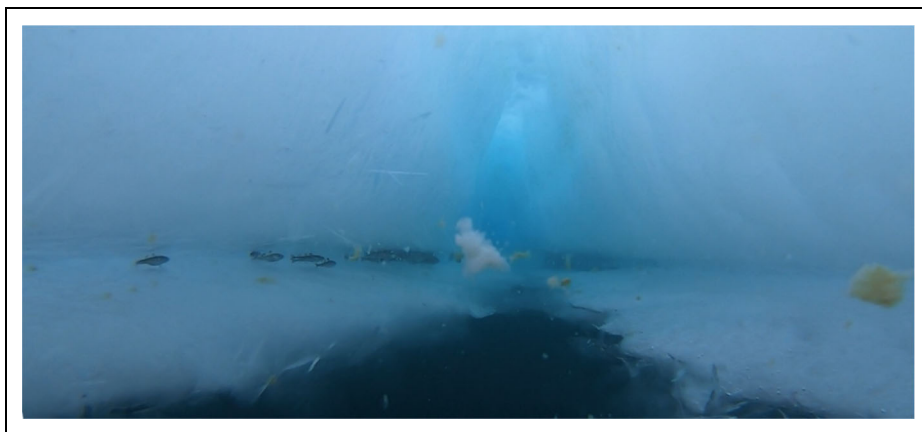

Figure 13. Polar cod using the void space between false bottom and pack ice as refuge. Photo was taken during a research cruise on RV *Polarstern* (PS131) in summer 2022. Also visible are brown and bleached algal aggregates.

biological carbon pump. The buoyancy of aggregates may be regulated by oxygen bubbles within the mucus that are formed during photosynthesis under favorable light conditions (Fernandéz-Mendéz et al., 2014). A working hypothesis is that the accumulation of cells at the meltwater-seawater interface is driven by 1) buoyancy of cells living underneath the meltwater layer that rise to the surface where light and nutrient availability allow these and other photoautotrophs to thrive (Hancke et al., 2022), and/or 2) the strong density gradient between meltwater and seawater acting as a barrier for continued upward (pelagic community) or downward (ice-associated community) movement of cells. This "entrapment" of cells leads to increased light exposure and stress, particularly in open leads where there is no snow/ice attenuation of UV radiation, resulting in reduced productivity and/or photodegradation of non-acclimated biomass (Alou-Font et al., 2013;

Elliott et al., 2015; Kauko et al., 2017). In meltwater layers observed later in the season and further north (August–September), biomass was no longer visibly enhanced at the meltwater halocline but suspended within the meltwater layer, with algal aggregates and bleached particulate organic matter potentially fueling secondary production and regeneration processes within the meltwater layer (**Figure 12c**). Similar drifting aggregates observed on other expeditions were dominated by pennate sea-ice diatoms within a mucous matrix, which can support high levels of local biological activity and zooplankton grazing (Assmy et al., 2013).

Indeed, the abundance of photoautotrophs in under-ice water creates an important feeding and nursery ground for zooplankton. They include sympagic sub-ice fauna that migrate there from the ice interior and pelagic sub-ice fauna that arrive from the water column. The

sympagic fauna—e.g., copepods *Halectinosoma* spp., *Tisbe* spp. and ice amphipods *Apherusa glacialis* and *Onisimus glacialis*—dominate the under-ice habitat during early summer when a pronounced layer of meltwater is present (Werner, 2006) and are derived from meltwater flushing, which expel the ice fauna from their brine channel habitat. Their high osmotic tolerance enables them to survive in the brackish meltwater (Aarset and Aunaas, 1990; Werner, 2006). In contrast, pelagic copepods (e.g., *Pseudocalanus* spp., *Oithona similis, Oncaea borealis* and *Calanus hyperboreus*) are more sensitive to low salinities (Grainger and Mohammed, 1990; Weslawski and Legezynska, 1998) and accumulate at the periphery of the meltwater layer, where they benefit from aggregated food (Hop et al., 2011). Indeed, meltwater layers can sometimes prove detrimental to sampling efforts of these more sensitive communities for experimental work. During July of the MOSAiC Expedition, a vertical zooplankton net tow underneath the ice (conducted 3 days after the meltwater layer was observed in a nearby lead) and subsequent rinsing of the net with surface water resulted in the death of all animals collected, most likely due to osmotic stress from meltwater (C. Gelfman, personal communication, 20/12/2022). With the progressive loss of sea ice over the summer, the sympagic fauna at the surface is gradually replaced by pelagic zooplankton. In previous studies, dense concentrations or "swarms" of the copepod *Calanus glacialis* were associated with the meltwater layer, and their green guts indicated the use of the rich food supply before overwintering (Werner, 2006; Hop et al., 2011). These swarms provide a potential food source to higher trophic levels. For example, cold-adapted fish, like polar cod, have been observed to congregate or take refuge in meltwater layers and associated habitats, such as the void space between false bottoms and pack ice (**Figure 13**).

The vertically condensed structure of lead meltwater also provides a unique habitat for examining intensive microbial loop processes that are involved in the decomposition of organic matter and regeneration of nutrients. One hypothesis that future work will test is that the meltwater and interface layers harbor separate microbial loop systems, with potentially different consequences for cycling of nutrients, organic matter, and the structuring of microbial assemblages as these layers change under future ice conditions (Lannuzel et al., 2020). Hypothetically, the microbial loop system within the meltwater layer could be dominated by recycling of sea ice organic matter, which was incorporated into the ice column during ice growth and released during the onset of melting. In some instances, the ratios of particulate organic carbon to nitrogen of sea ice organic matter could reflect higher proportions of refractory material relative to freshly generated organic matter during the growth season (Juhl et al., 2011; Jørgensen et al., 2015; Underwood et al., 2019). Proportions of refractory to labile organic matter in the meltwater layer, which are currently unknown, could influence the composition of microbial assemblages and rates of remineralization activity. Different nutrients, organic or inorganic, play a vital role in driving different microbial activities across the meltwater system. Genetic information on marine microbial assemblages provides insights into the capacity of microbes to utilize organic forms of dissolved nitrogen and phosphorus (Grossart et al., 2020), and the conditions under which these capacities would be advantageous. For instance, Chrysophyceae and ciliates tend to dominate the mixotrophic and heterotrophic microbial eukaryotes found in freshwater layers (Xu et al., 2020), which suggests that nutrient sources within this habitat are based mainly on the recycling of organic material present in the layer rather than mixing or upwelling. This suggestion is supported by studies reporting low concentrations of essential inorganic nutrients, e.g., phosphate and nitrate in freshwater melt ponds (Sørensen et al., 2017).

Despite these exciting insights from previous studies, many questions surrounding the ecology of these persistent (on the short-term) yet ephemeral (on the long-term) meltwater habitats remain to be quantified and addressed. Key questions for future work include identifying the primary sources of the microbes that thrive and/or accumulate in ephemeral meltwater habitats and the physiological adaptations that allow them to do so. The level of endemism and presence of novel species in freshwater microbial communities need to be identified to understand the overall contribution of ephemeral meltwater habitats to the biodiversity of the Arctic Ocean and how it might change in a warming Arctic. Using the wealth of genetic data collected during the MOSAiC Expedition (Mock et al., 2022), many of these questions will be explored in future studies. Additionally, the strategic interdisciplinary sampling scheme employed on MOSAiC and other upcoming cruises for these environments (Section 4), where sampling of meltwater habitats was co-located with biogeochemical variables and flux measurements, will allow further exploration of key biological drivers of meltwater biogeochemical cycling, such as identifying the impact of meltwater microbial communities on sea ice-seawater gas, nutrient, and particle exchange and quantifying the contributions of meltwater microbes to air-sea gas exchange.

9. Biogeochemical gradients across the meltwater/seawater interface and implications for air–sea exchange of gases and aerosols

Although recent observations indicate that some gas exchange does occur through sea ice (e.g., Delille et al., 2014), sea ice generally acts as a physical barrier for direct sea–air flux, leading to significant differences in gas concentrations between the atmosphere and ice-covered waters (Wand et al., 2006; Loose and Schlosser, 2011; Karlsson et al., 2013; Butterworth and Miller, 2016; Denfeld et al., 2018; Silyakova et al., 2022). Summer sea ice melt enhances exchange between the ocean and the atmosphere by increasing open water area and gas solubility (Bates et al., 2006; Parmentier et al., 2013), leading to climate feedbacks through effects on biogeochemical cycling and the emission of climate-active biogenic gases and aerosols (James et al., 2016). The Arctic Ocean generally acts as a net annual sink for atmospheric carbon dioxide (CO_2) during the melt season (e.g., Fransson et al.,
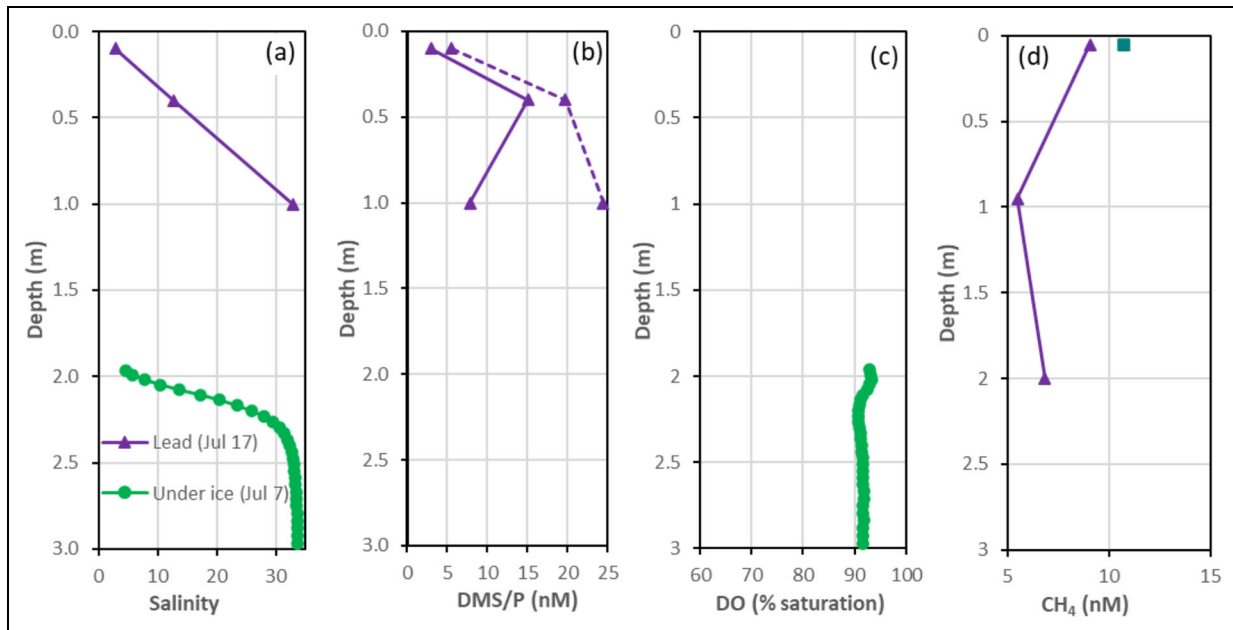
Figure 14. Example profiles of biogenic gases from meltwater layers during the MOSAiC melt season, July 2020. Example profiles from July 17 from leads (purple) and under-ice water (green), showing discrete samples for (a) salinity, measured using YSI (Smith et al., 2022a) and MSS (Schulz et al., 2022); (b) dimethylsulfide (DMS; solid lines) and dimethylsulfoniopropionate (DMSP, analysed using PTR-MS; dashed lines); (c) percentage saturation of dissolved oxygen (DO) calculated from MSS on July 7; and (d) dissolved methane (CH_4), measured with a Picarro G2201-I cavity ring-down spectrometer, coupled with a Small Sample Isotope Module, on July 11 due to unavailability of data on other dates.

2001; Fransson et al., 2009; Else et al., 2013; Chierici et al., 2019). However, the magnitude and duration of this sink can vary regionally and from year to year depending on factors such as the extent and timing of sea ice melt (e.g., Bates and Mathis, 2009; Mo et al., 2022) and the activity of the biomass that produces or consumes these gases (as outlined in Section 8). In addition, the stratification of the Arctic Ocean facilitated by the presence of meltwater layers in leads and in melt ponds and the subsequent formation of relatively fresh layers of ice may inhibit the transfer of gases between the atmosphere and the subsurface seawater.

Here, we summarize what is known about the impact of meltwater layers on the production and turnover of key climate-active biogenic gases and aerosols in the upper Arctic Ocean. Aggregated biological material immediately below the meltwater layer (e.g., Nansen, 1906; Perovich and Maykut, 1990) and strong stratification are expected to impact biogeochemical processes involved in elemental cycling. Observations during the MOSAiC expedition provide unique insight into concentrations in the near-surface meltwater layers during melt (**Figure 14**) and freeze-up (**Figure 15**) periods. We also consider the overall effect of thin meltwater layers on air-sea exchange of these gases and aerosols.

9.1. Dissolved oxygen

Total dissolved oxygen (DO) in the surface mixed layer of the Arctic Ocean generally shows saturated or supersaturated values. Conventional discrete sampling of DO from shipborne CTD Rosette samplers, followed by standard Winkler analysis (Langdon, 2010), shows a mean supersaturation in total DO of 102.6% ± 3.5% (n = 520) north of 85°N in the upper 10 m of the central Arctic Ocean (Lauvset et al., 2022). Biologically mediated DO supersaturation in the surface ocean reflects the net metabolic balance between photosynthesis and respiration, i.e., net community production (NCP). Historic underway measurements of $\Delta O_2/Ar$ from a depth of approximately 10 m show a mean biological DO supersaturation (ΔO_2^{bio}) of 3.4% ± 3.0% (n = 4477) north of 85°N, indicating net autotrophic conditions during late summer (Eveleth et al., 2014; Ulfsbo et al., 2014; Ouyang et al., 2021). This excess DO is produced photosynthetically or injected by the exclusion of dissolved gas by growing ice (Codispoti and Richards, 1971; Top et al., 1985; Sherr and Sherr, 2003; Loose et al., 2009; Timmermans et al., 2010). Trapping of dissolved gases by the sea ice cover likely increases the residence time of DO in the mixed layer relative to open ocean conditions (Eveleth et al., 2014), but conversely, sea ice melt is depleted in DO compared to the ambient seawater and can become a significant sink of DO compared to its sea ice precursor upon melting (Glud et al., 2002; Rysgaard and Glud, 2004; Rysgaard et al., 2008). Depending on melt rate and stratification, DO-depleted sea ice meltwater can lead to undersaturated surface waters, thereby driving a downward flux of oxygen at air-ice-sea interfaces (Rysgaard et al., 2008; Rysgaard et al., 2011).
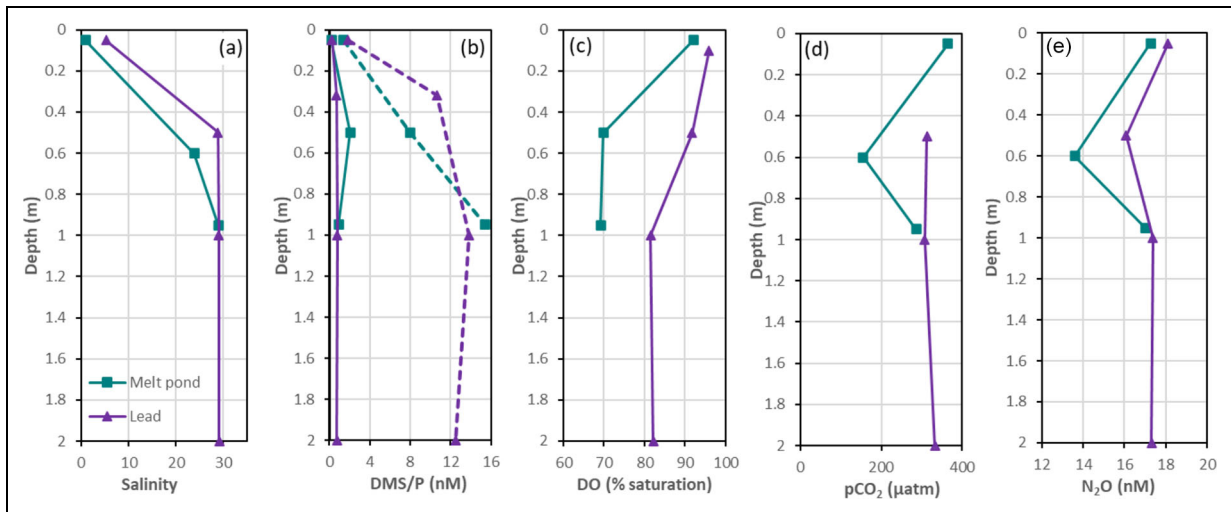
Figure 15. Example profiles of biogenic gases from meltwater layers during the MOSAiC freeze-up, September 2020. Example profiles from September 2 from melt ponds (teal) and leads (purple) showing discrete samples for (a) salinity, measured using RINKO CTD; (b) dimethylsulfide (DMS; solid lines) and dimethylsulfoniopropionate (DMSP, analysed using PTR-MS; dashed lines); (c) percentage saturation of dissolved oxygen (DO), calculated from RINKO CTD; (d) pCO_2, calculated from dissolved inorganic carbon and total alkalinity analyses; and (e) N_2O, analysed by GC-ECD.

During the MOSAiC melt period, DO was lower in the surface meltwater layer compared to the layer immediately below the halocline, presumably linked with high Chl *a* concentrations identified in the interface layer and subsequent photosynthesis (Section 8; **Figure 11**), which were disconnected with O_2 entering the water from the atmosphere. Disentangling the processes underlying the net DO content in the uppermost Arctic Ocean presents significant challenges, as biological production or consumption is likely to change with season from net primary to net secondary production, and may often be masked by a much larger physically induced flux under conditions of sea ice freezing or melting (Glud et al., 2014; Attard et al., 2018).

9.2. Carbon dioxide
The partial pressure of CO_2 (pCO_2) in the surface layer of the Arctic Ocean is driven by a complex interplay between abiotic and biotic processes. In the Arctic, meltwater, whether from sea ice and snow or glacial origin, dilutes marine carbonate system components, thus lead to decreasing dissolved inorganic carbon (DIC) and total alkalinity (TA; Chierici and Fransson, 2009), which can lead to decreased pCO_2. Geilfus et al. (2015) observed low pCO_2 in melt pond water on first-year sea ice in the Canadian Arctic due to the dilution effect of meltwater. Nomura et al. (2013) similarly showed that snow meltwater on Arctic and Antarctic sea ice results in a drastic decrease of TA and DIC in the sea ice environment, and that sea ice therefore supports atmospheric CO_2 uptake during periods of snowmelt and surface flooding. Temperature changes modulate the effects of dilution, as cold and fresh waters increase CO_2 solubility (Weiss, 1974).

In addition to being affected by biological and physical processes, sea ice formation also imposes changes in the carbonate chemistry. For instance, dissolution of the ikaite ($CaCO_3 \cdot 6H_2O$) crystals in sea ice during the melting season leads to enhanced TA in sea ice melt water, resulting in a reduction of pCO_2 (Fransson et al., 2011; Geilfus et al., 2015; Mo et al., 2022). Remineralization and production of organic matter respectively produce and remove CO_2 (Zeebe and Rolf-Gladrow, 2001). Sea ice meltwater contributions in the Arctic Ocean promote primary production through upper layer stratification and consequently CO_2 uptake (Chierici et al., 2019). Overall, the combined effects of dilution, ikaite dissolution, and biological primary production associated with sea ice meltwater in the Arctic suggest that meltwater is a driver of low surface water pCO_2. Although the above processes are expected to apply to the carbonate chemistry of the meltwater layer, their mechanistic interplay in this small-scale ephemeral feature, and thus the net effect on its pCO_2, is highly uncertain.

During the freeze-up phase of the MOSAiC expedition (August–September), the meltwater layer had higher DO and pCO_2 values compared to the underlying seawater. Indeed, DO percentage saturation on September 2 was 96% in the meltwater layer and 60% in the seawater (**Figure 15**). In the melt ponds, the pCO_2 in the surface layer of the melt pond (0.1 m) was about 364 µatm and a pCO_2 minimum of about 155 µatm occurred at the interface between the meltwater surface layer and the bottom melt pond water (M Yoshimura, unpublished data). This pCO_2 minimum was accompanied by low DO. While the latter suggests enhanced secondary production and regeneration (Section 8), with limited resupply from the atmosphere, these processes contradict the low

$p\text{CO}_2$ value, which is expected to be higher due to respiration based on the DO results. Instead, the unexpected $p\text{CO}_2$ minimum at the meltwater interface could be explained by the mixing process of the carbonate system parameters between sea ice meltwater near the surface and the water at the bottom of the melt pond, which has been in contact with the ocean below due to bottom ice porosity.

Whether or not CO_2 is absorbed from or released to the atmosphere depends on the gradient of $p\text{CO}_2$ at the sea-air interface. In the case of the melt ponds, the $p\text{CO}_2$ at the surface is lower than that of the atmosphere and thus indicates that melt ponds have the potential to absorb CO_2 from the atmosphere at this time in the year. A common method for estimating air-sea CO_2 flux is based on indirect bulk seawater $p\text{CO}_2$ measurements from the ship's seawater inlet, often at a depth of 5–6 m (Fransson et al., 2009; Pierrot et al., 2009) and 11 m on the R/V *Polarstern*, and flux calculations based on the pCO$_2$ gradient between air and seawater, wind speed and meteorological conditions (e.g., Weiss, 1974). This method assumes a well-mixed upper surface layer and has therefore been shown to lead to significant biases in CO_2 flux estimates when shallow stratification occurs in the top 10 m in the Arctic Ocean (Miller et al., 2019; Dong et al., 2021; Section 4.1). The detailed MOSAiC studies of meltwater process are showing how physical, chemical, and biological processes lead to strong vertical $p\text{CO}_2$ gradients on the order of centimeters, rendering measurements even deeper than 1 m potentially unrepresentative of the meltwater layer. These findings complicate accurate estimations of CO_2 fluxes in the Arctic Ocean, both by model simulations (limited by resolution) and observations (limited by logistics and practical limitations).

9.3. Nitrous oxide

In the Arctic Ocean, nitrous oxide (N_2O) concentrations are generally influenced by biogenic production rather than dissolution of anthropogenically derived N_2O from the atmosphere. This biogenic production is driven by archaea and bacteria that produce N_2O as an intermediate stage of their metabolism (Goreau et al., 1980; Smith and Zimmerman, 1981; Löscher et al., 2012). Near-surface water N_2O concentration in the North American Arctic Ocean was found to be associated with production from continental shelf sediments (Fenwick et al., 2017; Zhan et al., 2017; Zhan et al., 2020; Rees et al., 2022), whereas those in the Greenland Basin and Fram Strait were found to be undersaturated (Rees et al., 2021). N_2O profiles, for melt ponds and leads during MOSAiC, mimic $p\text{CO}_2$ profiles during the freeze-up season, with a minimum value at the bottom of the meltwater layer and an increase of concentrations toward the surface and underlying sea water (**Figure 15**).

Similar salinity, $p\text{CO}_2$ and N_2O concentrations at the bottom of melt ponds and in lead water at 1 m depth suggest connection of the melt pond with seawater. The minimum value of N_2O at the bottom of the meltwater layer can be related to the melting of N_2O-depleted sea ice, while the increase of N_2O at the surface could be due to atmospheric N_2O uptake. N_2O is undersaturated along

both profiles with regards to the atmosphere, with a minimum saturation at the bottom of the meltwater layer (81.0% and 76.2% for lead and melt pond, respectively), and a near-equilibrium saturation for underlying seawater (98.1%). Surface saturation is 94.0% and 88.2% for the lead and melt pond, respectively.

N_2O surface water samples were collected from 13 different melt ponds during the MOSAiC freeze-up period. The N_2O concentration ranged from 6.8 to 17.3 nmol L^{-1} (**Figure 15**; mean of 8.5 ± 2.85 nmol L^{-1}) and was markedly undersaturated compared to the atmosphere (34.9% to 88.2% with a mean of 44.4%). The concentrations of N_2O in the ice beneath the melt pond were lower than in the melt pond, ranging from 4.1 to 8.2 nmol L^{-1} (mean of 6.2 ± 1.1 nmol L^{-1}). The higher concentration in melt pond water compared to the underlying ice suggests that N_2O concentrations may increase during and following melt as a result of the uptake of atmospheric N_2O. Contrary to the concentrations of dimethylsulfide (DMS) that appear to be related to salinity (see below) and its impact on microbial processes, we did not observe a clear relationship between salinity and N_2O concentration in the melt ponds. This finding might suggest a weak contribution of microbial processes, with primary control by atmospheric exchange. Concentration of N_2O in the surface lead meltwater layer was higher than in the melt ponds, ranging from 9.0 to 18.1 nmol L^{-1} (**Figure 15**; mean of 14.2 ± 3.2 nmol L^{-1}) and therefore was also undersaturated relative to the atmosphere (51.6% to 97.0% with a mean of 79.7% ± 16.2%).

9.4. Methane

The methane (CH_4) cycle in the Arctic Ocean is highly dynamic, with intermittent sedimentary sources, sea ice cover, and dynamic circulation patterns influencing it. Evidence suggests that sea ice plays a role in Arctic methane cycling by serving as a vector for stored methane, transporting it to remote areas far from its sources, or reducing its content and hindering exchange between subsurface ocean layers and the atmosphere through stronger stratification/isolation (Damm et al., 2018; Verdugo et al., 2021; Silyakova et al., 2022). Nevertheless, the effect of rising freshwater input, whether at the basin level or from local meltwater, on CH_4 gas exchange at the ocean-atmosphere interface and emissions, is currently poorly understood (Lamarche-Gagnon et al., 2019; Manning et al., 2020; 2022). During MOSAiC, CH_4 was supersaturated in lead meltwater layers relative to the atmospheric CH_4 capacity (mean of 4.19 ± 0.35 nmol L^{-1}; n = 21), with concentrations higher in the lead meltwater layer compared to the underlying water (**Figure 15**). This observation was in line with earlier studies (e.g., Kitidis et al., 2010; Damm et al., 2015; Verdugo et al., 2021), suggesting the potential for ventilation into the atmosphere (see Text S4 for methods). The vertical profile of CH_4 followed the water stratification, which restricted downward mixing. As discussed in Damm et al. (2015), the decoupling between the deeper ocean and the atmosphere reduces the sink capacity of the Arctic Ocean.

Likely sources of methane were sea ice (mean of 14 ± 5 nmol L^{-1}) and the favorable conditions for biogenic methane production. This likelihood was corroborated by microbial community data, which suggested the potential for methanogenesis through the detection of methanogenic Archaea in the family Thermoplasmatales (Section 8). Methane can also be produced as a byproduct of primary production or the degradation of dissolved organic matter in the water column. The average methane concentration in the melt pond at 10 cm depth (within the meltwater) was >20 nmol L^{-1}, whereas in the lead meltwater layer concentrations averaged 12 ± 5 nmol L^{-1}. While the CH_4 excess in lead meltwater layers could translate into a significant water-to-air flux, the coupling of incubation experiments performed during MOSAiC to in situ measurements and microbial community structure analysis suggested potential microbial methane oxidation within the relatively fresh meltwater down to 50 cm depth, likely inhibiting CH_4 emissions into the atmosphere. The methane oxidation rate constant was in the range of 0.0003 to 0.004 d^{-1} with no negative values recorded, suggesting prevailing methanotrophy (i.e., bacterial use of methane as a source of carbon and of energy) in the upper 2 m of the open water leads. Within in situ waters, no clear evidence of methanotrophs was detected in the most abundant fraction (Section 8); however, the microbial community within the experimental samples could have shifted over time, giving the opportunity for CH_4 oxidizers to dominate at the end of the incubation experiment. Previous studies (e.g., Mau et al., 2013) have also reported elevated methane oxidation activity in marine environments, coincident with high CH_4 concentrations. These results suggest that CH_4 oxidizers may be able to increase oxidation rates rapidly in response to the abundance of CH_4. As with other gases, direct flux measurements performed during MOSAiC (Shupe et al., 2022) will allow verification of this hypothesis in future work.

9.5. Dimethylsulfide
The primary source of the climatically important gas dimethylsulfide (DMS; Simó, 2001) is dimethylsulfoniopropionate (DMSP), produced throughout marine microbial communities (Curson et al., 2017; McParland and Levine, 2019). In polar regions, DMSP production is generally closely associated with sea ice melt events (Trevena and Jones, 2006; Galindo et al., 2015; Gourdal et al., 2018; Stefels et al., 2018; Lizotte et al., 2020), but longer term summer processes and the drivers of DMSP and DMS turnover are poorly understood, likely due to sampling limitations of shipboard CTD rosette systems compared to the smaller scale of the meltwater layers (e.g., Matrai et al., 2008; Galí and Simó, 2010; Lizotte et al., 2020). Gourdal et al. (2018) found a positive relationship between DMS and salinity within Arctic Ocean melt ponds, with the implication that the low salinity water did not maintain the microbial community sufficiently to support DMSP production or subsequent turnover to DMS. Elevated concentrations of DMS were observed in melt ponds in the High Arctic by Park et al. (2019), but only in ponds that had melted through and contained relatively high salinity

environments. Otherwise, measurements of DMS and DMSP within the meltwater environment are very limited.

MOSAiC observations suggest that the presence of a meltwater layer inhibits emissions of DMS into the atmosphere. Concentrations of both DMS and DMSP in surface melt ponds during both the melting and freezing seasons were lower in the meltwater and associated with practical salinities <5, compared to order of magnitude higher values below the halocline (**Figures 14** and **15**). This trend was mirrored in the surrounding lead waters. These results give weight to the hypothesis of a limited water-to-air DMS flux in the Central Arctic. While autumn meltwater mixing and breakdown of the stratified layer could potentially release DMS towards the atmosphere, this process occurred at the time when surface ice was thickening, further limiting atmospheric flux (Section 6). While there is indirect evidence of a limited water-to-air DMS flux in the Central Arctic (e.g., low atmospheric levels of DMS and its oxidation products, or concentration spikes due to transport from the marginal ice zone (Baccarini et al., 2020; Schmale and Baccarini, 2021), direct flux measurements performed during the MOSAiC expedition by eddy covariance and dynamic/static flux chamber systems (Shupe et al., 2022) will confirm or refute this hypothesis. Further studies are also needed to evaluate implications for other aerosol precursors, such as iodic acid, which may be associated with sea ice processes (M Boyer, personal communication, 19/10/2022).

9.6. Aerosols
The presence of a meltwater layer likely also affects primary emissions of cloud condensation nuclei (CCN) and ice nucleating particles (INPs) and thus the regional radiation budget. Primary sea spray aerosol (SSA), namely sea salt, microbial cells and fragments (e.g., bacteria, viruses, and algae), and organic matter generated from marine biota (e.g., proteins, saccharides, lipids, fatty acids), as well as extracellular polymeric substances that can assemble into gels, can be emitted directly into the atmosphere via bubble bursting and wave-breaking production of airborne film, jet, and spume drops (Leck and Bigg, 2005; Quinn et al., 2015; Richter and Veron, 2016; Decho and Gutierrez, 2017; Malfatti et al., 2019). Only limited studies on SSA generation from leads in pack ice are available, and the results are conflicting (Kirpes et al., 2019; Chen et al., 2022). Wind is typically weak in the summertime Arctic (Shupe et al., 2022), when marine biological productivity peaks, limiting the emission of aerosols from whitecaps and waves. In addition, the presence of very low clouds in the summer, which were frequent during Leg 4 of the MOSAiC expedition, might provide a wet deposition sink for aerosols. Even fewer studies have evaluated primary aerosol emissions from relatively fresh melt ponds; those few have suggested that melt ponds may be a source of biological aerosol that serve as INPs (Zeppenfeld et al., 2019; Hartmann et al., 2021; Creamean et al., 2022). Evidence from MOSAiC suggests that melt ponds can be sources of primary biological aerosols and INPs (Creamean et al., 2022); however, the exchange of such particles across the air-water interface might have been limited as
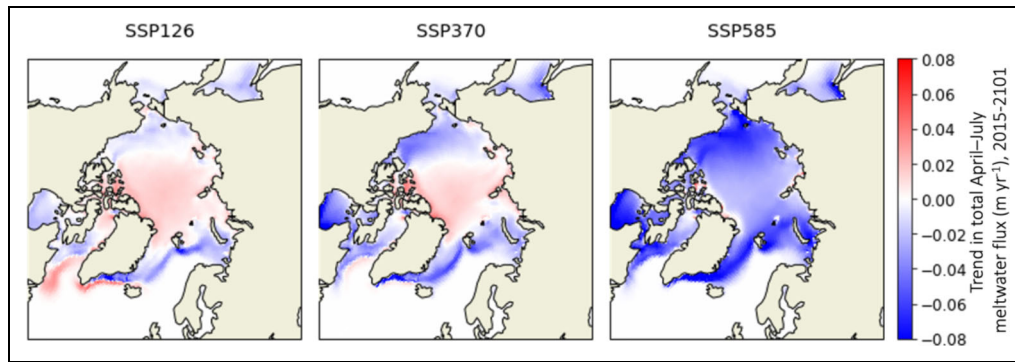
Figure 16. Projected future trends in Arctic summer snow and sea ice meltwater flux. Estimated projected trend in total April–July meltwater flux (m yr^{-1}) from 2015 to 2101 for three future scenarios SSP1-2.6, SSP3-7.0, and SSP5-8.5 from the CESM2 runs contributed to CMIP6. The meltwater flux shows a pattern of increases in the Central Basin with decreases in the margins for all scenarios, but with the area of increased flux decreasing in higher emissions scenarios.

subnivean ponds (i.e., pooling of meltwater beneath lingering snow on the ice surface) evolved into highly stratified melt ponds and meltwater layers on top of open leads (Webster et al., 2022). Future work is needed to better constrain the impact of meltwater layer characteristics and their contribution to primary aerosol CCN and INPs, particularly at a time of year when aerosol concentrations could be significantly influenced by meltwater processes.

9.7. Outlook for biogeochemical gradients and air-sea exchanges of meltwater interfaces

Together, recent observations suggest that evolution of the high-biomass layer trapped directly below the meltwater layer throughout the melt season drives variability in biogenic gas production, but there is no unifying trend in concentration profiles across the gases. This absence is unsurprising given the different production and consumption pathways, both biotic and abiotic, of oxygen, carbon, sulfur, and nitrogen. However, the MOSAiC dataset allows them to be compared side by side in the meltwater for the first time. Much of the existing data on processes involving these key elements has focused on the Canadian Archipelago or around Svalbard, with very little in the Central Arctic or other areas of pack ice. Further work to understand the dynamics of the large pack-ice areas that dominate the Arctic is essential to understand elemental cycling on the basin scale. Evidence of the impact of meltwater on gas/aerosol cycling in the literature has focused largely on melt ponds, applying a simple open or closed model, which observations from MOSAiC have shown cannot be broadly applied. While some gas concentrations have been suggested to vary directly with salinity, higher resolution data across a range of conditions would allow testing of this hypothesis. We also suggest investigating the capacity for gas production within thin meltwater layers (as indicated by CH$_4$), which would further impact concentrations of other gases in the surface layer beyond atmosphere dissolution. Finally, the increased gas transfer resistance associated with the stratified freshwater surface layer is likely quite variable in time and space. A better understanding of physical mixing is required before we can fully evaluate variability from biogenic factors.

10. Effects of climate change on meltwater layers

The anticipated future changes in the location and prevalence of meltwater layers depend on a number of factors, especially including the meltwater flux from the ice to the ocean during the melt season (April–July). We use CESM2 (Danabasoglu et al., 2020), a CMIP6 fully-coupled climate model, to visualize the trend in snow and sea ice meltwater input over the next century given different climate change scenarios (**Figure 16**). In all scenarios, the meltwater flux is expected to decrease around the margins and increase in the central Arctic Basin. In the "best case" scenario SSP1-2.6 and "moderate future pathway" SSP3-7.0, the majority of the area is expected to trend towards more meltwater input than at present. In the "high-emissions" scenario SSP5-8.5, almost no area is expected to have increasing meltwater input as the extent of sea ice cover is greatly reduced. A more seasonal sea ice cover in the Central Arctic results in more melt locally and less around the margins where there will no longer be ice. We note that "freshwater" from sea ice melt is more likely to remain in the Arctic compared to fresh meltwater from other sources, such as Greenland ice sheet melt, due primarily to the spatial distribution of such fluxes (e.g., Zanowski et al., 2021).

Of course, the propensity for the meltwater input to form thin stratified layers as described in this review depends on other factors, including sea ice morphology and concentration, and wind and drift speed, which are also likely to change in future scenarios. Thinning ice (Kwok and Cunningham, 2015) and accelerated ice motion (Rampal et al., 2011; Itkin et al., 2017) may reduce the potential for meltwater layers spatially in the future. Additionally, the Arctic is trending towards more seasonally ice-covered areas that support wave generation in the summer (i.e., Stopa et al., 2016), which may increase surface mixing and reduce the potential for stratification when ice concentrations are low.

Sea ice microbial communities may act as seeding stocks for the meltwater community, influencing both the taxonomic and metabolic diversity of the associated microbial communities present in meltwater habitats. Thinner ice may also support earlier development of phototrophic biomass in spring due to greater light transmission through thinner ice and snow cover (Nicolaus et al., 2012). Thinning ice could therefore change the bloom timing, composition and biomass levels of both sympagic and pelagic algae (Olsen et al., 2017). Shifting biodiversity could further influence biogeochemical cycling within meltwater layers, including compounds that play key roles in climate feedbacks (Edwards et al., 2020). Meanwhile, the environmental conditions in this habitat, including salinity, irradiance, and nutrients, are subject to change, with corresponding changes in physiology and productivity. In a more dynamic Arctic, more frequent occurrence, but also the erosion of such layers, may be expected, possibly increasing the potential for pulsed sinking events that export carbon efficiently to depth.

Current models project increasing magnitudes of DMS, CO_2, N_2O and CH_4 fluxes in the Arctic as a result of increased open water area (Kitidis et al., 2010; Levasseur, 2013; Parmentier et al., 2013; Galí et al., 2019; Galí et al., 2021). However, if open water in areas of partial ice cover is covered by a meltwater layer of different gas concentration with respect to that in under-ice water (Section 9), the magnitude of the fluxes will differ significantly, as observed in stratified coastal waters (Miller et al., 2019). Gas exchange rates and concentrations are thus likely to rely on the relative timing of peak melting, due to limited exchange through a stable meltwater layer. In a more distant future, as sea ice declines and the extent of the stable meltwater layer gradually diminishes, air-sea gas and aerosol exchanges could indeed increase substantially, leading to profound impacts on the emissions and uptake of climate-relevant gases and cloud-forming aerosols. In addition to increased air-sea gas exchange, the biogenic production of DMS, N_2O and CH_4 may also increase under scenarios with less sea ice coverage (Uhlig et al., 2019) either through the direct release of DMSP or through a shift in the onset of phytoplankton blooms (Vancoppenolle et al., 2013; Kurosaki et al., 2022). All current air-sea gas transfer models, both empirical and physical, assume a well-mixed ocean surface layer. Clearly these models cannot be applied to an open water environment with strong surface stratification. Global climate models, which rely on existing measurements and calculations of fluxes, require further research to account for the impact of thin meltwater layers during the summer in a rapidly changing Arctic.

11. Conclusion: Challenges and future directions
During the melt season, snow-and sea ice-derived meltwaters can accumulate under quiescent conditions in leads and under ice, resulting in strongly stratified layers on the order of 1 m thick situated directly at the interface between sea ice, ocean, and atmosphere. A key outcome of this review and the new observations from MOSAiC is an acknowledgement of the far-reaching implications of meltwater layers for nearly every component of the Arctic coupled system. Meltwater layers have been observed in most regions of the Arctic Basin (**Figure 3**). Some of their major impacts can be summarized as follow:

- The presence of meltwater layers can impact the icescape, in particular by resulting in the formation of false bottoms under the ice and even in leads. We have submitted a proposal to include false bottoms and other melt-related terminology in the WMO Sea Ice Nomenclature (JCOMM Expert Team on Sea Ice, 2014), which would help to support more standardized observation and discussion of these unique features.
- The strong stratification associated with meltwater layers has large implications for the distribution of heat. Meltwater layers can act to reduce heat fluxes from the mixed layer below, and the concentration of solar heating within meltwater layers can result in temperatures well above the salinity-dependent freezing temperature and melt rates above the local average (**Figure 6**).
- The strong stratification between the meltwater layer and the underlying ocean acts as a barrier to reduce vertical momentum fluxes from the atmosphere to the ocean (similar to sea ice). The high buoyancy of the meltwater layer requires considerable energy to mix downwards. Consequently, most of the wind-induced turbulence is trapped within the meltwater layer such that dissipation rates may be 1–2 orders of magnitude lower in the upper meters of the ocean than in the absence of a meltwater layer (e.g., **Figure 9**).
- Trapping of particles and organisms within the meltwater layer can increase the turbidity, further increasing solar absorption and scattering and also increasing the exposure of organisms to harmful levels of radiation.
- Meltwater stratification serves as a physiological barrier for biological growth and migration and for the exchange of nutrients and organic matter between habitable environments, thus impacting organismal diversity, distributions, and productivity. Further investigating and identifying the key ecological processes that are impacted by, and coupled to, this meltwater input will be critical to predicting and modeling future change in Arctic Ocean biodiversity and consequences for higher trophic levels.
- Evidence from the repeated meltwater sampling during MOSAiC suggests that the meltwater layer has a capping effect at lease at least as strong as previously proposed for the sea ice cover. With the increasing rate of sea ice loss across the Arctic Ocean as a whole, and changing duration and coverage of meltwater during the polar summer, existing estimates of gas and aerosol fluxes are likely to be significantly over- or under-estimated (e.g., Miller et al., 2019; Dong et al.,

2021). Due to the biogenic nature of many of the gases and aerosols considered here, changes to the ecology and productivity across the Arctic will likely also have significant effects on gas and aerosol production and projections by climate models.

The sparsity of observations of meltwater layers are a reflection of the inadequacy of traditional methods for capturing these layers and their impacts (e.g., Miller et al., 2019; Dong et al., 2021), rather than the rarity of the layer themselves. As such, the development of technology that is better suited for observing such small-scale millimeter-centimeter features over greater spatial and temporal scales is a key challenge for the future. Autonomous instruments offer opportunities for increasing observational capacity. New profilers through the ice are able to profile to within a few centimeters of the ice bottom, including a new generation of ice-tethered profilers, which profile closer to the surface than before and are able to survive in open water (Toole et al., 2011), and the D-TOP buoy designed by the Ocean University of China. Additionally, new methods are in development to expand the capability of IMB buoys by pairing conductivity cells that will allow identification of under-ice meltwater layers (I. Raphael, personal communication, 27/04/2022). Electromagnetic methods have been used to detect fresh under-ice river plumes (Prinsenberg et al., 2008) and may allow detection of low-conductivity meltwater layers beneath the ice on the large scale. These detailed in situ measurements could help guide focused discrete sampling of the relatively thin meltwater layers to be able to compare data from a wide range of physical, chemical, and biological measurements to the interface and seawater layers below.

While there is motivation to continue to move towards autonomous instrumentation, which increases the possibility for higher spatial and temporal coverage, the gap in our ability to observe these features with clarity currently motivates on-ice process studies. Further development of instruments that profile while rising upwards is promising for capturing near-surface or near-ice layers (Fer et al., 2022a). Another possible direction includes the development of a floating under-ice sensor package that follows the ice bottom, such that it would follow the development of the under-ice layer in a Lagrangian manner. There is also a need to develop of sensors that capture processes impacted by the presence of meltwater layers on the relevant millimeter-centimeter scales, including microbial and biogeochemical parameters. For example, development of sensors to measure in-water profiles of gases including DMS and N_2O and the magnitude of the air-water flux in both melt ponds and areas of open water is needed to address gaps in understanding. Similarly, better methods to accurately collect water samples from these microscale features and their interfaces for biological measurements, without too much disturbance, should be considered for future fieldwork targeting these environments.

The geographic distribution and temporal persistence of meltwater layers cannot yet be determined from current observations. For example, whether similar features develop, or can be expected to develop, associated with sea ice melt in Antarctica is unknown. While the greater density difference between sea ice meltwater and underlying seawater may increase the propensity for meltwater layers to form, the relative dominance of large waves from the Southern Ocean and strong coastal winds in many Antarctic regions are capable of breaking down near-surface stratification as it forms. Observations have indicated fresher surface layers in Antarctic coastal waters (e.g., van Leeuwe et al., 2020), but to our knowledge there are no measurements of sufficient resolution to identify layers of the scale discussed here. Additionally, if such layers were identified in Antarctic coastal regions, determining their origin would be complicated by the large influx of ice sheet meltwater. Dedicated upper ocean observations during the melt season and the development of satellite remote sensing methods to capture the likely presence of meltwater layers would be extremely beneficial to determining their global prevalence and impact.

The work reviewed here includes primarily process-scale observations, with some results from process-scale modeling, as climate-scale models do not accurately represent thin meltwater layers. For example, the minimum ocean surface layer thickness in many CMIP6 models is 5–10 m, which limits the ability to explicitly represent these thinner layers, even though their climatic impacts could be significant. Additionally, the relationships of meltwater layers in leads and under ice with other emergent variables such as melt pond coverage are not well defined, such that a parameterization is not yet feasible. Thus, in order to represent these often overlooked features in both process and large-scale models, our understanding of the meltwater layer evolution and controls needs to be refined, and higher model vertical resolution near the surface interface or appropriate sub-grid-scale parameterizations likely need to be implemented. Progress in these areas may allow additional constraints for atmospheric models, where the presence of meltwater layers significantly affects fluxes from the ocean to the atmosphere. Similarly, biogeochemical models in development using recent observations described here may better constrain fluxes of gases and nutrients based on impacts of thin meltwater layers.

Data accessibility statement

All data plotted in this manuscript are extracted from much larger data sets. Most full data sets are now published publicly online, and data from the following are used in the manuscript:

- MSS: http://dx.doi.org/10.1594/PANGAEA.939816
- VMP: http://dx.doi.org/10.1594/PANGAEA.946076
- YSI near-surface ocean measurements: http://dx.doi.org/10.18739/A2TT4FV1G
- Fishing-rod CTD: http://dx.doi.org/10.1594/PANGAEA.956142

- Mass balance transect data include melt pond depths: http://dx.doi.org/10.1594/PANGAEA.937781
- Autonomous SIMBA measurements at FYI site (2019T66): http://dx.doi.org/10.1594/PANGAEA.938134
- Amplicon sequence data: http://doi.org/10.18739/A2CC0TV5X
- Ice and false bottom temperature, density, salinity and isotope composition from FYI coring site: https://doi.pangaea.de/10.1594/PANGAEA.956732

A few data sets are not yet complete or are still under revision. Where possible, values used in this manuscript are published in the text or in the supplemental material, and direct access to these partial data sets can be granted by contacting the relevant contacts given below:

- Gas flux data: Daiki Nomura (daiki.nomura@fish.hokudai.ac.jp)
- Methane data: Alessandra D'Angelo (a_dangelo@uri.edu), Brice Loose (bloose@uri.edu), Emelia J. Chamberlain (echamber@ucsd.edu), Jeff Bowman (jsbowman@ucsd.edu)
- Cell count data: Oliver Müller (oliver.muller@uib.no)
- Photosynthetic yield data: Deborah Bozzato (d.bozzato@rug.nl)
- Chlorophyll *a* data: Clara Hoppe (Clara.Hoppe@awi.de)

Supplemental files

The supplemental files for this article can be found as follows:

Text S1. Methods for meltwater layer characterization in **Figures 5** and **6**.

Text S2. Methods for VMP upper-ocean turbulence in **Figure 9**.

Text S3. Methods for ecological characterization in **Figure 11**.

Text S4. Methods associated with air-sea gas exchange in Section 9.

Video S1. Under-ice GoPro video near FYI sediment trap on June 28, 2020.

Video S2. Under-ice GoPro video near FYI sediment trap on July 5, 2020.

Video S3. Under-ice GoPro video near FYI sediment trap on July 19, 2020.

Acknowledgments

Funding

Competing interests

The authors have declared that no competing interests exist. Hélène Angot, Byron W. Blomquist, and Jeff S. Bowman are associate editors at Elementa. They were not involved in the review process of this article.

Author contributions

Contributed to conception and design: MMS, MH, ALW, SK, EJC, MM, IF, MAG, MDS, HA, ESD.

Contributed to acquisition of data: MMS, EJC, MH, KMS, ES, SK, ESD, JB, DN, MM, DB, IF, ST, ALW, HA, SDA, AD.

Contributed to analysis and interpretation of data: MMS, KMS, SK, EJC, DN, ES, ESD, MY, MAG, MM, DB, IF, ST, ALW, HA, KS, SM, BD, TM, SDA, CJMH, OM, AD.

Drafted and/or revised the article: All authors.

Approved the submitted version for publication: All authors.

References

Aarset, AV, **Aunaas, T**. 1990. Influence of environmental salinity on oxygen consumption and ammonia excretion of the arctic under-ice amphipod *Onisimus glacialis*. *Marine Biology* **107**: 9–15. DOI: http://dx.doi.org/10.1007/BF01313237.

Abdullahi, AS, **Underwood, GJC**, **Gretz, MR**. 2006. Extracellular matrix assembly in diatoms Bacillariophyceae. V. Environmental effects on polysaccharide synthesis in the model diatom, *Phaeodactylum tricornutum*. *Journal of Phycology* **42**(2): 363–378. DOI: http://dx.doi.org/10.1111/j.1529-8817.2006.00193.x.

Alexandrov, DV, **Nizovtseva, IG**. 2008. To the theory of underwater ice evolution, or nonlinear dynamics of "false bottoms." *International Journal of Heat and Mass Transfer* **51**(21–22): 5204–5208. DOI: http://dx.doi.org/10.1016/j.ijheatmasstransfer.2007.11.061.

Allen, MB. 1971. High-latitude phytoplankton. *Annual Review of Ecology and Systematics* **2**: 261–276. DOI: http://dx.doi.org/10.1146/annurev.es.02.110171.001401.

Alou-Font, E, **Mundy, CJ**, **Roy, S**, **Gosselin, M**, **Agusti, S**. 2013. Snow cover affects ice algal pigment composition in the coastal Arctic Ocean during spring. *Marine Ecology Progress Series* **474**: 89–104. DOI: http://dx.doi.org/10.3354/meps10107.

Antoni, JS, **Almandoz, GO**, **Ferrario, ME**, **Hernando, MP**, **Varela, DE**, **Rozema, PD**, **Buma, AGJ**, **Paparazzo, FE**, **Schloss, IR**. 2020. Response of a natural Antarctic phytoplankton assemblage to changes in temperature and salinity. *Journal of Experimental Marine Biology and Ecology* **532**: 151444. DOI: http://dx.doi.org/10.1016/j.jembe.2020.151444.

Apollonio, S. 1980. Primary production in Dumbell Bay in the Arctic Ocean. *Marine Biology* **61**: 41–51. DOI: http://dx.doi.org/10.1007/BF00410340.

Apollonio, S. 1985. Arctic marine phototrophic systems: Functions of sea ice stabilization. *Arctic* **38**(3): 167–260. DOI: https://dx.doi.org/10.14430/arctic2129.

Apollonio, S, **Matrai, P**. 2011. Marine primary production in the Canadian Arctic, 1956, 1961–1963. *Polar Biology* **34**: 767–774. DOI: http://dx.doi.org/10.1007/s00300-010-0928-3.

Arrigo, KR, **Sullivan, CW**. 1992. The influence of salinity and temperature covariation on the photophyisiological characteristics of Antarctic sea ice microalgae. *Journal of Phycology* **28**(6): 746–756. DOI: http://dx.doi.org/10.1111/j.0022-3646.1992.00746.x.

Aslam, SN, **Cresswell-Maynard, T**, **Thomas, DN**, **Underwood, GJ**. 2012. Production and characterization of the intra-and extracellular carbohydrates and polymeric substances (EPS) of three sea-ice diatom species, and evidence for a cryoprotective role for EPS. *Journal of Phycology* **48**(6): 1494–1509. DOI: http://dx.doi.org/10.1111/jpy.12004.

Assmy, P, **Ehn, JK**, **Fernández-Méndez, M**, **Hop, H**, **Katlein, C**, **Sundfjord, A**, **Bluhm, K**, **Daase, M**, **Engel, A**, **Fransson, A**, **Granskog, MA**, **Hudson, SR**, **Kristiansen, S**, **Nicolaus, M**, **Peeken, I**, **Renner, AHH**, **Spreen, G**, **Tatarek, A**, **Wiktor, J**. 2013. Floating ice-algal aggregates below melting Arctic sea ice. *PLoS One* **8**(10): e76599. DOI: http://dx.doi.org/10.1371/journal.pone.0076599.

Attard, KM, **Søgaard, DH**, **Piontek, J**, **Lange, BA**, **Katlein, C**, **Sørensen, HL**, **McGinnis, DF**, **Rovelli, L**, **Rysgaard, S**, **Wenzhöfer, F**, **Glud, RN**. 2018. Oxygen fluxes beneath Arctic land-fast ice and pack ice: Towards estimates of ice productivity. *Polar Biology* **41**: 2119–2134. DOI: http://dx.doi.org/10.1007/s00300-018-2350-1.

Baccarini, A, **Karlsson, L**, **Dommen, J**, **Duplessis, P**, **Vüllers, J**, **Brooks, IM**, **Saiz-Lopez, A**, **Salter, M**, **Tjernström, M**, **Baltensperger, U**, **Zieger, P**, **Schmale, J**. 2020. Frequent new particle formation over the high Arctic pack ice by enhanced iodine emissions. *Nature Communications* **11**: 4924. DOI: http://dx.doi.org/10.1038/s41467-020-18551-0.

Bates, NR, **Mathis, JT**. 2009. The Arctic Ocean marine carbon cycle: Evaluation of air-sea CO_2 exchanges, ocean acidification impacts and potential feedbacks. *Biogeosciences* **6**: 2433–2459. DOI: http://dx.doi.org/10.5194/bg-6-2433-2009.

Bates, NR, **Moran, SB**, **Hansell, DA**, **Mathis, JT**. 2006. An increasing CO_2 sink in the Arctic Ocean due to sea-ice loss. *Geophysical Research Letters* **33**(23). DOI: https://dx.doi.org/10.1029/2006GL027028.

Bauerfeind, E, **Garrity, C**, **Krumbholz, M**, **Ramseier, RO**, **Voβ, M**. 1997. Seasonal variability of sediment trap collections in the Northeast Water Polynya. Part 2. Biochemical and microscopic composition of sedimenting matter. *Journal of Marine Systems* **10**(1–4): 371–389. DOI: http://dx.doi.org/10.1016/S0924-7963(96)00069-3.

Behrenfeld, MJ, **Halsey, KH**, **Milligan, AJ**. 2008. Evolved physiological responses of phytoplankton to their integrated growth environment. *Philosophical Transactions of the Royal Society B: Biological Sciences* **363**(1504): 2687–2703. DOI: http://dx.doi.org/10.1098/rstb.2008.0019.

Bélanger, S, **Cizmeli, SA**, **Ehn, J**, **Matsuoka, A**, **Doxaran, D**, **Hooker, S**, **Babin, M**. 2013. Light absorption and partitioning in Arctic Ocean surface waters: Impact of multiyear ice melting. *Biogeosciences* **10**(10):

6433–6452. DOI: http://dx.doi.org/10.5194/bg-10-6433-2013.

Boetius, A, Albrecht, S, Bakker, K, Bienhold, C, Felden, J, Fernández-Méndez, M, Hendricks, S, Katlein, C, Lalande, C, Krumpen, T, Nicolaus, M, Peeken, N, Rabe, B, Rogacheva, A, Rybakova, E, Somavilla, R, Wenzhöfer, F, RV Polarstern ARK27-3-Shipboard Science Party. 2013. Export of algal biomass from the melting Arctic sea ice. *Science* **339**(6126): 1430–1432. DOI: http://dx.doi.org/10.1126/science.1231346.

Boetius, A, Anesio, AM, Deming, JW, Mikucki, JA, Rapp, JZ. 2015. Microbial ecology of the cryosphere: Sea ice and glacial habitats. *Nature Reviews Microbiology* **13**(11): 677–690. DOI: http://dx.doi.org/10.1038/nrmicro3522.

Bowman, JS. 2015. The relationship between sea ice bacterial community structure and biogeochemistry: A synthesis of current knowledge and known unknowns. *Elementa: Science of the Anthropocene* **3**: 000072. DOI: http://dx.doi.org/10.12952/journal.elementa.000072.

Bowman, JS, Van Mooy, BA, Lowenstein, DP, Fredricks, HF, Hansel, CM, Gast, R, Collins, JR, Couto, N, Ducklow, HW. 2021. Whole community metatranscriptomes and lipidomes reveal diverse responses among Antarctic phytoplankton to changing ice conditions. *Frontiers in Marine Science* **8**: 593566. DOI: http://dx.doi.org/10.3389/fmars.2021.593566.

Brinkmeyer, R, Glöckner, FO, Helmke, E, Amann, R. 2004. Predominance of β-proteobacteria in summer melt pools on Arctic pack ice. *Limnology and Oceanography* **49**(4): 1013–1021. DOI: http://dx.doi.org/10.4319/lo.2004.49.4.1013.

Bursa, A. 1963. Phytoplankton in coastal waters of the Arctic Ocean at Point Barrow, Alaska. *Arctic* **16**(4): 239–262. DOI: http://dx.doi.org/10.14430/arctic3544.

Butterworth, BJ, Miller, SD. 2016. Air-sea exchange of carbon dioxide in the Southern Ocean and Antarctic marginal ice zone. *Geophysical Research Letters* **43**(13): 7223–7230. DOI: http://dx.doi.org/10.1002/2016GL069581.

Calmer, R, de Boer, G, Hamilton, J, Lawrence, D, Webster, MA, Wright, N, Shupe, MD, Cox, CJ, Cassano, JJ. 2023. Relationships between summertime surface albedo and melt pond fraction in the central Arctic Ocean: The aggregate scale of albedo obtained on the MOSAiC floe. *Elementa: Science of the Anthropocene* **11**(1): 00001. DOI: http://dx.doi.org/10.1525/elementa.2023.00001.

Carmack, EC. 2000. The Arctic ocean's freshwater budget: Sources, storage and export, in Lewis, EL, Jones, EP, Lemke, P, Prowse, TD, Wadhams, P eds., *The freshwater budget of the Arctic ocean*. Dordrecht, the Netherlands: Springer. (NATO science series, vol. 70). DOI: http://dx.doi.org/10.1007/978-94-011-4132-1_5.

Carmack, EC. 2007. The alpha/beta ocean distinction: A perspective on freshwater fluxes, convection,

nutrients and productivity in high-latitude seas. *Deep Sea Research Part II: Topical Studies in Oceanography* **54**(23–26): 2578–2598. DOI: http://dx.doi.org/10.1016/j.dsr2.2007.08.018.

Chamberlain EJ, Balmonte JP, Torstensson A, Fong AA, Snoeijs-Leijonmalm P, Bowman JS. 2022. Impacts of sea ice melt procedure on measurements of microbial community structure. *Elementa: Science of the Anthropocene* **10**(1): 00017. DOI: http://dx.doi.org/10.1525/elementa.2022.00017.

Chen, Q, Mirrielees, JA, Thanekar, S, Loeb, NA, Kirpes, RM, Upchurch, LM, Barget, AJ, Lata, NN, Raso, AR, McNamara, SM, China, S. 2022. Atmospheric particle abundance and sea salt aerosol observations in the springtime Arctic: A focus on blowing snow and leads. *Atmospheric Chemistry and Physics* **22**(23): 15263–15285. DOI: http://dx.doi.org/10.5194/acp-22-15263-2022.

Chierici, M, Fransson, A. 2009. Calcium carbonate saturation in the surface water of the Arctic Ocean: Undersaturation in freshwater influenced shelves. *Biogeosciences* **6**(11): 2421–2432. DOI: http://dx.doi.org/10.5194/bg-6-2421-2009.

Chierici M, Vernet, M, Fransson, A, Børsheim, Y. 2019. Net community production and carbon exchange from winter to summer in the Atlantic water inflow to the Arctic Ocean. *Frontiers in Marine Science* **6**: 528. DOI: http://dx.doi.org/10.3389/fmars.2019.00528.

Codispoti, LA, Richards, FA. 1971. Oxygen supersaturations in the Chukchi and East Siberian seas. *Deep Sea Research and Oceanographic Abstracts* **18**(3): 341–351. DOI: http://dx.doi.org/10.1016/0011-7471(71)90039-8.

Creamean, JM, Barry, K, Hill, TC, Hume, C, DeMott, PJ, Shupe, MD, Dahlke, S, Willmes, S, Schmale, J, Beck, I, Hoppe, CJ. 2022. Annual cycle observations of aerosols capable of ice formation in central Arctic clouds. *Nature Communications* **13**: 3537. DOI: http://dx.doi.org/10.1038/s41467-022-31182-x.

Crews, L, Lee, CM, Rainville, L, Thomson, J. 2022. Direct observations of the role of lateral advection of sea ice meltwater in the onset of autumn freeze up. *Journal of Geophysical Research* **127**(2): e2021JC017775. DOI: http://dx.doi.org/10.1029/2021JC017775.

Curson, AR, Liu, J, Bermejo Martínez, A, Green, RT, Chan, Y, Carrión, O, Williams, BT, Zhang, SH, Yang, GP, Bulman Page, PC, Zhang, XH. 2017. Dimethylsulfoniopropionate biosynthesis in marine bacteria and identification of the key gene in this process. *Nature Microbiology* **2**: 17009. DOI: http://dx.doi.org/10.1038/nmicrobiol.2017.9.

Damm, E, Bauch, D, Krumpen, T, Rabe, B, Korhonen, M, Vinogradova, E, Uhlig, C. 2018. The Transpolar Drift conveys methane from the Siberian Shelf to the central Arctic Ocean. *Scientific Reports* **8**: 4515. DOI: http://dx.doi.org/10.1038/s41598-018-22801-z.

Damm, E, Rudels, B, Schauer, U, Mau, S, Dieckmann, G. 2015. Methane excess in Arctic surface water-triggered by sea ice formation and melting. Sc*ientific Reports* **5**: 16179. DOI: http://dx.doi.org/10.1038/srep16179.

Danabasoglu, G, Lamarque, JF, Bacmeister, J, Bailey, DA, DuVivier, AK, Edwards, J, Emmons, LK, Fasullo, J, Garcia, R, Gettelman, A, Hannay, C, Holland, MM, Large, WG, Lauritzen, PH, Lawrence, DM, Lenaerts, JTM, Lindsay, K, Lipscomb, WH, Mills, MJ, Neale, R, Oleson, KW, Otto-Bliesner, B, Phillips, AS, Sacks, W, van Kampenhout, STL, Vertenstein, M, Bertini, A, Denni, J, Deser, C, Fischer, C, Fox-Kemper, B, Kay, JE, Kinnison, D, Kushner, PJ, Larson, VE, Long, MC, Mickelson, S, Moore, JK, Nienhouse, E, Polvani, L, Rasch, PJ, Strand, WG. 2020. The Community Earth System Model Version 2 (CESM2). *Journal of Advances in Modeling Earth Systems* **12**(2): e2019MS001916. DOI: http://dx.doi.org/10.1029/2019MS001916.

Decho, AW, Gutierrez, T. 2017. Microbial extracellular polymeric substances EPSs in ocean systems. *Frontiers in Microbiology* **8**: 922. DOI: http://dx.doi.org/10.3389/fmicb.2017.00922.

Delille, B, Vancoppenolle, M, Geilfus, N-X, Tilbrook, B, Lannuzel, D, Schoemann, V, Becquevort, S, Carnat, G, Delille, D, Lancelot, C, Chou, L, Dieckmann, GS, Tison, J-L. 2014. Southern Ocean CO_2 sink: The contribution of the sea ice. *Journal of Geophysical Research* **119**(9): 6340–6355. DOI: http://dx.doi.org/10.1002/2014JC009941.

Denfeld, BA, Baulch, HM, del Giorgio, PA, Hampton, SE, Karlsson, J. 2018. A synthesis of carbon dioxide and methane dynamics during the ice-covered period of northern lakes. *Limnology and Oceanography Letters* **3**(3): 117–131. DOI: http://dx.doi.org/10.1002/lol2.10079.

Divine DV, Pedersen, CA, Karlsen, TI, Aas, HF, Granskog, MA, Hudson, SR, Gerland, S. 2016. Photogrammetric retrieval and analysis of small scale sea ice topography during summer melt. *Cold Regions Science and Technolgy* **129**: 77–84. DOI: http://dx.doi.org/10.1016/j.coldregions.2016.06.006.

Dong, Y, Yang, M, Bakker, DC, Liss, PS, Kitidis, V, Brown, I, Chierici, M, Fransson, A, Bell, TG. 2021. Near-surface stratification due to ice melt biases Arctic air-sea CO_2 flux estimates. *Geophysical Research Letters* **48**(22): e2021GL095266. DOI: http://dx.doi.org/10.1029/2021GL095266.

Edwards, A, Cameron, KA, Cook, JM, Debbonaire, AR, Furness, E, Hay, MC, Rassner, SM. 2020. Microbial genomics amidst the Arctic crisis. *Microbial Genomics* **6**(5): e000375. DOI: http://dx.doi.org/10.1099/mgen.0.000375.

Ehn, JK, Mundy, CJ, Barber, DG, Hop, H, Rossnagel, A, Stewart, J. 2011. Impact of horizontal spreading on light propagation in melt pond covered seasonal sea ice in the Canadian Arctic. *Journal of Geophysical Research* **116**: C00G02. DOI: http://dx.doi.org/10.1029/2010JC006908.

Eicken, H. 1994. Structure of under-ice melt ponds in the central Arctic and their effect on, the sea-ice cover. *Limnology and Oceanography* **39**(3): 682–693. DOI: http://dx.doi.org/10.4319/lo.1994.39.3.0682.

Eicken, H, Grenfell, TC, Perovich, DK, Richter-Menge, JA, Frey, K. 2004. Hydraulic controls of summer Arctic pack ice albedo. *Journal of Geophysical Research* **109**(C8): C08007. DOI: http://dx.doi.org/10.1029/2003JC001989.

Eicken, H, Krouse, HR, Kadko, D, Perovich, DK. 2002. Tracer studies of pathways and rates of meltwater transport through Arctic summer sea ice. *Journal of Geophysical Research* **107**(C10): 8046. DOI: http://dx.doi.org/10.1029/2000JC000583.

Elliott, A, Mundy, CJ, Gosselin, M, Poulin, M, Campbell, K, Wang, F. 2015. Spring production of mycosporine-like amino acids and other UV-absorbing compounds in sea ice-associated algae communities in the Canadian Arctic. *Marine Ecology Progress Series* **541**: 91–104. DOI: http://dx.doi.org/10.3354/meps11540.

Else, BGT, Papkyriakou, TN, Asplin, MG, Barber, DG, Galley, RJ, Miller, LA, Mucci, A. 2013. Annual cycle of air-sea CO_2 exchange in an Arctic Polynya Region. *Global Biogeochemical Cycles* **27**: 388–398. DOI: http://dx.doi.org/10.1002/gbc.20016.

Eveleth, R, Timmermans, M-L, Cassar, N. 2014. Physical and biological controls on oxygen saturation variability in the upper Arctic Ocean. *Journal of Geophysical Research* **119**(11): 7420–7432. DOI: http://dx.doi.org/10.1002/2014JC009816.

Ewert, M, Deming JW. 2014. Bacterial responses to fluctuations and extremes in temperature and brine salinity at the surface of Arctic winter sea ice. *FEMS Microbiology Ecology* **89**(2): 476–489. DOI: http://dx.doi.org/10.1111/1574-6941.12363.

Farrell, SL, Duncan, K, Buckley, EM, Richter-Menge, J, Li, R. 2020. Mapping sea ice surface topography in high fidelity with ICESat-2. *Geophysical Research Letters* **47**(21): e2020GL090708. DOI: http://dx.doi.org/10.1029/2020GL090708.

Fenwick, L, Capelle, D, Damm, E, Zimmermann, S, Williams, WJ, Vagle, S, Tortell, PD. 2017. Methane and nitrous oxide distributions across the North American Arctic Ocean during summer, 2015. *Journal of Geophysical Research* **122**(1): 390–412. DOI: http://dx.doi.org/10.1002/2016JC012493.

Fer, I, Baumann, T, Fang, Y-C, Hoppmann, M, Karam, S, Koenig, Z, Kuznetsov, I, Muilwijk, M, Schulz, K, Schaffer, J, Sukhikh, N, Tippenhauer, S. 2022b. Under-ice temperature and dissipation rate profiles from uprising VMP250 during MOSAiC. *PANGAEA* [data set]. DOI: http://dx.doi.org/10.1594/PANGAEA.946076.

Fer, I, Baumann, T, Koenig, Z, Muilwijk, M, Tippenhauer, S. 2022a. Upper-ocean turbulence structure and ocean-ice drag coefficient estimates using an ascending microstructure profiler during the MOSAiC drift. *Journal of Geophysical Research*

127(9): e2022JC018751. DOI: http://dx.doi.org/10.1029/2022JC018751.

Fernández-Méndez, M, Turk-Kubo, KA, Buttigieg, PL, Rapp, JZ, Krumpen, T, Zehr, JP, Boetius, A. 2016. Diazotroph diversity in the sea ice, melt ponds, and surface waters of the Eurasian Basin of the Central Arctic Ocean. *Frontiers in Microbiology* **7**: 1884. DOI: http://dx.doi.org/10.3389/fmicb.2016.01884.

Fernández-Méndez, M, Wenzhöfer, F, Peeken, I, Sørensen, HL, Glud, RN, Boetius, A. 2014. Composition, buoyancy regulation and fate of ice algal aggregates in the Central Arctic Ocean. *PLoS One* **9**(9): e107452. DOI: http://dx.doi.org/10.1371/journal.pone.0107452.

Fetterer, F, Untersteiner, N. 1998. Observations of melt ponds on Arctic sea ice. *Journal of Geophysical Research* **103**(C11): 24821–24835. DOI: http://dx.doi.org/10.1029/98JC02034.

Fransson, A, Chierici, M, Anderson, LG, Bussman, I, Jones, EP, Swift, JH. 2001. The importance of shelf processes for the modification of chemical constituents in the waters of the eastern Arctic Ocean: Implication for carbon fluxes. *Continental Shelf Research* **21**: 225–242. DOI: http://dx.doi.org/10.1016/S0278-4343(00)00088-1.

Fransson, A, Chierici, M, Nojiri, Y. 2009. New insights into the spatial variability of the surface water CO_2 in varying sea ice conditions in the Arctic Ocean. *Continental Shelf Research* **29**(10): 1317–1328. DOI: http://dx.doi.org/10.1016/j.csr.2009.03.008.

Fransson, A, Chierici, M, Yager, P, Smith, WO. 2011. Antarctic sea ice carbon dioxide system and controls. *Journal of Geophysical Research* **116**: C12035. DOI: http://dx.doi.org/10.1029/2010JC006844.

Galí, M, Devred, E, Babin, M, Levasseur, M. 2019. Decadal increase in Arctic dimethylsulfide emission. *Proceedings of the National Academy of Sciences* **116**(39): 19311–19317. DOI: http://dx.doi.org/10.1073/pnas.1904378116.

Galí, M, Lizotte, M, Kieber, DJ, Randelhoff, A, Hussherr, R, Xue, L, Dinasquet, J, Babin, M, Rehm, E, Levasseur, M. 2021. DMS emissions from the Arctic marginal ice zone. *Elementa: Science of the Anthropocene* **9**(1): 00113. DOI: http://dx.doi.org/10.1525/elementa.2020.00113.

Galí, M, Simó, R. 2010. Occurrence and cycling of dimethylated sulfur compounds in the Arctic during summer receding of the ice edge. *Marine Chemistry* **122**(1–4): 105–117. DOI: http://dx.doi.org/10.1016/j.marchem.2010.07.003.

Galindo, V, Levasseur, M, Scarratt, M, Mundy, CJ, Gosselin, M, Kiene, RP, Gourdal, M, Lizotte, M. 2015. Under-ice microbial dimethylsulfoniopropionate metabolism during the melt period in the Canadian Arctic Archipelago. *Marine Ecology Progress Series* **524**: 39–53. DOI: http://dx.doi.org/10.3354/meps11144.

Geilfus, N-X, Galley, RJ, Crabeck, O, Papakyriakou, T, Landy, J, Tison J-L, Rysgaard, S. 2015. Inorganic carbon dynamics of melt-pond-covered first-year sea ice in the Canadian Arctic. *Biogeosciences* **12**(6): 2047–2061. DOI: http://dx.doi.org/10.5194/bg-12-2047-2015.

Glud, RN, Rysgaard, S, Kühl, M. 2002. A laboratory study on O_2 dynamics and photosynthesis in ice algal communities: Quantification by microsensors, O_2 exchange rates, ^{14}C incubations and a PAM fluorometer. *Aquatic Microbial Ecology* **27**(3): 301–311. DOI: http://dx.doi.org/10.3354/ame027301.

Glud, RN, Rysgaard, S, Turner, G, McGinnis, DF, Leakey, RJG. 2014. Biological- and physical-induced oxygen dynamics in melting sea ice of the Fram Strait. *Limnology and Oceanography* **59**(4): 1097–1111. DOI: http://dx.doi.org/10.4319/lo.2014.59.4.1097.

Golovin, PN, Ivanov, VV. 2015. Density stratification effects on the ice lead heat balance and perennial ice melting in the Central Arctic. *Russian Meteorology and Hydrology* **401**: 46–59. DOI: http://dx.doi.org/10.3103/S1068373915010070.

Goreau, TJ, Kaplan, WA, Wofsy, SC, McElroy, MB, Valois, FW, Watson, SW. 1980. Production of NO_2^- and N_2O by nitrifying bacteria at reduced concentrations of oxygen. *Applied and Environmental Microbiology* **40**(3): 526–532. DOI: http://dx.doi.org/10.1128/aem.40.3.526-532.1980.

Gourdal, M, Lizotte, M, Massé, G, Gosselin, M, Poulin, M, Scarratt, M, Charette, J, Levasseur, M. 2018. Dimethyl sulfide dynamics in first-year sea ice melt ponds in the Canadian Arctic Archipelago. *Biogeosciences* **15**(10): 3169–3188. DOI: http://dx.doi.org/10.5194/bg-15-3169-2018.

Gradinger, R. 1996. Occurrence of an algal bloom under Arctic pack ice. *Marine Ecology Progress Series* **131**: 301–305. DOI: http://dx.doi.org/10.3354/meps131301.

Grainger, EH, Mohammed, AA. 1990. High salinity tolerance in sea ice copepods. *Ophelia* **313**: 177–185. DOI: http://dx.doi.org/10.1080/00785326.1990.10430860.

Granskog, MA, Pavlov, AK, Sagan, S, Kowalczuk, P, Raczkowska, A, Stedmon, CA. 2015. Effect of sea-ice melt on inherent optical properties and vertical distribution of solar radiant heating in Arctic surface waters. *Journal of Geophysical Research* **120**(10): 7028–7039. DOI: http://dx.doi.org/10.1002/2015JC011087.

Grant, WS, Horner, RA. 1976. Growth responses to salinity variation in four Arctic ice diatoms. *Journal of Phycology* **12**(2): 180–185. DOI: http://dx.doi.org/10.1111/j.1529-8817.1976.tb00498.x.

Grossart, HP, Massana, R, McMahon, KD, Walsh, DA. 2020. Linking metagenomics to aquatic microbial ecology and biogeochemical cycles. *Limnology and Oceanography* **65**(S1): S2–S20. DOI: http://dx.doi.org/10.1002/lno.11382.

Ha, S-Y, Min, J-O, Joo, HM, Chung, KH, Shin, K-H, Yang, E, Kang, S-H. 2014. Production rate estimation of mycosporine-like amino acids in two Arctic melt ponds by stable isotope probing with NAH$^{13}CO_3$.

Journal of Phycology **50**(5): 901–907. DOI: http://dx.doi.org/10.1111/jpy.12221.

Hancke, K, Kristiansen, S, Lund-Hansen, LC. 2022. Highly productive ice algal mats in Arctic melt ponds: Primary production and carbon turnover. *Frontiers in Marine Science* **9**: 841720. DOI: http://dx.doi.org/10.3389/fmars.2022.841720.

Hanson, AM. 1965. Studies of the mass budget of Arctic pack-ice floes. *Journal of Glaciology* **5**(41): 701–709. DOI: http://dx.doi.org/10.3189/S0022143000018694.

Hartmann, M, Gong, X, Kecorius, S, van Pinxteren, M, Vogl, T, Welti, A, Wex, H, Zeppenfeld, S, Herrmann, H, Wiedensohler, A, Stratmann, F. 2021. Terrestrial or marine—Indications towards the origin of ice-nucleating particles during melt season in the European Arctic up to 83.7°N. *Atmospheric Chemistry and Physics* **21**(15): 11613–11636. DOI: http://dx.doi.org/10.5194/acp-21-11613-2021.

Hatam, I, Lange, B, Beckers, J, Haas, C, Lanoil, B. 2016. Bacterial communities from Arctic seasonal sea ice are more compositionally variable than those from multi-year sea ice. *The ISME Journal* **10**(10): 2543–2552. DOI: http://dx.doi.org/10.1038/ismej.2016.4.

Hernando, M, Schloss, IR, Almandoz, GO, Malanga, G, Varela, DE, De Troch, M. 2018. Combined effects of temperature and salinity on fatty acid content and lipid damage in Antarctic phytoplankton. *Journal of Experimental Marine Biology and Ecology* **503**: 120–128. DOI: http://dx.doi.org/10.1016/j.jembe.2018.03.004.

Hernando, M, Schloss, IR, Malanga, G, Almandoz, GO, Ferreyra, GA, Aguiar, MB, Puntarulo, S. 2015. Effects of salinity changes on coastal Antarctic phytoplankton physiology and assemblage composition. *Journal of Experimental Marine Biology and Ecology* **466**: 110–119. DOI: http://dx.doi.org/10.1016/j.jembe.2015.02.012.

Hop, H, Mundy, CJ, Gosselin, M, Rossnagel, AL, Barber, DG. 2011. Zooplankton boom and ice amphipod bust below melting sea ice in the Amundsen Gulf, Arctic Canada. *Polar Biology* **34**(12): 1947–1958. DOI: http://dx.doi.org/10.1007/s00300-011-0991-4.

Hoppmann, M, Richter, ME, Smith, IJ, Jendersie, S, Langhorne, PJ, Thomas, DN, Dieckmann, GS. 2020. Platelet ice, the Southern Ocean's hidden ice: A review. *Annals of Glaciology* **61**(83): 341–368. DOI: http://dx.doi.org/10.1017/aog.2020.54.

Horvat, C, Tziperman, E, Campin, JM. 2016. Interaction of sea ice floe size, ocean eddies, and sea ice melting. *Geophysical Research Letters* **43**(15): 8083–8090. DOI: http://dx.doi.org/10.1002/2016GL069742.

Hudson, SR, Granskog, MA, Sundfjord, A, Randelhoff, A, Renner, AH, Divine, DV. 2013. Energy budget of first-year Arctic sea ice in advanced stages of melt. *Geophysical Research Letters* **40**(11): 2679–2683. DOI: http://dx.doi.org/10.1002/grl.50517.

Itkin, P, Hendricks, S, Webster, M, von Albedyll, L, Arndt, S, Divine, D, Jaggi, M, Oggier, M, Raphael, I, Ricker, R, Rohde, J, Schneebeli, M, Liston, GE. 2023. Sea ice and snow characteristics from year-long transects at the MOSAiC Central Observatory. *Elementa: Science of the Anthropocene* **11**(1). DOI: http://dx.doi.org/10.1525/elementa.2022.00048.

Itkin, P, Spreen, G, Cheng, B, Doble, M, Girard-Ardhuin, F, Haapala, J, Hughes, N, Kaleschke, L, Nicolaus, M, Wilkinson, J. 2017. Thin ice and storms: Sea ice deformation from buoy arrays deployed during N-ICE 2015. *Journal of Geophysical Research* **122**(6): 4661–4674. DOI: http://dx.doi.org/10.1002/2016JC012403.

James, RH, Bousquet, P, Bussmann, I, Haeckel, M, Kipfer, R, Leifer, I, Niemann, H, Ostrovsky, I, Piskozub, J, Rehder, G, Treude, T, Vielstädte, L, Greinert, J. 2016. Effects of climate change on methane emissions from seafloor sediments in the Arctic Ocean: A review. *Limnology and Oceanography* **61**: S283–S299. DOI: http://dx.doi.org/10.1002/lno.10307.

JCOMM Expert Team on Sea Ice. 2014. Sea-Ice Nomenclature: Snapshot of the WMO Sea Ice Nomenclature WMO No. 259, volume 1—Terminology and Codes; Volume II—Illustrated Glossary and III—International System of Sea-Ice Symbols. Geneva, Switzerland: WMO-JCOMM: 1–121 (WMO-No. 259 I-III). DOI: http://dx.doi.org/10.25607/OBP-1515.

Jeffries, MO, Schwartz, K, Morris, K, Veazey, AD, Krouse, HR, Gushing, S. 1995. Evidence for platelet ice accretion in Arctic sea ice development. *Journal of Geophysical Research* **100**(C6): 10905–10914. DOI: http://dx.doi.org/10.1029/95JC00804.

Jørgensen, L, Stedmon, CA, Kaartokallio, H, Middelboe, M, Thomas, DN. 2015. Changes in the composition and bioavailability of dissolved organic matter during sea ice formation. *Limnology and Oceanography* **60**(3): 817–830. DOI: http://dx.doi.org/10.1002/lno.10058.

Juhl, AR, Krembs, C. 2010. Effects of snow removal and algal photoacclimation on growth and export of ice algae. *Polar Biology* **33**: 1057–1065. DOI: http://dx.doi.org/10.1007/s00300-010-0784-1.

Juhl, AR, Krembs, C, Meiners, KM. 2011. Seasonal development and differential retention of ice algae and other organic fractions in first-year Arctic sea ice. *Marine Ecology Progress Series* **436**: 1–16. DOI: http://dx.doi.org/10.3354/meps09277.

Junge K, Eicken H, Deming JW. 2004. Bacterial activity at −2 to −20°C in Arctic wintertime sea ice. *Applied and Environmental Microbiology* **70**(1): 550–557. DOI: http://dx.doi.org/10.1128/AEM.70.1.550-557.2004.

Kadko, D. 2000. Modeling the evolution of the Arctic mixed layer during the fall 1997 Surface Heat Budget of the Arctic Ocean (SHEBA) Project using measurements of ^{7}Be. *Journal of Geophysical Research* **105**(C2): 3369–3378. DOI: http://dx.doi.org/10.1029/1999JC900311.

Karam, S, **Tippenhauer, S**, **Allerholt, J**, **Hoppmann, M**, **Koenig, Z**, **Muilwijk, M**, **Schuffenhauer, I**, **Schulz, K**. 2023. Physical oceanography measurements from a hand-held CTD during Leg 4 and 5 of POLARSTERN cruise PS122—MOSAiC. *PANGAEA* [data set]. DOI: http://dx.doi.org/10.1594/PANGAEA.956142.

Karlsson, J, **Giesler, R**, **Persson, J**, **Lundin, E**. 2013. High emission of carbon dioxide and methane during ice thaw in high latitude lakes. *Geophysical Research Letters* **40**(6): 1123–1127. DOI: http://dx.doi.org/10.1002/grl.50152.

Katlein, C, **Schiller, M**, **Belter, HJ**, **Coppolaro, V**, **Wenslandt, D**, **Nicolaus, M**. 2017. A new remotely operated sensor platform for interdisciplinary observations under sea ice. *Frontiers in Marine Science* **4**: 281. DOI: http://dx.doi.org/10.3389/fmars.2017.00281.

Kauko, HM, **Taskjelle, T**, **Assmy, P**, **Pavlov, AK**, **Mundy, CJ**, **Duarte, P**, **Fernández-Méndez, M**, **Olsen, LM**, **Hudson, SR**, **Johnsen, G**, **Elliot, A**, **Wang, F**, **Granskog, MA**. 2017. Windows in Arctic sea ice: Light transmission and ice algae in a refrozen lead. *Journal of Geophysical Research* **122**(6): 1486–1505. DOI: https://doi.org/10.1002/2016JG003626.

Kawaguchi, Y, **Koenig, Z**, **Nomura, D**, **Hoppmann, M**, **Inoue, J**, **Fang, YC**, **Schulz, K**, **Gallagher, M**, **Katlein, C**, **Nicolaus, M**, **Rabe, B**. 2022. Turbulent mixing during late summer in the ice–ocean boundary layer in the Central Arctic Ocean: Results from the MOSAiC expedition. *Journal of Geophysical Research* **127**(8): e2021JC017975. DOI: http://dx.doi.org/10.1029/2021JC017975.

Kirillov, S, **Dmitrenko, I**, **Rysgaard, S**, **Babb, D**, **Ehn, J**, **Bendtsen, J**, **Boone, W**, **Barber, D**, **Geilfus, N**. 2018. The inferred formation of a subice platelet layer below the multiyear landfast sea ice in the Wandel Sea (NE Greenland) induced by meltwater drainage. *Journal of Geophysical Research* **123**(5): 3489–3506. DOI: http://dx.doi.org/10.1029/2017JC013672.

Kirpes, RM, **Bonanno, D**, **May, NW**, **Fraund, M**, **Barget, AJ**, **Moffet, RC**, **Ault, AP**, **Pratt, KA**. 2019. Wintertime Arctic sea spray aerosol composition controlled by sea ice lead microbiology. *ACS Central Science* **5**(11): 1760–1767. DOI: http://dx.doi.org/10.1021/acscentsci.9b00541.

Kirst, GO. 1989. Salinity tolerance of eukaryotic marine algae. *Annual Review of Plant Physiology and Plant Molecular Biology* **40**: 21–53. DOI: http://dx.doi.org/10.1146/annurev.pp.41.060190.000321.

Kitidis, V, **Upstill-Goddard, RC**, **Anderson, LG**. 2010. Methane and nitrous oxide in surface water along the North-West Passage, Arctic Ocean. *Marine Chemistry* **121**: 80–86. DOI: http://dx.doi.org/10.1016/j.marchem.2010.03.006.

König, M, **Oppelt, N**. 2020. A linear model to derive melt pond depth on Arctic sea ice from hyperspectral data. *The Cryosphere* **14**(8): 2567–2579. DOI: http://dx.doi.org/10.5194/tc-14-2567-2020.

Krembs, C, **Eicken, H**, **Junge, K**, **Deming, JW**. 2002. High concentrations of exopolymeric substances in Arctic winter sea ice: Implications for the polar ocean carbon cycle and cryoprotection of diatoms. *Deep Sea Research Part I: Oceanographic Research Papers* **49**(12): 2163–2181. DOI: http://dx.doi.org/10.1016/S0967-0637(02)00122-X.

Krumpen, T, **Birrien, F**, **Kauker, F**, **Rackow, T**, **von Albedyll, L**, **Angelopoulos, M**, **Belter, HJ**, **Bessonov, V**, **Damm, E**, **Dethloff, K**, **Haapala, J**, **Haas, C**, **Harris, C**, **Hendricks, S**, **Hoelemann, J**, **Hoppmann, M**, **Kaleschke, L**, **Karcher, M**, **Kolabutin, N**, **Lei, R**, **Lenz, J**, **Morgenstern, A**, **Nicolaus, M**, **Nixdorf, U**, **Petrovsky, T**, **Rabe, B**, **Rabenstein, L**, **Rex, M**, **Ricker, R**, **Rohde, J**, **Shimanchuk, E**, **Singha, S**, **Smolyanitsky, V**, **Sokolov, V**, **Stanton, T**, **Timofeeva, A**, **Tsamados, M**, **Watkins, D**. 2020. The MOSAiC ice floe: Sediment-laden survivor from the Siberian shelf. *The Cryosphere* **14**(7): 2173–2187. DOI: http://dx.doi.org/10.5194/tc-14-2173-2020.

Kudryavtsev, VN, **Soloviev, AV**. 1990. Slippery near-surface layer of the ocean arising due to daytime solar heating. *Journal of Physical Oceanography* **20**(5): 617–628. DOI: http://dx.doi.org/10.1175/1520-0485(1990)020<0617:SNSLOT>2.0.CO;2.

Kurosaki, Y, **Matoba, S**, **Iizuka, Y**, **Fujita, K**, **Shimada, R**. 2022. Increased oceanic dimethyl sulfide emissions in areas of sea ice retreat inferred from a Greenland ice core. *Communications Earth & Environment* **3**(1): 327. DOI: http://dx.doi.org/10.1038/s43247-022-00661-w.

Kwok, R, **Cunningham, GF**. 2015. Variability of Arctic sea ice thickness and volume from CryoSat-2. *Philosophical Transactions of the Royal Society A: Mathematical, Physical and Engineering Sciences* **373**(2045). DOI: http://dx.doi.org/10.1098/rsta.2014.0157.

Lamarche-Gagnon, G, **Wadham, JL**, **Sherwood Lollar, B**, **Arndt, S**, **Fietzek, P**, **Beaton, AD**, **Tedstone, AJ**, **Telling, J**, **Bagshaw, EA**, **Hawkings, JR**, **Kohler, TJ**. 2019. Greenland melt drives continuous export of methane from the ice-sheet bed. *Nature* **565**(7737): 73–77. DOI: http://dx.doi.org/10.1038/s41586-018-0800-0.

Landy, J, **Ehn, J**, **Shields, M**, **Barber, D**. 2014. Surface and melt pond evolution on landfast first-year sea ice in the Canadian Arctic Archipelago. *Journal of Geophysical Research: Oceans* **119**(5): 3054–3075. DOI: http://dx.doi.org/10.1002/2013JC009617.

Langdon, C. 2010. Determination of dissolved oxygen in seawater by winkler titration using amperometric technique, in Hood, EM, Sabine, CL, Sloyan, BM eds., *The GO-SHIP repeat hydrography manual: A collection of expert reports and guidelines. Version 1.* (IOCCP Report Number 14; ICPO Publication Series Number 134): 18. DOI: http://dx.doi.org/10.25607/OBP-1350.

Lange, BA, **Granskog, MA**, **Meyer, H**, **Bauch, D**, **Smith, MM**, **von Albedyll, L**, **Raphael, I**, **Matero, I**, **Salganik, E**. 2022. Oxygen and hydrogen isotopic ratios from sea ice bottom, false bottom ice, under-ice

meltwater layer and surface melt pond samples collected during MOSAiC leg 4 (PS122.4). *PANGAEA* [data set]. DOI: http://dx.doi.org/pangaea.de/10.1594/PANGAEA.943734.

Lange, BA, Salganik, E, Macfarlane, A, Schneebeli, M, Høyland, K, Gardner, J, Müller, O, Divine, DV, Kohlbach, D, Katlein, C, Granskog, MA. 2023. Snowmelt contribution to Arctic first-year ice ridge mass balance and rapid consolidation during summer melt. *Elementa: Science of the Anthropocene* **11**(1): 00037. DOI: http://dx.doi.org/10.1525/elementa.2022.00037.

Langleben, MP. 1966. On the factors affecting the rate of ablation of sea ice. *Canadian Journal of Earth Sciences* **3**(4): 431–439. DOI: http://dx.doi.org/10.1139/e66-032.

Lannuzel, D, Tedesco, L, Van Leeuwe, M, Campbell, K, Flores, H, Delille, B, Miller, L, Stefels, J, Assmy, P, Bowman, J, Brown, K. 2020. The future of Arctic sea-ice biogeochemistry and ice-associated ecosystems. *Nature Climate Change* **10**(11): 983–992. DOI: http://dx.doi.org/10.1038/s41558-020-00940-4.

Lauvset, SK, Lange, N, Tanhua, T, Bittig, HC, Olsen, A, Kozyr, A, Alin, S, Álvarez, M, Azetsu-Scott, K, Barbero, L, Becker, S, Brown, PJ, Carter, BR, Cotrim da Cunha, L, Feely, RA, Hoppema, M, Humphreys, MP, Ishii, M, Jeansson, E, Jiang, LQ, Jones, SD, Lo Monaco, C, Murata, A, Müller, JD, Pérez, FF, Pfeil, B, Schirnick, C, Steinfeldt, R, Suzuki, T, Tilbrook, B, Ulfsbo, A, Velo, A, Woosley, RJ, Key, RM. 2022. GLODAPv2.2022: The latest version of the global interior ocean biogeochemical data product. *Earth System Science Data* **14**: 5543–5572. DOI: http://dx.doi.org/10.5194/essd-14-5543-2022.

Leck, C, Bigg, EK. 2005. Biogenic particles in the surface microlayer and overlaying atmosphere in the central Arctic Ocean during summer. *Tellus B: Chemical and Physical Meteorology* **57**: 305–316. DOI: http://dx.doi.org/10.3402/tellusb.v57i4.16546.

Lei, R, Cheng, B, Hoppmann, M, Zhang, F, Zuo, G, Hutchings, JK, Lin, L, Lan, M, Wang, H, Regnery, J, Krumpen, T. 2022. Seasonality and timing of sea ice mass balance and heat fluxes in the Arctic transpolar drift during 2019–2020. *Elementa: Science of the Anthropocene* **10**(1): 000089. DOI: http://dx.doi.org/10.1525/elementa.2021.000089.

Levasseur, M. 2013. Impact of Arctic meltdown on the microbial cycling of sulphur. *Nature Geoscience* **6**: 691–700. DOI: http://dx.doi.org/10.1038/ngeo1910.

Lewis, KM, Arntsen, AE, Coupel, P, Joy-Warren, H, Lowry, KE, Matsuoka, A, Mills, MM, van Dijken, GL, Selz, V, Arrigo, KR. 2019. Photoacclimation of Arctic Ocean phytoplankton to shifting light and nutrient limitation. *Limnology and Oceanography* **64**: 284–301. DOI: http://dx.doi.org/10.1002/lno.11039.

Lizotte, M, Levasseur, M, Galindo, V, Gourdal, M, Gosselin, M, Tremblay, JÉ, Blais, M, Charrette, J,

Hussherr, R. 2020. Phytoplankton and dimethylsulfide dynamics at two contrasting Arctic ice edges. *Biogeosciences* **17**(6): 1557–1581. DOI: http://dx.doi.org/10.5194/bg-17-1557-2020.

Loose, B, McGillis, WR, Schlosser, P, Perovich, D, Takahashi, T. 2009. Effects of freezing, growth, and ice cover on gas transport processes in laboratory seawater experiments. *Geophysical Research Letters* **36**(5): L05603. DOI: http://dx.doi.org/10.1029/2008GL036318.

Loose, B, Schlosser, P. 2011. Sea ice and its effect on CO_2 flux between the atmosphere and the Southern Ocean interior. *Journal of Geophysical Research* **116**: C11019. DOI: http://dx.doi.org/10.1029/2010JC006509.

Löscher, CR, Kock, A, Könneke, M, LaRoche, J, Bange, HW, Schmitz, RA. 2012. Production of oceanic nitrous oxide by ammonia-oxidizing archaea. *Biogeosciences* **9**(7): 2419–2429. DOI: http://dx.doi.org/10.5194/bg-9-2419-2012.

Malfatti, F, Lee, C, Tinta, T, Pendergraft, MA, Celussi, M, Zhou, Y, Sultana, CM, Rotter, A, Axson, JL, Collins, DB, Santander, MV. 2019. Detection of active microbial enzymes in nascent sea spray aerosol: Implications for atmospheric chemistry and climate. *Environmental Science & Technology Letters* **6**(3): 171–177. DOI: http://dx.doi.org/10.1021/acs.estlett.8b00699.

Manning, CC, Preston, VL, Jones, SF, Michel, AP, Nicholson, DP, Duke, PJ, Ahmed, MM, Manganini, K, Else, BG, Tortell, PD. 2020. River inflow dominates methane emissions in an Arctic coastal system. *Geophysical Research Letters* **47**(10): e2020GL087669. DOI: http://dx.doi.org/10.1029/2020GL087669.

Manning, CC, Zheng, Z, Fenwick, L, McCulloch, RD, Damm, E, Izett, RW, Williams, WJ, Zimmermann, S, Vagle, S, Tortell, PD. 2022. Interannual variability in methane and nitrous oxide concentrations and sea-air fluxes across the North American Arctic Ocean (2015–2019). *Global Biogeochemical Cycles* **36**(4): e2021GB007185. DOI: http://dx.doi.org/10.1029/2021GB007185.

Marchenko, A. 2022. Modeling of thermodynamic consolidation of sea ice ridges drifting in the water with changing temperature. *Journal of Marine Science and Engineering* **10**(12): 1858. DOI: http://dx.doi.org/10.3390/jmse10121858.

Martin, S, Kauffman, P. 1974. The evolution of under-ice melt ponds, or double diffusion at the freezing point. *Journal of Fluid Mechanics* **64**(3): 507–528. DOI: http://dx.doi.org/10.1017/S0022112074002527.

Martin, T, Steele, M, Zhang, J. 2014. Seasonality and long-term trend of Arctic Ocean surface stress in a model. *Journal of Geophysical Research* **119**(3): 1723–1738. DOI: http://dx.doi.org/10.1002/2013JC009425.

Matrai, PA, Tranvik, L, Leck, C, Knulst, JC. 2008. Are high Arctic surface microlayers a potential source of aerosol organic precursors? *Marine Chemistry*

108(1–2): 109–122. DOI: http://dx.doi.org/10.1016/j.marchem.2007.11.001.

Matthes, LC, Mundy, CJ, Girard, SL, Babin, M, Verin, G, Ehn, JK. 2020. Spatial heterogeneity as a key variable influencing spring-summer progression in UVR and PAR transmission through Arctic sea ice. *Frontiers in Marine Science* **7**(183): 1–15. DOI: http://dx.doi.org/10.3389/fmars.2020.00183.

Mau, S, Blees, J, Helmke, E, Niemann, H, Damm, E. 2013. Vertical distribution of methane oxidation and methanotrophic response to elevated methane concentrations in stratified waters of the Arctic fjord Storfjorden (Svalbard, Norway). *Biogeosciences* **10**(10): 6267–6268. DOI: http://dx.doi.org/10.5194/bg-10-6267-2013.

McDougall, TJ, Barker, PM. 2011. Getting started with TEOS-10 and the Gibbs Seawater (GSW) oceanographic toolbox. SCOR/IAPSO Working Group 127: 1–28.

McDougall, TJ, Jackett, DR, Millero, FJ, Pawlowicz, R, Barker, PM. 2012. A global algorithm for estimating absolute salinity. *Ocean Science* **8**(6): 1123–1134. DOI: http://dx.doi.org/10.5194/os-8-1123-2012.

McLaren, IA. 2011. Primary production and nutrients in Ogac Lake, a landlocked fiord on Baffin Island. *Journal of the Fisheries Research Board of Canada* **26**(6): 1561–1576. DOI: http://dx.doi.org/10.1139/f69-140.

McParland, EL, Levine, NM. 2019. The role of differential DMSP production and community composition in predicting variability of global surface DMSP concentrations. *Limnology and Oceanography* **64**(2): 757–773. DOI: http://dx.doi.org/10.1002/lno.11076.

McPhee, MG, Kantha, LH. 1989. Generation of internal waves by sea ice. *Journal of Geophysical Research* **94**(C3): 3287–3302. DOI: http://dx.doi.org/10.1029/JC094iC03p03287.

McPhee, MG, Maykut, GA, Morison, JH. 1987. Dynamics and thermodynamics of the ice/upper ocean system in the marginal ice zone of the Greenland Sea. *Journal of Geophysical Research* **92**(C7): 7017–7031. DOI: http://dx.doi.org/10.1029/JC092iC07p07017.

Miao, X, Xie, H, Ackley, SF, Perovich, DK, Ke, C. 2015. Object-based detection of Arctic sea ice and melt ponds using high resolutionaerial photographs. *Cold Regions Science and Technology* **119**: 211–222. DOI: http://dx.doi.org/10.1016/j.coldregions.2015.06.014.

Michel, C, Legendre, L, Taguchi, S. 1997. Coexistence of microalgal sedimentation and water column recycling in a seasonally ice-covered ecosystem (Saroma-ko Lagoon, Sea of Okhotsk, Japan). *Journal of Marine Systems* **11**(1–2): 133–148. DOI: http://dx.doi.org/10.1016/S0924-7963(96)00034-6.

Miller, LA, Burgers, TM, Burt, WJ, Granskog, MA, Papakyriakou, TN. 2019. Air-sea CO_2 flux estimates in stratified Arctic coastal waters: How wrong can we be? *Geophysical Research Letters* **46**(1): 235–243. DOI: http://dx.doi.org/10.1029/2018GL080099.

Mo, A, Yang, EJ, Kang, S-H, Kim, D, Lee, K, Ko, YH, Kim, K, Kim, T-W. 2022. Impact of sea ice melting on summer air-sea CO_2 exchange in the east Siberian Sea. *Frontiers in Marine Science* **9**: 766810. DOI: http://dx.doi.org/10.3389/fmars.2022.766810.

Mock, T, Boulton, W, Balmonte, JP, Barry, K, Bertilsson, S, Bowman, J, Buck, M, Bratbak, G, Chamberlain, EJ, Cunliffe, M, Creamean, J. 2022. Multiomics in the central Arctic Ocean for benchmarking biodiversity change. *PLoS Biology* **20**(10): e3001835. DOI: http://dx.doi.org/10.1371/journal.pbio.3001835.

Mock, T, Otillar, RP, Strauss, J, McMullan, M, Paajanen, P, Schmutz, J, Salamov, A, Sanges, R, Toseland, A, Ward, BJ, Allen, AE. 2017. Evolutionary genomics of the cold-adapted diatom *Fragilariopsis cylindrus*. *Nature* **541**: 536–540. DOI: http://dx.doi.org/10.1038/nature20803.

Morison, JH, Long, CE, Levine, MD. 1985. Internal wave dissipation under sea ice. *Journal of Geophysical Research* **90**(C6): 11959–11966. DOI: http://dx.doi.org/10.1029/JC090iC06p11959.

Muilwijk, M, Koenig, Z, Fer, I, Schulz, K, Tippenhauer, S, Schuffenhauer, I, Karam, S, Hoppmann, M, Allerholt, J. 2022. Videos and extracted frames from Blueye ROV camera during MOSAiC Leg 4 (PS122/4) and Leg 5 (PS122/5). PANGAEA [data set]. DOI: http://dx.doi.org/10.1594/PANGAEA.941553.

Mundy, CJ, Gosselin, M, Ehn, JK, Belzile, C, Poulin, M, Alou, E, Roy, S, Hop, H, Lessard, S, Papakyriakou, TN, Barber, DG. 2011. Characteristics of two distinct high-light acclimated algal communities during advanced stages of sea ice melt. *Polar Biology* **34**: 1869–1886. DOI: http://dx.doi.org/10.1007/s00300-011-0998-x.

Nansen, F. 1902. The oceanography of the North Polar Basin, in Nansen, F ed., *The Norwegian North polar expedition 1893–1896 scientific results* (vol. 3). New York, NY: Greenwood Press.

Nansen, F. 1906. Protozoa on the ice-floes of the North Polar Sea, in Nansen, F ed., *The Norwegian North polar expedition 1893–1896 scientific results* (vol. 5). New York, NY: Greenwood Press.

Nazintsev, YL. 1964. The heat balance of the surface of the multiyear ice cover in the central Arctic (in Russian). *Trudy Arkticheskogo i Antarkticheskogo Nauchno-Issledovatel'skogo Instituta* **267**: 110–126.

Neckel, N, Fuchs, N, Birnbaum, G, Hutter, N, Jutila, A, Buth, L, von Albedyll, L, Ricker, R, Haas, C. 2022. Helicopter-borne RGB orthomosaics and photogrammetric digital elevation models from the MOSAiC expedition. PANGAEA [data set]. DOI: http://dx.doi.org/10.1594/PANGAEA.949433.

Nicolaus, M, Katlein, C, Maslanik, J, Hendricks, S. 2012. Changes in Arctic sea ice result in increasing light transmittance and absorption. *Geophysical Research Letters* **39**(24). DOI: http://dx.doi.org/10.1029/2012GL053738.

Nicolaus, M, Perovich, DK, Spreen, G, Granskog, MA, Albedyll, LV, Angelopoulos, M, Anhaus, P, Arndt, S, Belter, HJ, Bessonov, V, Birnbaum, G, Brauchle,

J, Calmer, R, Cardellach, E, Cheng, B, Clemens-Sewall, D, Dadic, R, Damm, E, de Boer, G, Demir, O, Dethloff, K, Divine, DV, Fong, AA, Fons, S, Frey, MM, Fuchs, N, Gabarró, C, Gerland, S, Goessling, HF, Gradinger, R, Haapala, J, Haas, C, Hamilton, J, Hannula, H-R, Hendricks, S, Herber, A, Heuzé, C, Hoppmann, M, Høyland, KV, Huntemann, M, Hutchings, JK, Hwang, B, Itkin, P, Jacobi, H-W, Jaggi, M, Jutila, A, Kaleschke, L, Katlein, C, Kolabutin, N, Krampe, D, Kristensen, SS, Krumpen, T, Kurtz, N, Lampert, A, Lange, BA, Lei, R, Light, B, Linhardt, F, Liston, GE, Loose, B, Macfarlane, AR, Mahmud, M, Matero, IO, Maus, S, Morgenstern, A, Naderpour, R, Nandan, V, Niubom, A, Oggier, M, Oppelt, N, Pätzold, F, Perron, C, Petrovsky, T, Pirazzini, R, Polashenski, C, Rabe, B, Raphael, IA, Regnery, J, Rex, M, Ricker, R, Riemann-Campe, K, Rinke, A, Rohde, J, Salganik, E, Scharien, RK, Schiller, M, Schneebeli, M, Semmling, M, Shimanchuk, E, Shupe, MD, Smith, MM, Smolyanitsky, V, Sokolov, V, Stanton, T, Stroeve, J, Thielke, L, Timofeeva, A, Tonboe, RT, Tavri, A, Tsamados, M, Wagner, DN, Watkins, D, Webster, M, Wendisch, M. 2022. Overview of the MOSAiC expedition: Snow and sea ice. *Elementa: Science of the Anthropocene* **10**(1): 000046. DOI: http://dx.doi.org/10.1525/elementa.2021.000046.

Nixdorf, U, Dethloff, K, Rex, M, Shupe, M, Sommerfeld, A, Perovich, DK, Nicolaus, M, Heuzé, C, Rabe, B, Loose, B, Damm, E, Gradinger, R, Fong, A, Maslowski, W, Rinke, A, Kwok, R, Spreen, G, Wendisch, M, Herber, A, Hirsekorn, M, Mohaupt, Ve, Frickenhaus, S, Immerz, A, Weiss-Tuider, K, König, B, Mengedoht, D, Regnery, J, Gerchow, P, Ransby, D, Krumpen, T, Morgenstern, A, Haas, C, Kanzow, T, Rack, FR, Saitzev, V, Sokolov, V, Makarov, A, Schwarze, S, Wunderlich, T, Wurr, K, Boetius, A. 2021. MOSAiC extended acknowledgement. Zenodo. DOI: http://dx.doi.org/10.5281/zenodo.5541624.

Nomura, D, Granskog, MA, Assmy, P, Simizu, D, Hashida, G. 2013. Arctic and Antarctic sea ice acts as a sink for atmospheric CO_2 during periods of snowmelt and surface flooding. *Journal of Geophysical Research* **118**(12): 6511–6524. DOI: http://dx.doi.org/10.1002/2013JC009048.

Nomura, D, Kawaguchi, Y, Webb, A, Li, Y, Dall'osto, M, Schmidt, K, Droste, ES, Chamberlain, EJ, Kolabutin, N, Shimanchuk, E, Hoppmann, M, Gallagher, MR, Meyer, H, Ardakani, MM, Bauch, D, Gabarró, C, Smith, MM, Inoue, J, Damm, E, Delille, B. 2023. Meltwater layer dynamics in a central Arctic lead: Effects of width, re-freezing, and mixing during late summer. *Elementa: Science of the Anthropocene* **11**(1): 00102. DOI: http://dx.doi.org/10.1525/elementa.2022.00102.

Notz, D, McPhee, MG, Worster, MG, Maykut, GA, Schlünzen, KH, Eicken, H. 2003. Impact of underwater-ice evolution on Arctic summer sea ice.

Journal of Geophysical Research **108**(C7): 3223. DOI: http://dx.doi.org/10.1029/2001JC001173.

Olsen, LM, Laney, SR, Duarte, P, Kauko, HM, Fernández-Méndez, M, Mundy, CJ, Rösel, A, Meyer, A, Itkin, P, Cohen, L, Peeken, I, Tatarek, A, Różańska-Pluta, M, Wiktor, J, Taskjelle, T, Pavlov, AK, Hudson, SR, Granskog, MA, Hop, H, Assmy, P. 2017. The seeding of ice algal blooms in Arctic pack ice: The multiyear ice seed repository hypothesis. *Journal of Geophysical Research Biogeosciences* **122**: 1529–1548. DOI: http://dx.doi.org/10.1002/2016JG003668.

Ouyang, Z, Qi, D, Zhong, W, Chen, L, Gao, Z, Lin, H, Sun, H, Li, T, Cai, WJ. 2021. Summertime evolution of net community production and CO_2 flux in the western Arctic Ocean. *Global Biogeochemical Cycles* **35**(3): e2020GB006651. DOI: http://dx.doi.org/10.1029/2020GB006651.

Park, K, Kim, I, Choi, JO, Lee, Y, Jung, J, Ha, SY, Kim, JH, Zhang, M. 2019. Unexpectedly high dimethyl sulfide concentration in high-latitude Arctic sea ice melt ponds. *Environmental Science: Processes & Impacts* **21**(10): 1642–1649. DOI: http://dx.doi.org/10.1039/c9em00195f.

Parmentier, FJW, Christensen, TR, Sørensen, LL, Rysgaard, S, McGuire, AD, Miller, PA, Walker, DA. 2013. The impact of lower sea-ice extent on Arctic greenhouse-gas exchange. *Nature Climate Change* **3**(3): 195–202. DOI: http://dx.doi.org/10.1038/nclimate1784.

Pavlov, AK, Taskjelle, T, Kauko, HM, Hamre, B, Hudson, SR, Assmy, P, Duarte, P, Fernández-Méndez, M, Mundy, CJ, Granskog, MA. 2017. Altered inherent optical properties and estimates of the underwater light field during an Arctic under-ice bloom of *Phaeocystis pouchetii. Journal of Geophysical Research Oceans* **122**(6): 4939–4961. DOI: http://dx.doi.org/10.1002/2016JC012471.

Pegau, WS. 2002. Inherent optical properties of the central Arctic surface waters. *Journal of Geophysical Research* **107**(C10): SHE 16-1–SHE 16-7. DOI: http://dx.doi.org/10.1029/2000JC000382.

Peralta-Ferriz, C, Woodgate, RA. 2015. Seasonal and interannual variability of pan-Arctic surface mixed layer properties from 1979 to 2012 from hydrographic data, and the dominance of stratification for multiyear mixed layer depth shoaling. *Progress in Oceanography* **134**: 19–53. DOI: http://dx.doi.org/10.1016/j.pocean.2014.12.005.

Perovich, D, Smith, M, Light, B, Webster, M. 2021. Meltwater sources and sinks for multiyear Arctic sea ice in summer. *The Cryosphere* **15**(9): 4517–4525. DOI: http://dx.doi.org/10.5194/tc-15-4517-2021.

Perovich, DK, Grenfell, TC, Richter-Menge, JA, Light, B, Tucker III, WB, Eicken, H. 2003. Thin and thinner: Sea ice mass balance measurements during SHEBA. *Journal of Geophysical Research* **108**: 8050. DOI: http://dx.doi.org/10.1029/2001JC001079.

Perovich, DK, Maykut, GA. 1990. Solar heating of a stratified ocean in the presence of a static ice cover.

Journal of Geophysical Research **95**(C10): 18233–18245. DOI: http://dx.doi.org/10.1029/JC095iC10p18233.

Petrich, C, Eicken, C, Polashenski, CM, Sturm, M, Harbeck, JP, Perovich, DK, Finnegan, DC. 2012. Snow dunes: A controlling factor of melt pond distribution on Arctic sea ice. *Journal of Geophysical Research* **117**: C09029. DOI: http://dx.doi.org/10.1029/2012JC008192.

Petrou, K, Doblin, MA, Ralph, PJ. 2011. Heterogeneity in the photoprotective capacity of three Antarctic diatoms during short-term changes in salinity and temperature. *Marine Biology* **158**: 1029–1041. DOI: http://dx.doi.org/10.1007/s00227-011-1628-4.

Pierrot, D, Neill, C, Sullivan, K, Castle, R, Wanninkhof, R, Lüger, H, Johannessen, T, Olsen, A, Feeley, RA, Cosca, CE. 2009. Recommendations for autonomous underway pCO_2 measuring systems and data-reduction routines. *Deep Sea Research Part II: Topical Studies in Oceanography* **56**(8–10): 512–522. DOI: http://dx.doi.org/10.1016/j.dsr2.2008.12.005.

Polashenski, C, Golden, KM, Perovich, DK, Skyllingstad, E, Arnsten, A, Stwertka, C, Wright, N. 2017. Percolation blockage: A process that enables melt pond formation on first year Arctic sea ice. *Journal of Geophysical Research* **122**: 413–440. DOI: http://dx.doi.org/10.1002/2016JC011994.

Polashenski, C, Perovich, DK, Courville, Z. 2012. The mechanisms of sea ice melt pond formation and evolution. *Journal of Geophysical Research* **117**: C01001. DOI: http://dx.doi.org/10.1029/2011JC007231.

Polashenski, C, Perovich, DK, Frey, KE, Cooper, LW, Logvinova, CI, Dadic, R, Light, B, Kelly, HP, Trusel, LD, Webster, M. 2015. Physical and morphological properties of sea ice in the Chukchi and Beaufort Seas during the 2010 and 2011 NASA ICESCAPE missions. *Deep Sea Research Part II: Topical Studies in Oceanography* **118**(Part A): 7–17. DOI: http://dx.doi.org/10.1016/j.dsr2.2015.04.006.

Prinsenberg, SJ, Peterson, IK, Holladay, JS. 2008. Measuring the thicknesses of the freshwater-layer plume and sea ice in the land-fast ice region of the Mackenzie Delta using helicopter-borne sensors. *Journal of Marine Systems* **74**(3–4): 783–793. DOI: http://dx.doi.org/10.1016/j.jmarsys.2008.02.009.

Provost, C, Sennéchael, N, Sirven, J. 2019. Contrasted summer processes in the sea ice for two neighboring floes north of 84°N: Surface and basal melt and false bottom formation. *Journal of Geophysical Research* **124**(6): 3963–3986. DOI: http://dx.doi.org/10.1029/2019JC015000.

Quinn, PK, Collins, DB, Grassian, VH, Prather, KA, Bates, TS. 2015. Chemistry and related properties of freshly emitted sea spray aerosol. *Chemical Reviews* **115**(10): 4383–4399. DOI: http://dx.doi.org/10.1021/cr500713g.

Rabe, B, Heuzé, C, Regnery, J, Aksenov, Y, Allerholt, J, Athanase, M, Bai, Y, Basque, C, Bauch, D, Baumann, TM, Chen, D, Cole, ST, Craw, L, Davies, A, Damm, E, Dethloff, K, Divine, DV, Doglioni, F, Ebert, F, Fang, Y-C, Fer, I, Fong, AA, Gradinger, R, Granskog, MA, Graupner, R, Haas, C, He, H, He, Y, Hoppmann, M, Janout, M, Kadko, D, Kanzow, T, Karam, S, Kawaguchi, Y, Koenig, Z, Kong, B, Krishfield, RA, Krumpen, T, Kuhlmey, D, Kuznetsov, I, Lan, M, Laukert, G, Lei, R, Li, T, Torres-Valdés, S, Lin, L, Lin, L, Liu, H, Liu, N, Loose, B, Ma, X, MacKay, R, Mallet, M, Mallett, RDC, Maslowski, W, Mertens, C, Mohrholz, V, Muilwijk, M, Nicolaus, M, O'Brien, JK, Perovich, D, Ren, J, Rex, M, Ribeiro, N, Rinke, A, Schaffer, J, Schuffenhauer, I, Schulz, K, Shupe, MD, Shaw, W, Sokolov, V, Sommerfeld, A, Spreen, G, Stanton, T, Stephens, M, Su, J, Sukhikh, N, Sundfjord, A, Thomisch, K, Tippenhauer, S, Toole, JM, Vredenborg, M, Walter, M, Wang, H, Wang, L, Wang, Y, Wendisch, M, Zhao, J, Zhou, M, Zhu, J. 2022. Overview of the MOSAiC expedition: Physical oceanography. *Elementa: Science of the Anthropocene* **10**(1): 00062. DOI: http://dx.doi.org/10.1525/elementa.2021.00062.

Ralph, PJ, McMinn, A, Ryan, KG, Ashworth, C. 2005. Short-term effect of temperature on the photokinetics of microalgae from the surface layers of Antarctic pack ice. *Journal of Phycology* **41**(4): 763–769. DOI: http://dx.doi.org/10.1111/j.1529-8817.2005.00106.x.

Ralph, PJ, Ryan, KG, Martin, A, Fenton, G. 2007. Melting out of sea ice causes greater photosynthetic stress in algae than freezing in. *Journal of Phycology* **43**(5): 948–956. DOI: http://dx.doi.org/10.1111/j.1529-8817.2007.00382.x.

Rampal, P, Weiss, J, Dubois, C, Campin, JM. 2011. IPCC climate models do not capture Arctic sea ice drift acceleration: Consequences in terms of projected sea ice thinning and decline. *Journal of Geophysical Research* **116**(C8). DOI: http://dx.doi.org/10.1029/2011JC007110.

Randelhoff, A, Fer, I, Sundfjord, A. 2017. Turbulent upper-ocean mixing affected by meltwater layers during Arctic summer. *Journal of Physical Oceanography* **474**: 835–853. DOI: http://dx.doi.org/10.1175/JPO-D-16-0200.1.

Randelhoff, A, Sundfjord, A, Renner, AH. 2014. Effects of a shallow pycnocline and surface meltwater on sea ice–ocean drag and turbulent heat flux. *Journal of Physical Oceanography* **448**: 2176–2190. DOI: http://dx.doi.org/10.1175/JPO-D-13-0231.1.

Rapp, JZ, Sullivan, MB, Deming, JW. 2021. Divergent genomic adaptations in the microbiomes of Arctic subzero sea-ice and cryopeg brines. *Frontiers in Microbiology* **12**: 701186. DOI: http://dx.doi.org/10.3389/fmicb.2021.701186.

Rees, AP, Bange, HW, Arévalo-Martínez, DL, Artioli, Y, Ashby, DM, Brown, I, Campen, HI, Clark, DR, Kitidis, V, Lessin, G, Tarran, GA, Turley, C. 2022. Nitrous oxide and methane in a changing Arctic

Ocean. *Ambio* **51**: 398–410. DOI: http://dx.doi.org/10.1007/s13280-021-01633-8.

Rees, AP, **Brown, IJ**, **Jayakumar, A**, **Lessin, G**, **Somerfield, PJ**, **Ward, BB**. 2021. Biological nitrous oxide consumption in oxygenated waters of the high latitude Atlantic Ocean. *Communications Earth & Environment* **2**: 36. DOI: http://dx.doi.org/10.1038/s43247-021-00104-y.

Richter, DH, **Veron, F**. 2016. Ocean spray: An outsized influence on weather and climate. *Physics Today* **69**(11): 34–39. DOI: http://dx.doi.org/10.1063/PT.3.3363.

Richter-Menge, JA, **Perovich, DK**, **Pegau, WS**. 2001. Summer ice dynamics during SHEBA and its effect on the ocean heat content. *Annals of Glaciology* **33**: 201–206. DOI: http://dx.doi.org/10.3189/172756401781818176.

Riebesell, U, **Schloss, I**, **Smetacek, V**. 1991. Aggregation of algae released from melting sea ice: Implications for seeding and sedimentation. *Polar Biology* **11**: 239–248. DOI: http://dx.doi.org/10.1007/BF00238457.

Rinke, A, **Cassano, JJ**, **Cassano, EN**, **Jaiser, R**, **Handorf, D**. 2021. Meteorological conditions during the MOSAiC expedition: Normal or anomalous? *Elementa: Science of the Anthropocene* **9**(1): 00023. DOI: http://dx.doi.org/10.1525/elementa.2021.00023.

Rösel, A, **Kaleschke, L**. 2012. Exceptional melt pond occurrence in the years 2007 and 2011 on the Arctic sea ice revealed from MODIS satellite data. *Journal of Geophysical Research: Oceans* **117**(C5). DOI: http://dx.doi.org/10.1029/2011JC007869.

Rudels, B. 2012. Arctic Ocean circulation and variability–advection and external forcing encounter constraints and local processes. *Ocean Science* **8**(2): 261–286. DOI: http://dx.doi.org/10.5194/os-8-261-2012.

Rudels, B. 2016. Arctic Ocean stability: The effects of local cooling, oceanic heat transport, freshwater input, and sea ice melt with special emphasis on the Nansen Basin. *Journal of Geophysical Research* **121**(7): 4450–4473. DOI: http://dx.doi.org/10.1002/2015JC011045.

Ryan, KG, **Ralph, P**, **McMinn, A**. 2004. Acclimation of Antarctic bottom-ice algal communities to lowered salinities during melting. *Polar Biology* **27**: 679–686. DOI: http://dx.doi.org/10.1007/s00300-004-0636-y.

Rysgaard, S, **Bendtsen, J**, **Delille, B**, **Dieckmann, GS**, **Glud, RN**, **Kennedy, H**, **Mortensen, J**, **Papadimitriou, S**, **Thomas, DN**, **Tison, J-L**. 2011. Sea ice contribution to the air–sea CO_2 exchange in the Arctic and Southern Oceans. *Tellus B: Chemical and Physical Meteorology* **63**(5): 823–830. DOI: http://dx.doi.org/10.1111/j.1600-0889.2011.00571.x.

Rysgaard, S, **Glud, RN**. 2004. Anaerobic N_2 production in Arctic sea ice. *Limnology and Oceanography* **49**(1): 86–94. DOI: http://dx.doi.org/10.4319/lo.2004.49.1.0086.

Rysgaard, S, **Glud, RN**, **Sejr, MK**, **Blicher, ME**, **Stahl, HJ**. 2008. Denitrification activity and oxygen dynamics in Arctic sea ice. *Polar Biology* **31**: 527–537. DOI: http://dx.doi.org/10.1007/s00300-007-0384-x.

Salganik, E, **Katlein, C**, **Lange, BA**, **Matero, I**, **Lei, R**, **Fong, AA**, **Fons, SW**, **Divine, D**, **Oggier, M**, **Castellani, G**, **Bozzato, D**, **Chamberlain, EJ**, **Hoppe, CJM**, **Müller, O**, **Gardner, J**, **Rinke, A**, **Pereira, PS**, **Ulfsbo, A**, **Marsay, C**, **Webster, MA**, **Maus, S**, **Høyland, KV**, **Granskog, MA**. 2023. Temporal evolution of under-ice meltwater layers and false bottoms and their impact on summer Arctic sea ice mass balance. *Elementa: Science of the Anthropocene* **11**(1): 00035. DOI: http://dx.doi.org/10.1525/elementa.2022.00035.

Schmale, J, **Baccarini, A**. 2021. Progress in unraveling atmospheric new particle formation and growth across the Arctic. *Geophysical Research Letters* **48**(14): e2021GL094198. DOI: http://dx.doi.org/10.1029/2021GL094198.

Schulz, K, **Mohrholz, V**, **Fer, I**, **Janout, M**, **Hoppmann, M**, **Schaffer, J**, **Koenig, Z**. 2022. A full year of turbulence measurements from a drift campaign in the Arctic Ocean 2019–2020. *Scientific Data* **9**: 472. DOI: http://dx.doi.org/10.1038/s41597-022-01574-1.

Sherr, BF, **Sherr, EB**. 2003. Community respiration/production and bacterial activity in the upper water column of the central Arctic Ocean. *Deep Sea Research Part I: Oceanographic Research Papers* **50**(4): 529–542. DOI: http://dx.doi.org/10.1016/S0967-0637(03)00030-X.

Shupe, MD, **Rex, M**, **Blomquist, B**, **Persson, POG**, **Schmale, J**, **Uttal, T**, **Althausen, D**, **Angot, H**, **Archer, S**, **Bariteau, L**, **Beck, I**, **Bilberry, J**, **Bucci, S**, **Buck, C**, **Boyer, M**, **Brasseur, Z**, **Brooks, IM**, **Calmer, R**, **Cassano, J**, **Castro, V**, **Chu, D**, **Costa, D**, **Cox, CJ**, **Creamean, J**, **Crewell, S**, **Dahlke, S**, **Damm, E**, **de Boer, G**, **Deckelmann, H**, **Dethloff, K**, **Dütsch, M**, **Ebell, K**, **Ehrlich, A**, **Ellis, J**, **Engelmann, R**, **Fong, AA**, **Frey, MM**, **Gallagher, MR**, **Ganzeveld, L**, **Gradinger, R**, **Graeser, J**, **Greenamyer, V**, **Griesche, H**, **Griffiths, S**, **Hamilton, J**, **Heinemann, G**, **Helmig, D**, **Herber, A**, **Heuzé, C**, **Hofer, J**, **Houchens, T**, **Howard, D**, **Inoue, J**, **Jacobi, H-W**, **Jaiser, R**, **Jokinen, T**, **Jourdan, O**, **Jozef, G**, **King, W**, **Kirchgaessner, A**, **Klingebiel, M**, **Krassovski, M**, **Krumpen, T**, **Lampert, A**, **Landing, W**, **Laurila, T**, **Lawrence, D**, **Lonardi, M**, **Loose, B**, **Lüpkes, C**, **Maahn, M**, **Macke, A**, **Maslowski, W**, **Marsay, C**, **Maturilli, M**, **Mech, M**, **Morris, S**, **Moser, M**, **Nicolaus, M**, **Ortega, P**, **Osborn, J**, **Pätzold, F**, **Perovich, DK**, **Petäjä, T**, **Pilz, C**, **Pirazzini, R**, **Posman, K**, **Powers, H**, **Pratt, KA**, **Preußer, A**, **Quéléver, L**, **Radenz, M**, **Rabe, B**, **Rinke, A**, **Sachs, T**, **Schulz, A**, **Siebert, H**, **Silva, T**, **Solomon, A**, **Sommerfeld, A**, **Spreen, G**, **Stephens, M**, **Stohl, A**, **Svensson, G**, **Uin, J**, **Viegas, J**, **Voigt, C**, **von der Gathen, P**, **Wehner, B**, **Welker, JM**, **Wendisch, M**, **Werner, M**, **Xie, ZQ**, **Yue, F**.

2022. Overview of the MOSAiC expedition: Atmosphere. *Elementa: Science of the Anthropocene* **10**(1): 00060. DOI: http://dx.doi.org/10.1525/elementa.2021.00060.

Sigman, DM, **Jaccard, SL**, **Haug, GH**. 2004. Polar ocean stratification in a cold climate. *Nature* **428**: 59–63. DOI: http://dx.doi.org/10.1038/nature02357.

Silyakova, A, **Nomura, D**, **Kotovitch, M**, **Fransson, A**, **Delille, B**, **Chierici, M**, **Granskog, MA**. 2022. Methane release from open leads and new ice following an Arctic winter storm event. *Polar Science* **33**: 100874. DOI: http://dx.doi.org/10.1016/j.polar.2022.100874.

Simó, R. 2001. Production of atmospheric sulfur by oceanic plankton: Biogeochemical, ecological and evolutionary links. *Trends in Ecology and Evolution* **16**(6): 287–294. DOI: http://dx.doi.org/10.1016/S0169-5347(01)02152-8.

Skyllingstad, ED, **Paulson, CA**, **Pegau, WS**. 2005. Simulation of turbulent exchange processes in summertime leads. *Journal of Geophysical Research* **110**(C5). DOI: http://dx.doi.org/10.1029/2004JC002502.

Smith, M, **Bozzato, D**, **Chamberlain, E**, **Dietrich, U**, **Droste, E**, **Fong, A**, **Light, B**, **Linhardt, F**, **Matero, I**, **Perovich, D**, **Raphael, I**, **Regnery, J**, **Salganik, E**, **Tavri, A**, **von Albedyll, L**, **Webster, M**. 2022a. Near-surface ocean temperature and salinity measurements (using YSI and Castaway) during the summer component of the Multidisciplinary drifting Observatory for the Study of Arctic Climate (MOSAiC) campaign in the Central Arctic Ocean, July–September 2020. Arctic Data Center. DOI: http://dx.doi.org/10.18739/A2TT4FV1G.

Smith, MM, **Holland, M**, **Light, B**. 2022c. Arctic sea ice sensitivity to lateral melting representation in a coupled climate model. *The Cryosphere* **16**(2): 419–434. DOI: http://dx.doi.org/10.5194/tc-16-419-2022.

Smith, MM, **von Albedyll, L**, **Raphael, IA**, **Lange, BA**, **Matero, I**, **Salganik, E**, **Webster, MA**, **Granskog, MA**, **Fong, A**, **Lei, R**, **Light, B**. 2022b. Quantifying false bottoms and under-ice meltwater layers beneath Arctic summer sea ice with fine-scale observations. *Elementa: Science of the Anthropocene* **10**(1): 000116. DOI: http://dx.doi.org/10.1525/elementa.2021.000116.

Smith, MS, **Zimmerman, K**. 1981. Nitrous oxide production by nondenitrifying soil nitrate reducers. *Soil Science Society of America Journal* **45**(5): 865–871. DOI: http://dx.doi.org/10.2136/sssaj1981.03615995004500050008x.

Smith, N. 2019. Mathematical modelling of under-ice melt ponds and their impact on the thermohaline interaction between sea ice and the oceanic mixed layer [PhD thesis]. Reading: University of Reading. DOI: http://dx.doi.org/10.48683/1926.00085363.

Sørensen, HL, **Thamdrup, B**, **Jeppesen, E**, **Rysgaard, S**, **Glud, RN**. 2017. Nutrient availability limits biological production in Arctic sea ice melt ponds. *Polar Biology* **40**: 1593–1606. DOI: http://dx.doi.org/10.1007/s00300-017-2082-7.

Stefels, J, **van Leeuwe, M**, **Jones, E**, **Meredith, M**, **Venables, H**, **Webb, A**, **Henley, S**. 2018. Impact of sea-ice melt on dimethyl sulfide (sulfoniopropionate) inventories in surface waters of Marguerite Bay, West Antarctic Peninsula. *Philosophical Transactions of the Royal Society A* **376**: 20170169. DOI: http://dx.doi.org/10.1098/rsta.2017.0169.

Stopa, JE, **Ardhuin, F**, **Girard-Ardhuin, F**. 2016. Wave climate in the Arctic 1992–2014: Seasonality and trends. *The Cryosphere* **10**(4): 1605–1629. DOI: http://dx.doi.org/10.5194/tc-10-1605-2016.

Taskjelle, T, **Granskog, MA**, **Pavlov, AK**, **Hudson, SR**, **Hamre, B**. 2017. Effects of an Arctic under-ice bloom on solar radiant heating of the water column. *Journal of Geophysical Research: Oceans* **122**(1): 126–138. DOI: http://dx.doi.org/10.1002/2016JC012187.

Thielke, L, **Fuchs, N**, **Spreen, G**, **Tremblay, B**, **Birnbaum, G**, **Huntemann, M**, **Hutter, N**, **Itkin, P**, **Jutila, A**, **Webster, MA**. 2022. Preconditioning of summer melt ponds from winter sea ice surface temperature. *Geophysical Research Letters* **50**(4): e2022GL101493. DOI: http://dx.doi.org/10.1029/2022GL101493.

Thornton, DCO. 2014. Dissolved organic matter (DOM) release by phytoplankton in the contemporary and future ocean. *European Journal of Phycology* **49**(1): 20–46. DOI: http://dx.doi.org/10.1080/09670262.2013.875596.

Timmermans, ML, **Krishfield, R**, **Laney, S**, **Toole, J**. 2010. Ice-tethered profiler measurements of dissolved oxygen under permanent ice cover in the Arctic Ocean. *Journal of Atmospheric and Oceanic Technology* **27**(11): 1936–1949. DOI: http://dx.doi.org/10.1175/2010JTECHO772.1.

Timmermans, ML, **Winsor, P**. 2013. Scales of horizontal density structure in the Chukchi Sea surface layer. *Continental Shelf Research* **52**: 39–45. DOI: http://dx.doi.org/10.1016/j.csr.2012.10.015.

Toole, JM, **Krishfield, RA**, **Timmermans, M-L**, **Proshutinsky, A**. 2011. The ice-tethered profiler: Argo of the Arctic. *Oceanography* **24**(3): 126–135. DOI: http://dx.doi.org/10.2307/24861307.

Top, Z, **Martin, S**, **Becker, P**. 1985. On the dissolved surface oxygen supersaturation in the Arctic. *Geophysical Research Letters* **12**(12): 821–823. DOI: http://dx.doi.org/10.1029/GL012i012p00821.

Tremblay, C, **Runge, J**, **Legendre, L**. 1989. Grazing and sedimentation of ice algae during and immediately after a bloom at the ice-water interface. *Marine Ecology Progress Series* **56**(3): 291–300. DOI: http://dx.doi.org/10.3354/meps056291.

Trevena, AJ, **Jones, GB**. 2006. Dimethylsulphide and dimethylsulphoniopropionate in Antarctic sea ice and their release during sea ice melting. *Marine Chemistry* **98**(2–4): 210–222. DOI: http://dx.doi.org/10.1016/j.marchem.2005.09.005.

Tsamados, M, **Feltham, D**, **Petty, A**, **Schroeder, D**, **Flocco, D**. 2015. Processes controlling surface, bottom and lateral melt of Arctic sea ice in a state of the art sea ice model. *Philosophical Transactions of the*

Royal Society A: Mathematical, Physical and Engineering Sciences **373**(2052): 20140167. DOI: http://dx.doi.org/10.1098/rsta.2014.0167.

Uhlig, C, Damm, E, Peeken, I, Krumpen, T, Rabe, B, Korhonen, M, Ludwichowski, KU. 2019. Sea ice and water mass influence dimethylsulfide concentrations in the central Arctic Ocean. *Frontiers in Earth Science* **7**: 179. DOI: http://dx.doi.org/10.3389/feart.2019.00179.

Ulfsbo, A, Cassar, N, Korhonen, M, van Heuven, S, Hoppema, M, Kattner, G, Anderson, LG. 2014. Late summer net community production in the central Arctic Ocean using multiple approaches. *Global Biogeochemical Cycles* **28**(10): 1129–1148. DOI: http://dx.doi.org/10.1002/2014GB004833.

Underwood, GJ, Michel, C, Meisterhans, G, Niemi, A, Belzile, C, Witt, M, Dumbrell, AJ, Koch, BP. 2019. Organic matter from Arctic sea-ice loss alters bacterial community structure and function. *Nature Climate Change* **9**(2): 170–176. DOI: http://dx.doi.org/10.1038/s41558-018-0391-7.

Untersteiner, N, Badgley, FI. 1958. Preliminary results of thermal budget studies on Arctic pack ice during summer and autumn. *Arctic Sea Ice* **598**: 85–92.

Uusikivi, J, Vähätalo, AV, Granskog, MA, Sommeruga, R. 2010. Contribution of mycosporine-like amino acids and colored dissolved and particulate matter to sea ice optical properties and ultraviolet attenuation. *Limnology and Oceanography* **55**(2): 703–713. DOI: http://dx.doi.org/10.4319/lo.2010.55.2.0703.

Van Leeuwe, MA, Webb, AL, Venables, HJ, Visser, RJ, Meredith, MP, Elzenga, JTM, Stefels, J. 2020. Annual patterns in phytoplankton phenology in Antarctic coastal waters explained by environmental drivers. *Limnology and Oceanography* **65**(7): 1651–1668. DOI: http://dx.doi.org/10.1002/lno.11477.

Vancoppenolle, M, Meiners, KM, Michel, C, Bopp, L, Brabant, F, Carnat, G, Delille, B, Lannuzel, D, Madec, G, Moreau, S, Tison, JL. 2013. Role of sea ice in global biogeochemical cycles: Emerging views and challenges. *Quaternary Science Reviews* **79**: 207–230. DOI: http://dx.doi.org/10.1016/j.quascirev.2013.04.011.

Verdugo, J, Damm, E, Nikolopoulos, A. 2021. Methane cycling within sea ice: Results from drifting ice during late spring, north of Svalbard. *The Cryosphere* **15**(6): 2701–2717. DOI: http://dx.doi.org/10.5194/tc-15-2701-2021.

Vihma, T, Pirazzini, R, Fer, I, Renfrew, IA, Sedlar, J, Tjernström, M, Lüpkes, C, Nygård, T, Notz, D, Weiss, J, Marsan, D, Cheng, B, Birnbaum, G, Gerland, S, Chechin, D, Gascard, JC. 2014. Advances in understanding and parameterization of small-scale physical processes in the marine Arctic climate system: A review. *Atmospheric Chemistry and Physics* **14**(17): 9403–9450. DOI: http://dx.doi.org/10.5194/acp-14-9403-2014.

Wadhams, P, Martin, S. 1990. Processes determining the bottom topography of multiyear Arctic sea ice, in Ackley, SF, Weeks, WF eds., *Sea ice properties and processes*, CRREL Monogr. 90-1. Hanover, NH: U.S. Army Cold Regions Research and Engineering Laboratory: 136–141.

Wand, U, Samarkin, VA, Nitzsche, H-M, Hubberten, H-W. 2006. Biogeochemistry of methane in the permanently ice-covered Lake Untersee, central Dronning Maud land, East Antarctica. *Limnology and Oceanography* **51**(2): 1180–1194. DOI: http://dx.doi.org/10.4319/lo.2006.51.2.1180.

Wang, C, Shi, L, Gerland, S, Granskog, MA, Renner, AH, Li, Z, Hansen, E, Martma, T. 2013. Spring sea-ice evolution in Rijpfjorden (80°N), Svalbard, from in situ measurements and ice mass-balance buoy (IMB) data. *Annals of Glaciology* **54**(62): 253–260. DOI: http://dx.doi.org/10.3189/2013AoG62A135.

Wang, M, Su, J, Landy, J, Leppäranta, M, Guan, L. 2020. A new algorithm for sea ice melt pond fraction estimation from high-resolution optical satellite imagery. *Journal of Geophysical Research* **125**(10): e2019JC015716. DOI: http://dx.doi.org/10.1029/2019JC015716.

Webster, MA, Holland, M, Wright, NC, Hendricks, S, Hutter, N, Itkin, P, Light, B, Linhardt, F, Perovich, DK, Raphael, IA, Smith, MM, Albedyll, Lv, Zhang, J. 2022. Spatiotemporal evolution of melt ponds on Arctic sea ice: MOSAiC observations and model results. *Elementa: Science of the Anthropocene* **10**(1): 000072. DOI: http://dx.doi.org/10.1525/elementa.2021.000072.

Weiss, RF. 1974. Carbon dioxide in water and seawater: The solubility of a non-ideal gas. *Marine Chemistry* **2**: 203–215.

Werner, I. 2006. Seasonal dynamics of sub-ice fauna below pack ice in the Arctic (Fram Strait). *Deep Sea Research Part I: Oceanographic Research Papers* **53**(2): 294–309. DOI: http://dx.doi.org/10.1016/j.dsr.2005.11.001.

Weslawski, JM, Legezynska, J. 1998. Glaciers caused zooplankton mortality? *Journal of Plankton Research* **20**(7): 1233–1240. DOI: http://dx.doi.org/10.1093/plankt/20.7.1233.

Wright, DG, Pawlowicz, R, McDougall, TJ, Feistel, R, Marion, GM. 2011. Absolute Salinity, "Density Salinity" and the Reference-Composition Salinity Scale: Present and future use in the seawater standard TEOS-10. *Ocean Science* **7**(1): 1–26. DOI: http://dx.doi.org/10.5194/os-7-1-2011.

Wright, NC, Polashenski, CM, McMichael, ST, Beyer, RA. 2020. Observations of sea ice melt from Operation IceBridge imagery. *The Cryosphere* **14**(10): 3523–3536. DOI: http://dx.doi.org/10.5194/tc-14-3523-2020.

Xu, D, Kong, H, Yang, EJ, Li, X, Jiao, N, Warren, A, Wang, Y, Lee, Y, Jung, J, Kang, SH. 2020. Contrasting community composition of active microbial eukaryotes in melt ponds and sea water of the Arctic Ocean revealed by high throughput sequencing. *Frontiers in Microbiology* **11**: 1170. DOI: http://dx.doi.org/10.3389/fmicb.2020.01170.

Zanowski, H, **Jahn, A**, **Holland, MM**. 2021. Arctic Ocean freshwater in CMIP6 ensembles: Declining sea ice, increasing ocean storage and export. *Journal of Geophysical Research* **126**(4): e2020JC016930. DOI: http://dx.doi.org/10.1029/2020JC016930.

Zeebe, RE, **Wolf-Gladrow, DA**. 2001. CO_2 in seawater: Equilibrium, kinetics, isotopes. Amsterdam, the Netherlands: Elsevier. (Elsevier Oceanography Series; vol. 65).

Zeng, YX, **Zhang, F**, **He, JF**, **Lee, SH**, **Qiao, ZY**, **Yu, Y**, **Li, HR**. 2013. Bacterioplankton community structure in the Arctic waters as revealed by pyrosequencing of 16S rRNA genes. *Antonie Van Leeuwenhoek* **103**: 1309–1319. DOI: http://dx.doi.org/10.1007/s10482-013-9912-6.

Zeppenfeld, S, **van Pinxteren, M**, **Hartmann, M**, **Bracher, A**, **Stratmann, F**, **Herrmann, H**. 2019. Glucose as a potential chemical marker for ice nucleating activity in Arctic seawater and melt pond samples. *Environmental Science & Technology* **53**(15): 8747–8756. DOI: http://dx.doi.org/10.1021/acs.est.9b01469.

Zhan, L, **Wu, M**, **Chen, L**, **Zhang, J**, **Li, Y**, **Liu, J**. 2017. The air-sea nitrous flux along cruise tracks to the Arctic Ocean and Southern Ocean. *Atmosphere* **8**(11): 216. DOI: http://dx.doi.org/10.3390/atmos8110216.

Zhan, L, **Zhang, J**, **Ouyang, Z**, **Xu, S**, **Qi, D**, **Gao, Z**, **Sun, H**, **Li, Y**, **Wu, M**, **Liu, J**, **Chen, L**. 2020. High-resolution distribution pattern of surface water nitrous oxide along a cruise track from the Okhotsk Sea to the western Arctic Ocean. *Limnology and Oceanography* **66**(51): S401–S410. DOI: http://dx.doi.org/10.1002/lno.11604.

Zhang, Q, **Gradinger, R**, **Spindler, M**. 1999. Experimental study on the effect of salinity on growth rates of Arctic-sea-ice algae from the Greenland Sea. *Boreal Environment Research* **4**(1): 1–8.

Elem Sci Anth is a peer-reviewed open access journal published by University of California Press.

OPEN ACCESS